MELT AND GLASSY DYNAMICS IN COMPLEX POLYMER SYSTEMS: MISCIBLE BLENDS AND STAR-SHAPED POLYMER FILMS

by

Bradley Raymond Frieberg

A dissertation submitted in partial fulfillment
of the requirements for the degree of
Doctor of Philosophy
(Macromolecular Science and Engineering)
in the University of Michigan
2014

Doctoral Committee:

Professor Peter F. Green, Chair
Associate Professor Anastasios John Hart, Massachusetts Institute of Technology
Professor Richard E. Robertson
Assistant Professor Anish Tuteja

To my loving wife,

Audrey,

my parents,

Raymond and Tammy,

and my brother and sister

Nathan and Kimberly

ACKNOWLEDGEMENTS

As I look back at the many years I have spent at the University of Michigan, I cannot express how grateful I am for all the love and support I received from my friends, family and colleagues. After this long, exhausting week of finishing up my Ph.D. degree I have to stop and look back at the many amazing moments I have had throughout both my undergraduate and graduate degrees at such an amazing university.

First, I need to take the time to especially thank my advisor and mentor, Professor Peter F. Green. I first started working for Professor Green as a junior in my undergraduate degree, and ever since the first day in the lab I knew that this was the right place for me. His work style and point of view in terms of research were the perfect fit for me, in that he allowed me to work on projects that I felt passionate about and he encouraged me to follow my intuitions. I cannot thank him enough for the support and advice he has given me throughout the years, as I know they will help me have a successful career.

I would also like to thank my committee members, Professor John Hart, Professor Richard Robertson and Professor Anish Tuteja, for their support, comments and suggestions throughout my degree. I especially want to thank Professor Richard Robertson, as his suggestions and mentoring throughout my undergraduate and graduate career helped shaped the projects I chose and where I am today. I would also like to give a special thank you to Dr. Suresh Narayanan at Argonne National Laboratory and Dr. Madhusudan Tyagi at the National Institute for Standards and Technology for their particular help with X-ray and Neutron scattering experiments respectively, which gave me so much insight and further improved my research.

I must also thank all the former and current members of Peter Green's research group. I especially would like to thank Dr. Emmanouil Glynos for his guidance throughout my research career. I am glad that I was not scared away from the group on

my first day from his thirst for research and trying to explain complex polymer physics with a heavy Greek accent. But without his help and support I would not have made it as far as I did. I of course need to thank all the other members of the Green group that contributed to my work either directly or indirectly: Dr. Aaron Tan, Dr. Hyun Joon Oh, Dr. Chelsea Chen, Dr. Jenny Kim, Dr. Ernest McIntyre, Hengxi Yang, Jojo Amonoo, Ravi Sharma, Kyle Johnson, Anton Li, Peter Chung, Bingyuan Huang, Junnan Zhao, Ban Dong, and the undergraduates that have worked with me: Brittany Auld, Marjorie Bridgewater and Desmond Pressey.

Many thanks to my collaborators David Bilby, Professor Jinsang Kim, Adam Barito, Matthew Sykes, Kanika Agrawal and Professor Max Shtein for their collaboration on connecting electrical properties and optical properties of organic electronics.

Finally, I would like to express my greatest thanks to my family and friends at the University of Michigan. Without these people I would have gone crazy, stuck in the lab 24 hours a day. First, I would like to thank my loving wife, Audrey Frieberg, for her unconditional love and support. I would like to thank my parents, Ray and Tammy Frieberg, my brother, Nathan, and sister, Kimberly, for their love and unwavering support throughout my educational career. I would also like to thank my in-laws, for giving me that home away from home, as it is not always easy being 600 miles from your parents. And of course a special thanks to the many friends that I have made, both at and outside the University of Michigan, that give me the moral support and moments of sanity outside of the lab. It is with the help and support of all these people, and any others I forgot to mention, that made this dissertation possible.

TABLE OF CONTENTS

LIST OF FIGURES

LIST OF TABLES

LIST OF APPENDICES

ABSTRACT

Considerable effort has been given towards using polymers as active materials in many types of organic devices such as photovoltaics, active membranes and sensors as well as drug delivery. A number of the applications of polymeric materials involve thin film geometries; therefore the role of interfacial interactions has garnered a lot of interest of late. However, the influence of interfaces on the physical properties of polymer films in not well understood. One such property is physical aging, which leads to a time-dependence of many properties, including: increased brittleness, enhanced modulus and reduced permeability. Therefore, there is a strong technological and scientific importance to understanding the underlying phenomenon behind this process. In this dissertation three classes of polymers are used in order to investigate the role of interfaces on the dynamic properties of polymer thin films: (1) glassy structural relaxation in star-shaped polymers, (2) free surface dynamics of miscible A/B polymer/polymer blends, and (3) polymer nanocomposites.

The structural relaxation rate of polystyrene in the bulk and micron thick films is strongly influenced by the chain architecture. Due to the decreased conformational freedom, and entropic constraints of the chains grafted to a central core exhibited by the star-shaped molecules, the stars exhibit up to a 40% reduction in the relaxation rate relative to their linear counterparts.

In the case of supported thin films, interfacial interactions can strongly influence the structural relaxation rate. By changing the chain architecture, the entropic loss upon adsorption to an interface as well as the surface tension can be controlled. The thickness dependence of the structural relaxation rate can be described with a universal model that accounts for to the temperature dependence of the structural relaxation rate as well as the distribution in local T_g throughout the film.

In a miscible A/B polymer blend, the local surface composition can vastly differ from the bulk. The lower surface tension of the B component will lead to a surface excess. Because of the differences in the composition near the surface, the polymer chain dynamics near that interface can be vastly different from that of the bulk.

Lastly, polymer grafted inorganic nanofillers are incorporated into the miscible blends in order to introduce additional surface area into the system. The addition of these nanoparticles decreased the local viscosity near the free surface for two reasons. The first reason is that the addition of a third component further changed the local composition near the free surface; the second reason is the reduced friction coefficient experienced by the polymer chains in the vicinity of the nanoparticles.

All of these findings have implications in the processing and long term implementation of polymer films in many different applications.

CHAPTER 1
INTRODUCTION

1.1 MOTIVATION AND RESEARCH OBJECTIVES

Polymers are incorporated into a number of current technologies used today from packaging such as plastic bags and bottles to functional materials such as organic electronics and sensors. The use of polymeric materials allows for cheaper manufacturing costs and flexible, light weight alternatives to inorganics. In order to meet the ever growing needs of current technologies, tailoring material structure on the nano-scale has been of utmost importance. A number of strategies have been employed in order to tailor the properties of polymeric materials on the nano-scale: from changing the monomer structure and molecular weight, to copolymers and polymer blends. One topic of interest of late has been macromolecular topology. By changing the molecular architecture, different macroscopic properties can be achieved while maintaining the same chemical constituents.

Many applications involving polymeric materials, such as membranes,[1-4] LEDs[5, 6] or organic photovoltaics, are utilized in thin film geometries. It has been well reported that in thin film geometries a number of physical properties depend on film thickness: viscosity,[7] physical aging rate[8, 9] and glass transition temperatures.[10, 11] The influence of a solid or free interface will alter the average properties of a polymer film, through the entropic and enthalpic interactions with the molecules. One of the more intriguing properties is the dynamics of the polymer chains at temperatures both above and below the glass transition temperature. It is how fast or slow the polymer chains will move that will govern the processibility or longevity of a particular material.

A long-standing problem in polymer physics over the past 70 years has been understanding how material properties will change below the glass transition temperature.[9, 12-16] When an amorphous material is quenched below the glass transition

temperature, it resides in a non-equilibrium state. Over time the polymer molecules will undergo a series of structural relaxations in order to return to an equilibrium state. It is through this process that a number of properties become time-dependent. When used in a technological application, this results in device characteristics that will also change with time. Due to the length-scales and time-scales required to fully understand the process of structural relaxations, a number of unique experimental protocols have been implemented in order to further understand this phenomenon. Yet, there is still debate to this day as to the specific mechanisms behind glassy structural relaxation in polymeric systems.

By introducing branching points into a polymer chain a number of macroscopic properties can be influenced including crystallinity, viscosity and glass transition temperatures. One of the most controllable branched systems is star-shaped molecules, in which a number of linear polymer chain arms are connected at a single branching point. Star-shaped molecules have also been shown to have significantly different interfacial interactions than their linear analogs. This allows for a tailoring of the film thickness dependence of properties such as wetting[17] and glass transition[18] without altering the chemical constituents. This is accomplished through the reduced entropic penalty for star-shaped molecules to adsorb to an interface.

Another material system in which interfacial interactions play a significant role is in miscible polymer blends. Although they may be miscible in the bulk state, one of the components will have a lower surface energy, making it energetically favorable for that polymer to reside at the surface; resulting in surface properties that differ from the bulk material.[19, 20] If one of the polymers resides preferentially at the surface, the local composition near the surface will have an excess of the low surface energy component.[21] Therefore, by introducing interfaces into a blend system, the phase diagram and stability of the blend can often be altered.[22-26]

A number of researchers have demonstrated that when confining polymeric materials at the nano-scale a number of properties will differ from the bulk.[7, 8, 27, 28] Some such properties include the glass transition temperature (T_g),[10, 11, 28] viscosity (η)[7] and physical aging rate.[8, 9] Of particular interest due to their many technological applications are thin supported films. It has been shown that in the case when there are non-specific interactions between the polymer and the substrate, i.e. polystyrene on silicon oxide, the

T_g has been found to decrease with decreasing film thickness.[10, 11] This has generally been attributed to the additional configurational freedom gained near a free surface leads to a higher chain mobility and hence lower local T_g relative to the bulk material.[29-33] As the film thickness is decreased, the surface layer becomes a larger fraction of the film and dominates the average value. However, when there is a specific interaction, such as hydrogen bonding between the polymer molecule and the substrate, i.e. polymethyl methacrylate on silicon oxide, the average T_g tends to increase with decreasing film thickness.[34]

Recently it was demonstrated that polymers of star-shaped architecture can be used in order to tailor the thickness dependence without changing the chemical structure of the molecule.[18] It was shown that purely through changes in the polymer architecture the T_g vs. h dependence could be varied from decreasing, akin to the linear polymer, to independent and even increase with decreasing thickness. Therefore, it is the main goal of my research is to gain a better understanding of how complex polymer architectures influence the polymer dynamics in both the bulk state and in confined geometries. To this end, the research in this dissertation can be categorized into three different material systems: (1) star-shaped polymers of varying functionality and molecular weight; (2) miscible A/B homopolymer blends; and (3) nanostructure composites in which polymer grafted nanoparticles are incorporated into miscible A/B homopolymer blends. In the first system, the goal is to understand the influence of chain architecture on the glassy segmental dynamics and structural relaxation in the bulk and confined states. The latter two systems are used in order to further understand the influence of interfaces on the miscibility and viscosity in supported polymer films.

1.2 BACKGROUND

1.2.1 Glassy Structural Relaxation

When a polymeric material is cooled at a sufficiently fast rate to avoid crystallization and is cooled below its T_g, the material resides in a non-equilibrium state. In its non-equilibrium state the material possesses an excess of thermodynamic properties such as volume, density, enthalpy, etc. Over time the material will undergo a series of structural relaxations in order to return to its equilibrium state; this process is termed

physical aging.[15] Physical aging thus leads to a time-dependence of many physical properties of the material that will influence their performance, such: as brittleness, enhanced modulus and reduced permeability.

When a material is aged isothermally below its T_g, the ensuing time-dependent recovery of such thermodynamic properties is sigmoidal with respect to the logarithm of aging time, t_{age}.[35] The sigmoidal behavior can be thought of as three different regimes: the initial plateau, power law and equilibrium plateau regimes. It is from the intermediate power law regime in which the physical aging rate is calculated. It is well accepted that there is a non-monotonic temperature dependence of the aging rate, which depends on the aging temperature, T_{age}, relative to its T_g. This difference is termed ΔT_A, and is depicted in Figure 1.1.

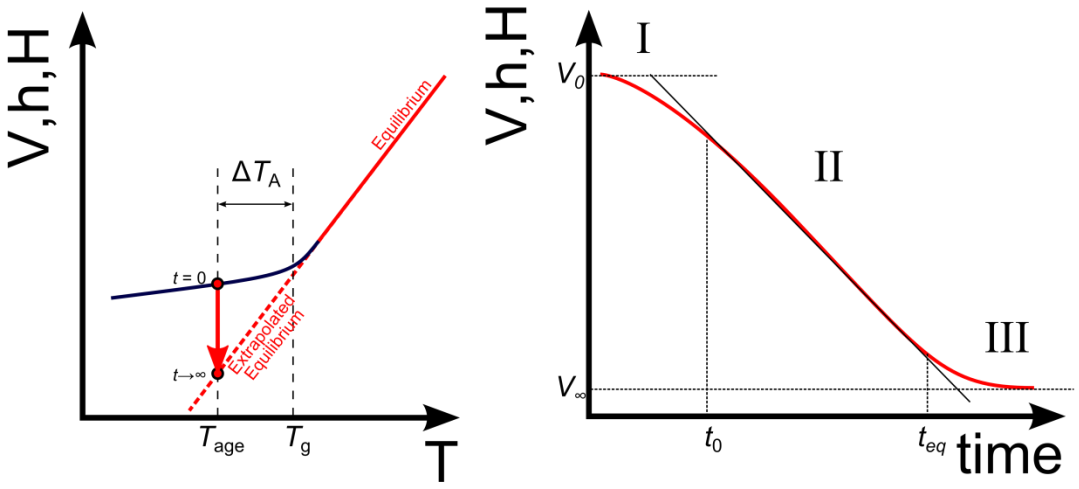

Figure 1.1 A schematic representation of the physical parameters of an amorphous polymer evolving with temperature (left) and time (right).

The physical aging rate can be determined from region II, as shown in Figure 1.1. The evolution of volume with time after a single temperature jump has been well described by Kovacs[14]:

$$\frac{V_0 - V(t_{age})}{V_0} = \beta \left[\log\left(\frac{t_{age}}{t_0} + 1\right) - \log\left(\frac{t_{age}}{t_{eq}} + 1\right)\right] \quad (1.1)$$

where t_0 and t_{eq} are shown as the dashed lines as the transition between region I and II and II and III respectively, v_0 is the extrapolated volume at t=0, and β is the aging rate; all the parameters are shown graphically in Figure 1.1.

However after the aging temperature is reduced to more than 10K below the T_g of the equilibrium time, t_{eq}, approaches years to centuries. Therefore it is not experimentally feasible to measure t_{eq}; $t_{eq} \rightarrow \infty$. Therefore, the volume recovery can be approximated as:

$$\frac{V_0 - V(t_{age})}{V_0} = \beta \log\left(\frac{t_{age}}{t_0} + 1\right)` \quad (1.2)$$

This equation can then be rearranged to solve for the aging rate in terms of the volume:

$$\beta = \frac{1}{V_0} \frac{\partial V}{\log(t_{age} - t_0)} \quad (1.3)$$

To this end, the aging rate of the polymeric material can be expressed in terms of the rate of change of the physical parameter (*V*, *H* or *h*) with respect to the logarithm of the aging time. In the case of supported thin films, this can be done through tracking changes in the film thickness using spectroscopic ellipsometry and in bulk materials in terms of the enthalpy recovered using differential scanning calorimetry.

1.2.2 Star-Shaped Molecules

To date, research in the thin polymer film field has been primarily devoted to materials composed of linear polymer chains, blends of linear chains, and block copolymers. The influence of changing the chain architecture has largely been neglected and unexplored in supported thin films. Many molecules composed of different architectures are available: branched, combs and star-shaped polymers.[36, 37] This study will investigate the influence of chain architecture, specifically branching, on the properties of thin polymer films.

The structure and dynamics of polymeric molecules that possess star-shaped architectures have received considerably more attention in recent years.[37-45] A star-shaped polymer is a polymer molecule that contains a number of linear chains covalently bonded to a core molecule or macromolecule. The core can be a comprised of variety of different species ranging from dendrimeric to highly cross-linked molecules.[36] The primary characteristic that differentiates a star-shaped polymer from other types of highly branched molecules is that star-shaped polymers have a number of linear chains all bonded to a single core molecule and the size of the arms:core ratio is very high (>>1). The size of the arms is generally taken to be the root mean square end-to-end distance. It

has been shown that these molecules possess properties, generally associated with entropic effects that differ from their linear analogs. Specifically, these differences in properties are due to their unique conformations that differ significantly from those of linear polymers.

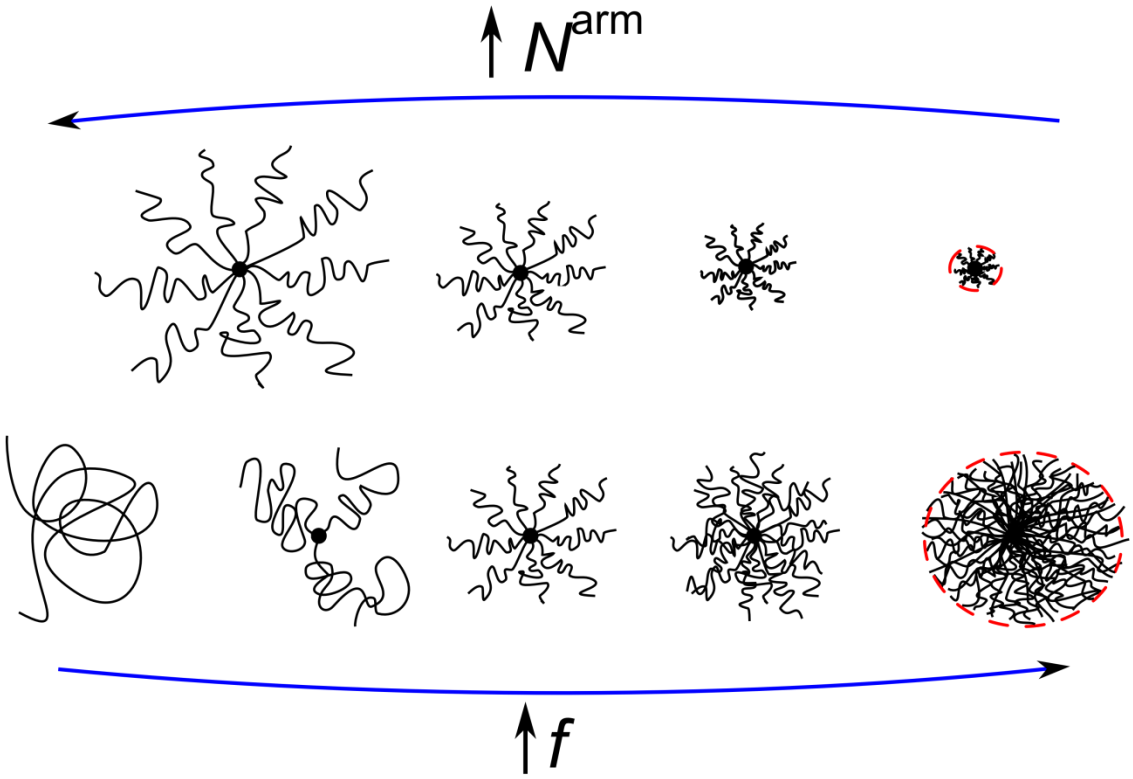

Figure 1.2 A schematic representation of star-shaped molecules, showing the interplay of the functionality and degree of polymerization of the arm.

There are a number of scientific reasons for studying star-shaped polymers.[38, 46] Star-shaped polymers have been shown to exhibit stronger adsorption to substrates than their linear analogs of the same chemical structure and degree of polymerization, which has been shown experimentally, in simulations as well as theory.[42] This is due to the decrease in the loss of entropy from adsorbing the arms of these branched molecules to surfaces. Because the star-shaped molecules do not have to change their configuration as much as a linear polymer chain would upon adsorption. This change in configuration is often associated with a penalty as it is entropically unfavorable. The magnitude of the

loss in entropy is associated with the number of arms, or functionality, *f* and the degree of polymerization of the arm, N_{arm}. The changes in functionality and degree of polymerization are depicted schematically in Figure 1.2. As illustrated in Figure 1.2, for sufficiently high *f* and small *N* the shape of the molecule, and consequently the physical properties, become more soft colloidal-like.

It has been previously demonstrated that the chain architecture can have significant influences on the scaling of viscosity and longest relaxation time. The viscosity, η, of star-shaped molecules is exponentially dependent on the degree of polymerization of an arm N_a, $e^{-\nu N_a / N_e}$, where N_e is the molecular weight between entanglements and $\nu \approx 1$ is a constant.[47, 48] The viscosity is independent of the number of arms, *f*, when *f* is not extremely large. Thus changing the number of arms, for reasonable values of *f*, does not significantly influence the viscosity or relaxation time, τ. This difference in scaling for the viscosity is dictated by the breakdown of the "tube-model" often associated with the diffusion of linear chains. In order for a star-shaped molecule to observe center of mass diffusion, it must retract all but 2 of its arms. This is an entropically unfavorable situation, and the probability of this occurring scales exponentially with the degree of polymerization.

In mixtures with linear chains, star-shaped molecules have been demonstrated to preferentially segregate toward the interfaces.[37, 39, 43-45] This is due to the smaller loss in entropy near an interface. They also tend to possess smaller cohesive energy densities, leading to a lower surface energy than their linear analogs of identical *N*.

The properties of star-shaped molecules show more promise than their linear counterparts in applications such as coatings and biomedical devices, where adhesive properties are especially important.[36, 49] Star-shaped molecules also exhibit properties ideal for battery and sensor applications, as it is possible to take advantage of the multi-arm architecture for attachment of molecules/nanoparticles of varying functionalities.[50] A deeper understanding of the role of chain architecture on the properties of thin films will have a profound impact on various technological applications.

1.2.3 Miscible Polymer Blends

Another means of tailoring the properties of a material, rather than synthesizing a whole new polymer, is to simply blend two different polymers with unique properties. By blending two different polymers, one can achieve a unique blend of the properties of the individual components. However, it is not always energetically favorable for two polymers to be homogeneously mixed together. The blending of polymers has been a long standing problem that has been well described by the free energy of mixing which depends largely on the degree of polymerization of the two components as well the Flory-Huggins interaction parameter, X_{AB}.

In the case of these A/B polymer/polymer blends in thin films, the free surface composition is dominated by the polymer with a lower surface tension.[19, 20] The surface of these polymer blends provides a means to alter the phase diagram as has been seen with surface directed spinodal decomposition.[22-26] However to date, there are a number of open questions as to how blend dynamics will differ near an interface relative to the bulk.

The idea of understanding how the polymer chain dynamics near a free surface will differ from that of the bulk has been of particular importance of late. As described in section 1.1, the local mobility near a free surface is significantly enhanced from that of the bulk. This is often associated with the increased configurational freedom and the reduction in entanglement density. The viscosity of a melt is governed by reptation theory in which an entangled polymer chain reptates through the confines of a tube formed by entanglements of its nearest neighbors.[51-53] As a polymer chain reptates through the tube, the longest reptation time, τ_{rep},, is dictated by the molecular friction, ζ, it observes. Therefore near an interface where there is enhanced configurational freedom, and the amount of entanglements is reduced, the local friction the chain experiences will be reduced reducing the relaxation time and local viscosity. While this has been demonstrated to be the case for homopolymer systems, the case of miscible A/B polymer blends, the influence of an interface on the polymer dynamics is relatively unknown.

1.2.4 Experimental Techniques

A number of experimental techniques were used in order to investigate the dynamics of polymers with complex architectures and structures. Variable angle

spectroscopic ellipsometry (VASE) and differential scanning calorimetry (DSC) were used in order to measure the physical aging in terms of the volumetric and enthalpic recovery respectively. As using VASE and DSC for determining the physical aging of a material are not traditional methods, the basic procedures will be outline in the following sections.

The glassy and rubbery dynamics of bulk polymeric materials was investigated using incoherent elastic neutron scattering, using the high flux backscatter spectrometer at the national institute of standards and technology (NIST) center for neutron research; using beam line NG2. The viscosity of polymer blends and blend nanocomposite structures were investigated using x-ray photon correlation spectroscopy. The x-ray photon correlation spectroscopy experiments were conducted at the advanced photon source at Argonne National Laboratory; using beam line 8-ID-I.

1.2.4.1 Variable Angle Spectroscopic Ellipsometry

Variable angle spectroscopic ellipsometry (VASE) is a non-destructive optical technique often used in coatings and semiconductor industries in order to obtain the optical properties and film thickness of a thin supported film. VASE is an extremely versatile technique that has been employed throughout the literature as it is very sensitive to subtle changes in surface roughness, density and film thickness. VASE has also been demonstrated to be able to measure the influence of various environments such as changes in temperature, vacuum, liquids and supercritical fluids.

The principles of VASE have been discussed in detail elsewhere,[54] but will be briefly outlined here for the purposes of clarity in this document. Ellipsometry takes advantage of polarized light and how the polarization state changes after it is reflected from the surface of a material. When linearly polarized light is reflected from a surface it becomes elliptically polarized with a shift in the phase, δ, and amplitude, A. VASE measures this shift in polarization in terms of Ψ and Δ, known as the elliposmetric angles. Ψ and Δ are often expressed in terms of the changes in polarization using the Fresnel reflection coefficients, R_s and R_p, for the ratio of the reflected, r, and incident, i, electric field vectors in the s and p polarization directions respectively. The relations connection these parameters can be seen in the equation below:

$$\frac{R_p}{R_s} = \frac{A_{rp}/A_{ip}}{A_{rs}/A_{is}} = \left|\frac{R_p}{R_s}\right| \exp\left[i\left(\delta_p - \delta_s\right)\right] = \tan(\Psi)\exp(i\Delta) \quad (1.4)$$

Therefore one can deduce that Δ is simply the difference in phase shift of the *s* and *p* polarization directions and $tan(\Psi)$ is the ratio of the amplitude changes. Additionally the Fresnel coefficients can be related to the complex refractive index of the media and the angle of incidence according to the equations below:

$$R_s = \frac{n_0 \cos\varphi_0 - n_1 \cos\varphi_1}{n_0 \cos\varphi_0 + n_1 \cos\varphi_1} \quad (1.5)$$

$$R_s = \frac{n_1 \cos\varphi_0 - n_0 \cos\varphi_1}{n_1 \cos\varphi_0 + n_0 \cos\varphi_1} \quad (1.6)$$

As discussed in section 1.1, the main interest of this manuscript is the case of thin supported films in which there is more than one interface that reflects the incident light. In this case the situation becomes more complex and the Fresnel coefficients can be rewritten as follows:

$$R_{p(s)} = \frac{R_{01}^{p(s)} + R_{12}^{p(s)} \exp(-i2\beta)}{1 + R_{01}^{p(s)} R_{12}^{p(s)} \exp(-i2\beta)} \quad (1.7)$$

where the subscripts 01 and 12 represent the interfaces between materials 0 and 1 and 1 and 2. The term β, the phase thickness, is related to the film thickness through the refractive index and the wavelength of light through the following relation:

$$\beta = \frac{2\pi h}{\lambda} n_1 \cos\varphi_1 \quad (1.8)$$

where *h* is the film thickness. Therefore, when looking at a thin supported film in isothermal conditions, the ellipsometric parameters measured by ellipsometry are directly related to *h* and *n*. The parameters involved are shown schematically in Figure 1.2. Because of this, VASE is ideally suited to measure the process of structural relaxation of thin films outlined in Section 1.2.1, as one of the consequences of structural relaxations is a change in density, which due to conservation of mass and the lateral constraints imposed by the substrate, results in a change in film thickness.

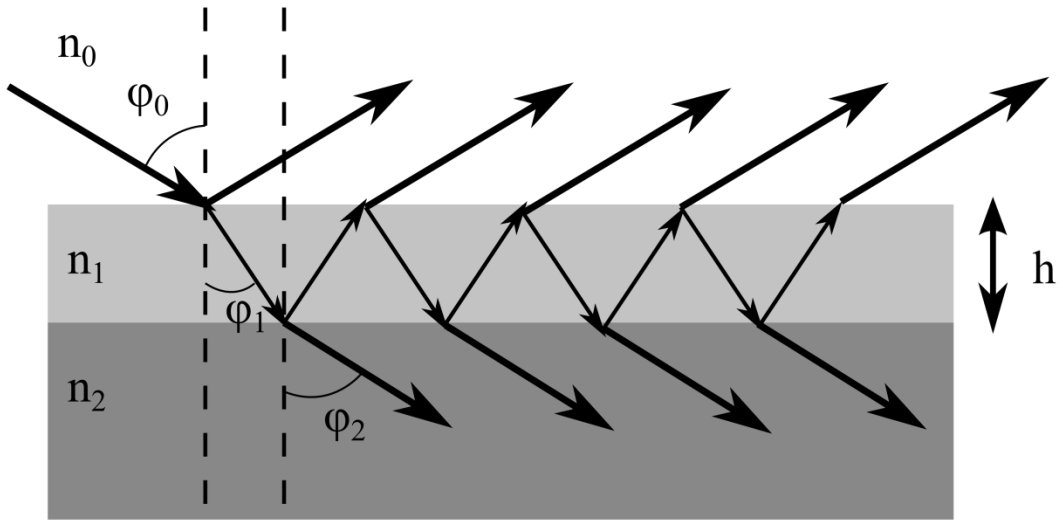

Figure 1.3 A schematic representation of the reflection and refraction of the incident light upon a multilayered planar surface.

1.2.4.2 Differential Scanning Calorimetry

Differential scanning calorimetry (DSC) is a conventional method that has been used for many years in order to measure the glass transition temperature of polymers. But in this manuscript, since DSC will be used in order to measure the enthalpy relaxation of polymeric materials, the differences in the procedure for determining the enthalpy recovery will be noted, and are also well described in the following references.[12, 13, 55-60]

As DSC traces measure the change in heat capacity at constant pressure (C_p) as a function of temperature, and the heat capacity is defined as:

$$\left(\frac{\partial H}{\partial T}\right)_P = \left(\frac{\partial Q}{\partial T}\right)_P = C_P \qquad (1.9)$$

where H is the enthalpy. Therefore the H in a given scan can be estimated by integrating C_p with respect to T. After isothermally aging a sample for a given amount of time, temperature profile shown in Figure 1.1, the amount of enthalpy recovered with change. This can be determined by the difference in enthalpy between an aged scan and an unaged scan as governed by:

$$\Delta H = \frac{1}{m}\int_{T_a}^{T_b}\left(\dot{Q}_{aged} - \dot{Q}_{unaged}\right)dT \qquad (1.10)$$

where m is the heating rate, and $\dot{Q}_{aged}$ and $\dot{Q}_{unaged}$ are the heat flows of the aged and unaged scans. This is shown graphically in Figure 1.4. The enthalpy recovered, ΔH, can then be monitored as a function of time, and from this one can estimate the aging rate of a polymer at a given temperature.

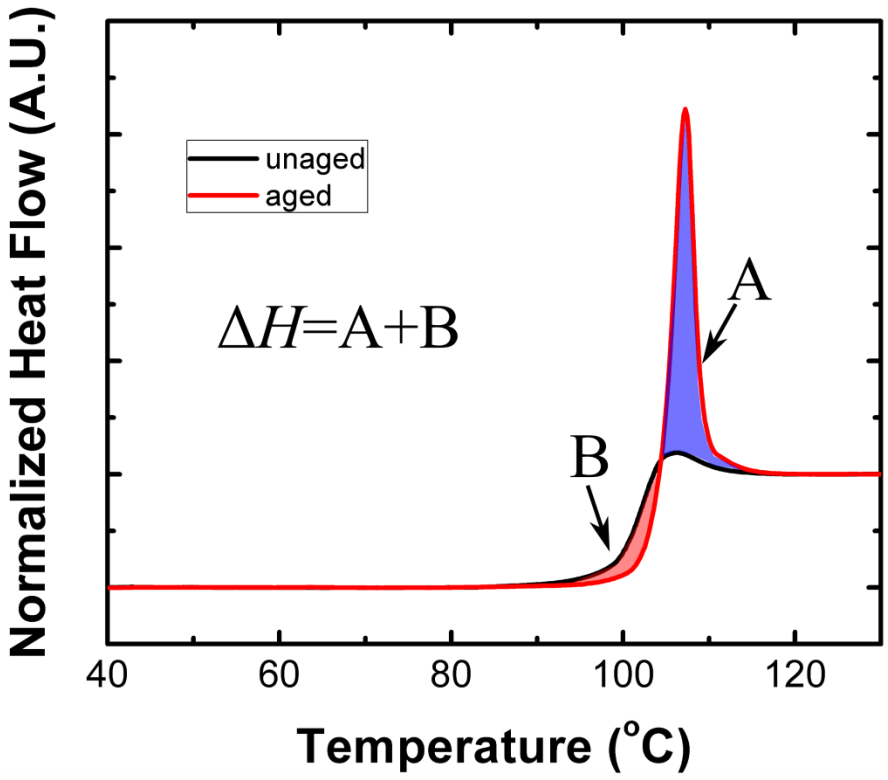

Figure 1.4 A schematic representation of the normalized heat flow traces extracted from a DSC experiment. The shaded areas represent the enthalpy recovered during aging described by equation 1.10.

Generally, in order to appropriately compare the aging behavior at various temperatures, the ΔH is generally given in reference to the value for ΔH_∞.

$$\Delta H_\infty = -\int_{T_g}^{T_{age}} \Delta C_P dT \qquad (1.11)$$

where $\Delta C_p = C_{pl} - C_{pg}$, the difference between the liquid and glassy heat capacities respectively. As the C_p values often have a linear slope with respect to temperature this equation is simple to solve for polystyrene, as seen in Figure 1.3.

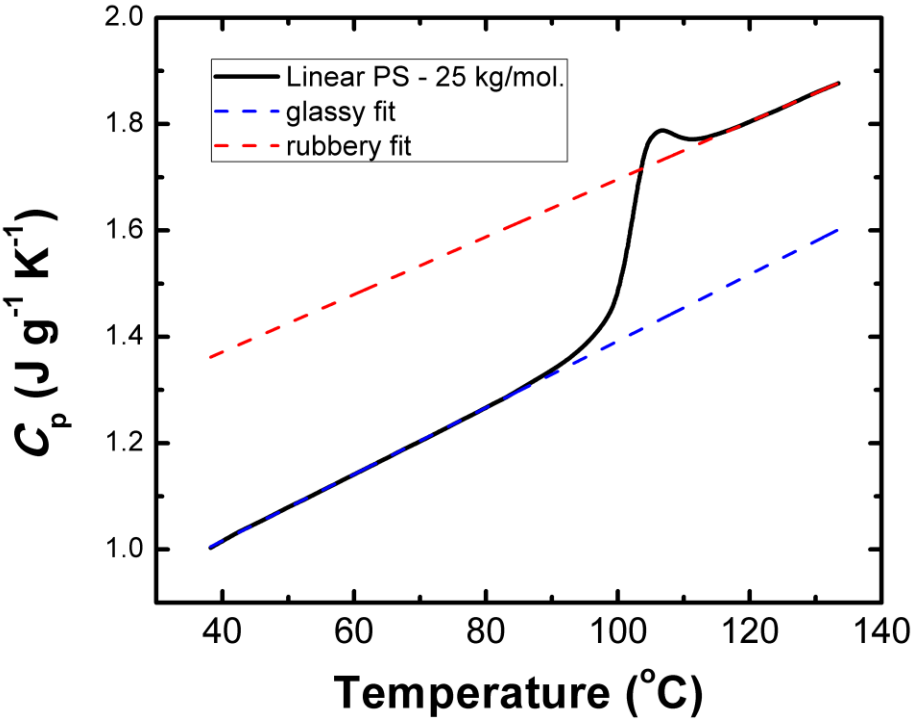

Figure 1.5 A representative heat capacity trace obtained from modulated DSC, in order to obtain the absolute heat capacity necessary to estimate the equilibrium value for the enthalpy recovery experiments.

1.2.4.3 Incoherent Neutron Scattering

Neutron scattering is a useful set of techniques that have widely been used in polymer physics due to the time-scales and length-scales achievable amount to uncovering information about the structure and dynamics of polymer chains in various environments. The use of incoherent neutron scattering to measure the glassy dynamics of amorphous polymers is well outlined in the literature.[61-64] The scattering of neutrons can be well described by the double-differential scattering cross section, which is the probability that a neutron will be scattered:

$$\frac{\partial^2\sigma}{\partial\Omega\,\partial \mathrm{E}} = \frac{k_f}{4\pi\hbar k_i} N[\sigma_{inc} S_{inc}(Q,\omega) + \sigma_{coh} S_{con}(Q,\omega)] \qquad (1.12)$$

where σ is the scattering cross section, dΩ is an angle element, k is the wave vector, N is the number of neutrons, $\hbar$ is Plank's constant, E is the energy, and the subscripts i and f are the initial and scattered neutron values. The subscripts *coh* and *inc* stand for the coherent and incoherent components to the signal. The coherent and incoherent cross sections of some of the elements contained within polystyrene are shown in Table 1.1. As one can see in the table, the incoherent neutron scattering signal for hydrogen is an order of magnitude larger than any other element. Therefore, when conducting experiments using incoherent neutron beams the signal will be dominated by the oscillatory motions of the hydrogen atoms.

Table 1.1 Incoherent and coherent cross section for neutron scattering for the elements found in linear and star-shaped polystyrene.

Element	**σ_{inc} (barns)**	**σ_{coh} (barns)**
Hydrogen	82	2
Deuterium	2	5
Carbon	0	5
Oxygen	0	4

Incoherent neutron scattering is a technique that has widely been used in the recent literature as a means to measure the amplitude of the local atomic motions in polymers in both bulk materials as well as in confinement. The use of incoherent neutron scattering yields information on length scales on the order of angstroms and time scales on the order of pico- to nano- seconds; therefore, neutron scattering is an ideal technique in order to measure the dynamics in the glassy state as well as in the melt for polymeric materials. The incoherent neutron scattering spectrum can be described by the one-phonon approximation:

$$S_{inc}(Q,\omega) = \frac{3N\hbar}{2M}\, e^{-2W}\, Q^2\, \frac{n(\omega)+1}{\omega}\, g(\omega) \qquad (1.13)$$

where Q and ω are the momentum transfer vector of the neutron, N is the number of neutrons scattered, $\hbar$ is plank's constant, M is the molar mass, $n(\omega)+1$ is the Bose population factor, $g(\omega)$ is the density of states and W is the Debye-Waller factor. Therefore, $S_{inc}(Q,\omega)$ contains information about both the structure and dynamics of the

material. However, in order to obtain comparable information within the glassy state larger than the noise of the equipment only the elastically scattered neutrons yield information about the sample, $S_{inc}(Q,\omega = 0) \approx I_{elastic}$. In the limit of elastically scattered neutrons, $S_{inc}(Q,\omega = 0)$ is reduced to the Debye-Waller factor:

$$\frac{S_{inc}(Q,0)_T}{S_{inc}(Q,0)_{T=0}} = \frac{I_{elastic}(Q,T)}{I_{elastic}(Q,T=0)} \approx \exp\left[-\frac{1}{3} Q^2\langle\mu^2\rangle\right] \qquad (1.14)$$

In this case, due to the conservation of scattered neutrons, a decrease in the elastic scattering intensity is a result of an increase in inelastically scattered neutrons, which yields information about the dynamics. Inherent within the Debye-Waller approximation, the atomic motions are assumed to be harmonic, which is a crude approximation for polymeric materials in which the motions are predominantly anharmonic. However, it has been well reported that although the absolute values for the $\langle\mu^2\rangle$ are overestimated, the Debye-Waller approximation has been useful in characterizing the dynamics of polymers as well as biological molecules.

1.2.4.4 X-ray Photon Correlation Spectroscopy

A number of different experimental techniques have been employed in order to determine the melt dynamics, i.e. viscosity, of thin polymer films. One technique that is emerging in order to measure the viscosity through the damping of thermally induced surface capillary waves is x-ray photon correlation spectroscopy (XPCS).[65, 66] XPCS, is surface sensitive grazing incidence x-ray scattering technique that makes use of the off-specular diffuse scattering of x-rays. By limiting the incident angle of the x-ray beam, the penetration depth of the x-rays can be limited to less than 9 nm. The benefit of using XPCS, is that the beam is collimated through an aperture to limit the size of the beam to be comparable to the coherence length of the incident x-ray beam. This gives rise to a partially coherent x-ray beam. When a partially coherent x-ray beam is reflected from the surface of a disordered material, the temporal evolution of the resultant "speckled" scattering signal gives information about the dynamics of the thermal fluctuations. An example of the "speckled" scattering from a polymer surface is given in Figure 1.6.

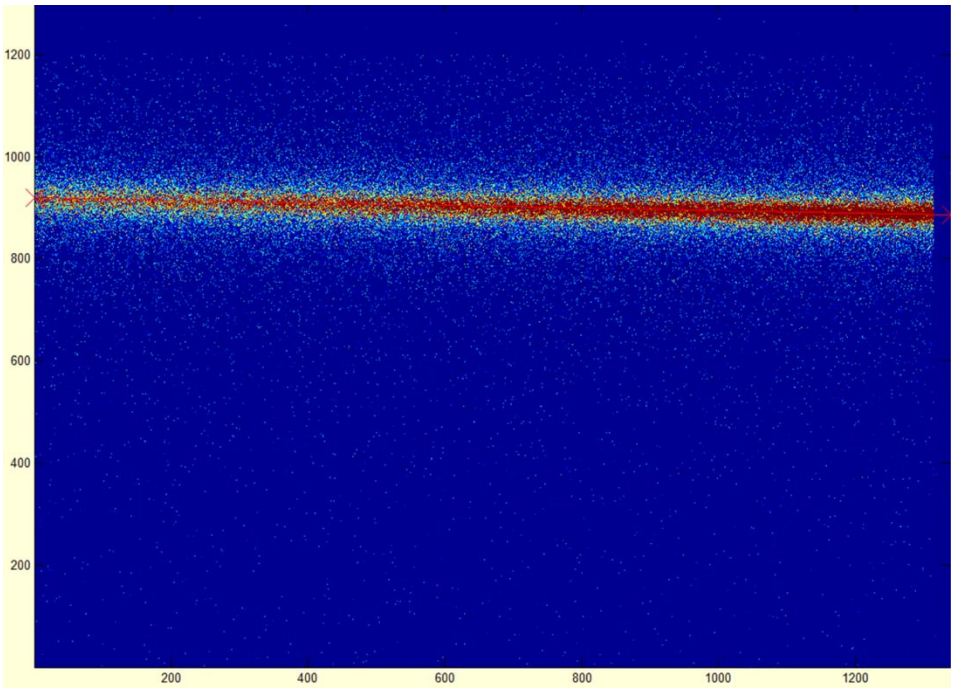

Figure 1.6 An example of a speckle pattern captured from a full frame CCD camera after reflection of the X-ray beam from the polymer film surface.

By monitoring the temporal evolution of the speckle scattering intensity, a time-scale dictated by the surface fluctuations can be determined using an intensity-intensity autocorrelation function:

$$g_2(Q,t) = \frac{\langle I(Q,t)I(Q,t+\Delta t)\rangle}{\langle I(Q,t)\rangle^2} \qquad (1.15)$$

where I is the intensity at a given, Q and time t, and Δt is the time delay between frames being compared. A typical autocorrelation function is shown in Figure 1.7, which follows a simple exponential decay.

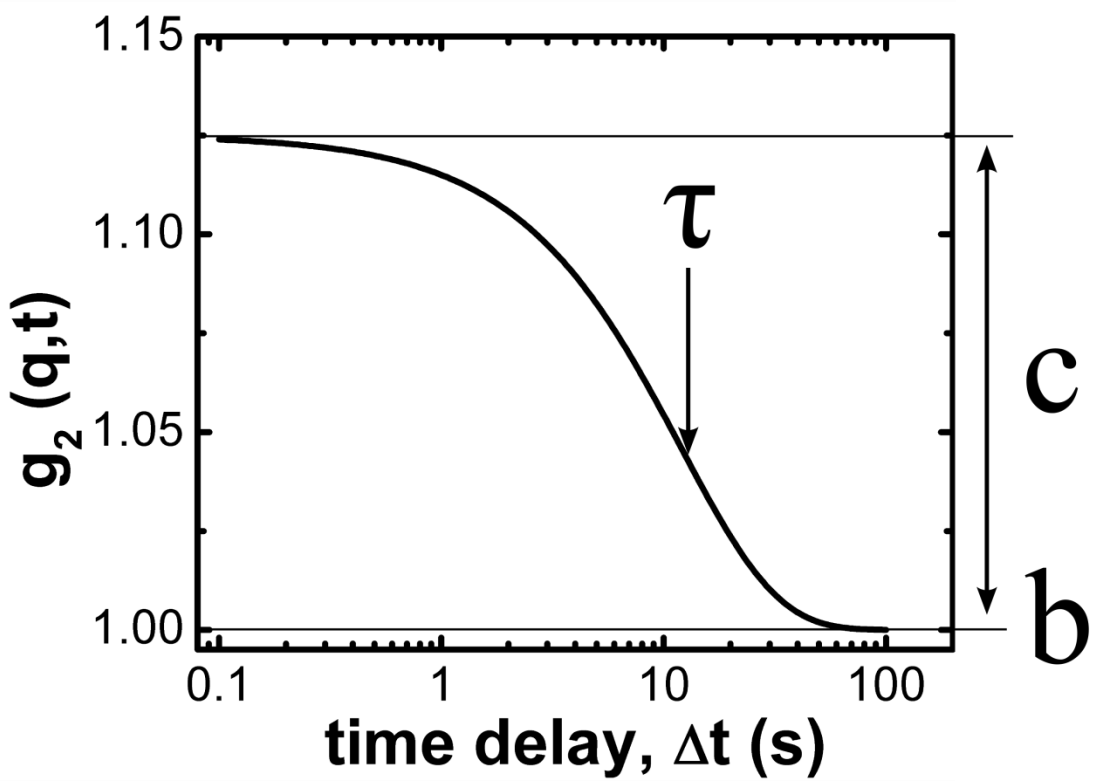

Figure 1.7 A schematic of the intensity-intensity autocorrelation function from XPCS, schematically showing the fitting parameters used to fit a simple exponential decay.

The decay rate can be characterized by a time scale, τ, which depends on the scattering vector, Q. According to hydrodynamic theory,[67] the characteristic relaxation time is a function of the viscosity of the film, η, the film thickness, h, and surface tension, γ:

$$\tau = \frac{2\,\eta\,(cosh^2(Q\,d) + Q^2 d^2)}{\gamma Q(\sinh(Qd)\cosh(Qd) - Qd)} \qquad (1.16)$$

This equation has been successfully applied to hompolymer films, from which the viscosity was extracted.[66] A schematic of the experimental setup is shown in Figure 1.8.

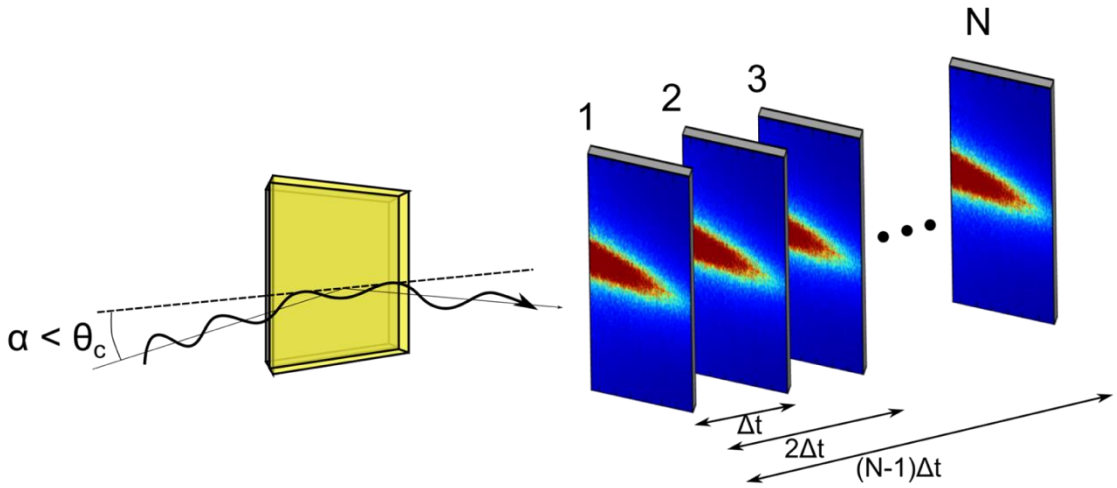

Figure 1.8 Schematic representation of the XPCS experiment, in which an autocorrelation function is generated in order to find the correlation between the speckle patterns obtained at different times.

1.3 REFERENCES

1. McCaig, M. S.; Paul, D. R. *Polymer* **2000,** 41, (2), 629-637.
2. McCaig, M. S.; Paul, D. R.; Barlow, J. W. *Polymer* **2000,** 41, (2), 639-648.
3. Rowe, B. W.; Freeman, B. D.; Paul, D. R. *Polymer* **2009,** 50, (23), 5565-5575.
4. Rowe, B. W.; Pas, S. J.; Hill, A. J.; Suzuki, R.; Freeman, B. D.; Paul, D. R. *Polymer* **2009,** 50, (25), 6149-6156.
5. Baldo, M. A.; Thompson, M. E.; Forrest, S. R. *Nature* **2000,** 403, (6771), 750-753.
6. Tang, C. W.; Vanslyke, S. A. *Applied Physics Letters* **1987,** 51, (12), 913-915.
7. Masson, J. L.; Green, P. F. *Physical Review E* **2002,** 65, (3).
8. Priestley, R. D. *Soft Matter* **2009,** 5, (5), 919-926.
9. Priestley, R. D.; Ellison, C. J.; Broadbelt, L. J.; Torkelson, J. M. *Science* **2005,** 309, (5733), 456-459.
10. Keddie, J. L.; Jones, R. A. L.; Cory, R. A. *Faraday Discussions* **1994,** 98, 219-230.
11. Keddie, J. L.; Jones, R. A. L.; Cory, R. A. *Europhysics Letters* **1994,** 27, (1), 59-64.
12. Tool, A. Q. *Journal of the American Ceramic Society* **1946,** 29, (9), 240-253.
13. Narayana.Os. *Journal of the American Ceramic Society* **1971,** 54, (10), 491-&.
14. Kovacs, A. J. *Annals of the New York Academy of Sciences* **1981,** 371, (OCT), 38-66.
15. Struik, L. C. E., *Physical Aging in Amorphous polymers*. Elsevier Scientific Publishing Company: Amsterdam, 1978.
16. Hodge, I. M. *Science* **1995,** 267, (5206), 1945-1947.
17. Glynos, E.; Frieberg, B.; Green, P. F. *Physical Review Letters* **2011,** 107, (11), 118303.
18. Glynos, E.; Frieberg, B.; Oh, H.; Liu, M.; Gidley, D. W.; Green, P. F. *Physical Review Letters* **2011,** 106, (12), 128301.
19. Nakanishi, H.; Pincus, P. *Journal of Chemical Physics* **1983,** 79, (2), 997-1003.
20. Schmidt, I.; Binder, K. *Journal De Physique* **1985,** 46, (10), 1631-1644.
21. Jones, R. A. L.; Kramer, E. J. *Polymer* **1993,** 34, (1), 115-118.
22. Bank, M.; Thies, C.; Leffingw.J. *Journal of Polymer Science Part a-2-Polymer Physics* **1972,** 10, (6), 1097-&.
23. Coleman, M. M.; Graf, J. F.; Painter, P. C., *Specific interactions and the Miscibility of Polymer Blends*. Technomic Publishing: Lancaster, PA, 1991.
24. Coleman, M. M.; Painter, P. C. *Progress in Polymer Science* **1995,** 20, (1), 1-59.
25. Dudowicz, J.; Freed, K. F. *Macromolecules* **1991,** 24, (18), 5076-5095.
26. Dudowicz, J.; Freed, K. F. *Macromolecules* **1991,** 24, (18), 5112-5123.
27. Keddie, J. L.; Jones, R. A. L.; Cory, R. A. *Faraday Discussions* **1994,** 98, (Polymers at Surfaces and Interfaces), 219-30.
28. Forrest, J. A.; DalnokiVeress, K.; Dutcher, J. R. *Physical Review E* **1997,** 56, (5), 5705-5716.
29. Baschnagel, J.; Varnik, F. *Journal of Physics-Condensed Matter* **2005,** 17, (32), R851-R953.

30. Lipson, J. E. G.; Milner, S. T. *European Physical Journal B* **2009,** 72, (1), 133-137.
31. Long, D.; Lequeux, F. *European Physical Journal E* **2001,** 4, (3), 371-387.
32. Mittal, J.; Shah, P.; Truskett, T. M. *Journal of Physical Chemistry B* **2004,** 108, (51), 19769-19779.
33. Truskett, T. M.; Ganesan, V. *Journal of Chemical Physics* **2003,** 119, (4), 1897-1900.
34. Kim, J. H.; Jang, J.; Zin, W. C. *Langmuir* **2001,** 17, (9), 2703-2710.
35. Hutchinson, J. M. *Progress in Polymer Science* **1995,** 20, (4), 703-760.
36. Lapienis, G. *Progress in Polymer Science* **2009,** 34, (9), 852-892.
37. Qian, Z. Y.; Minnikanti, V. S.; Archer, L. A. *Journal of Polymer Science Part B-Polymer Physics* **2008,** 46, (17), 1788-1801.
38. Freire, J. J., Conformational properties of branched polymers: Theory and simulations. In *Branched Polymers Ii*, Springer-Verlag Berlin: Berlin, 1999; Vol. 143, pp 35-112.
39. Foster, M. D.; Greenberg, C. C.; Teale, D. M.; Turner, C. M.; Corona-Galvan, S.; Cloutet, E.; Butler, P. D.; Hammouda, B.; Quirk, R. P. *Macromolecular Symposia* **2000,** 149, 263-268.
40. Greenberg, C. C.; Foster, M. D.; Turner, C. M.; Corona-Galvan, S.; Cloutet, E.; Quirk, R. P.; Butler, P. D.; Hawker, C. *Journal of Polymer Science Part B-Polymer Physics* **2001,** 39, (21), 2549-2561.
41. Minnikanti, V. S.; Archer, L. A. *Macromolecules* **2006,** 39, (22), 7718-7728.
42. Striolo, A.; Prausnitz, J. M. *Journal of Chemical Physics* **2001,** 114, (19), 8565-8572.
43. Yethiraj, A. *Physical Review Letters* **1995,** 74, (11), 2018-2021.
44. Yethiraj, A. *Computational and Theoretical Polymer Science* **2000,** 10, (1-2), 115-123.
45. Qian, Z. Y.; Minnikanti, V. S.; Sauer, B. B.; Dee, G. T.; Archer, L. A. *Macromolecules* **2008,** 41, (13), 5007-5013.
46. Likos, C. N. *Physics Reports-Review Section of Physics Letters* **2001,** 348, (4-5), 267-439.
47. McLeish, T. C. B.; Milner, S. T., Entangled dynamics and melt flow of branched polymers. In *Branched Polymers Ii*, Springer-Verlag Berlin: Berlin, 1999; Vol. 143, pp 195-256.
48. Vlassopoulos, D.; Fytas, G.; Pakula, T.; Roovers, J. *Journal of Physics-Condensed Matter* **2001,** 13, (41), R855-R876.
49. Gasteier, P.; Reska, A.; Schulte, P.; Salber, J.; Offenhausser, A.; Moeller, M.; Groll, J. *Macromolecular Bioscience* **2007,** 7, (8), 1010-1023.
50. Yang, X. H.; Sun, X. Y.; Shao, J. J.; Liu, Y. H.; Wang, X. L. *Journal of Polymer Science Part B-Polymer Physics* **2004,** 42, (22), 4195-4198.
51. Doi, M.; Edwards, S. F., *The Theory of Polymer Dynamics*. Oxford University Press: New York, 1988.
52. Lodge, T. P.; McLeish, T. C. B. *Macromolecules* **2000,** 33, (14), 5278-5284.
53. Lorthioir, C.; Alegria, A.; Colmenero, J. *Physical Review E* **2003,** 68, (3).
54. Tompkins, H. G.; McgGahan, W. A., *Spectroscopic ellipsometry and reflectometry: A user's guide*. Wiley: New York, 1999; Vol. xiv.

55. Moynihan, C. T.; Macedo, P. B.; Montrose, C. J.; Gupta, P. K.; Debolt, M. A.; Dill, J. F.; Dom, B. E.; Drake, P. W.; Easteal, A. J.; Elterman, P. B.; Moeller, R. P.; Sasabe, H.; Wilder, J. A. *Annals of the New York Academy of Sciences* **1976,** 279, (OCT15), 15-35.
56. Kovacs, A. J.; Aklonis, J. J.; Hutchinson, J. M.; Ramos, A. R. *Journal of Polymer Science Part B-Polymer Physics* **1979,** 17, (7), 1097-1162.
57. Koh, Y. P.; Simon, S. L. *Macromolecules* **2013,** 46, (14), 5815-5821.
58. Simon, S. L.; Sobieski, J. W.; Plazek, D. J. *Polymer* **2001,** 42, (6), 2555-2567.
59. Cangialosi, D.; Boucher, V. M.; Alegria, A.; Colmenero, J. *Physical Review Letters* **2013,** 111, (9).
60. Cangialosi, D.; Boucher, V. M.; Alegria, A.; Colmenero, J. *Soft Matter* **2013,** 9, (36), 8619-8630.
61. Kanaya, T.; Kaji, K. *Polymer Physics and Engineering* **2001,** 154, 87-141.
62. Kanaya, T.; Tsukushi, I.; Kaji, K. *Progress of Theoretical Physics Supplement* **1997**, (126), 133-140.
63. Soles, C.; Douglas, J.; Wu, W. l.; Dimeo, R. *Physical Review Letters* **2002,** 88, (3).
64. Soles, C. L.; Douglas, J. F.; Wu, W.-L. *Journal of Polymer Science Part B: Polymer Physics* **2004,** 42, (17), 3218-3234.
65. Leheny, R. L. *Current Opinion in Colloid & Interface Science* **2012,** 17, (1), 3-12.
66. Kim, H.; Ruhm, A.; Lurio, L. B.; Basu, J. K.; Lal, J.; Lumma, D.; Mochrie, S. G. J.; Sinha, S. K. *Physical Review Letters* **2003,** 90, (6).
67. Jackle, J. *Journal of Physics-Condensed Matter* **1998,** 10, (32), 7121-7131.

CHAPTER 2
THE PHYSICAL AGING OF STAR-SHAPED MACROMOLECULES

Reprinted with permission from:

Frieberg, B.; Glynos, E.; Sakellariou, G.; Green, P.F.; *ACS Macro. Lett.* **2012**, 1, 636-640.

2.1 INTRODUCTION

Structural relaxations, physical aging, below the glass transition temperature, T_g, are known to be responsible for time-dependent changes of physical properties, including the specific volume, thermal conductivity, gas permeability and optical properties, in materials.[1-5] Physical aging ensues after a liquid is rapidly cooled to a temperature, T_{age}, below its T_g. While below T_g, the material resides in a non-ergodic state and possesses excess configurational entropy, excess free volume; while in the non-equilibrium state, the material attempts to reach equilibrium via a structural relaxation mechanism.[1-5]

The driving force for aging is determined by $T_{age} - T_g = \Delta T_{age}$ and the rate at which a thermodynamic property, such as the specific volume or enthalpy, would approach equilibrium is known to exhibit a sigmoidal dependence on aging time, t_{age}.[5] Specifically an initial, nearly time-independent plateau regime, is followed by an intermediate regime where a thermodynamic parameter decreases with time, in a manner proportional to $\log(t_{age})$.[5-7] The third and final regime, terminal response, follows. The physical aging is believed to be accommodated by local chain segmental relaxations, also referred to as structural relaxation.[8] The aging rate is known to depend on the structure of the polymer chain, including the stiffness of the backbone, the side-groups and the cohesive energy densities.[9-12] Phenomenological theories based on time-dependent changes in free

volume,[13] or configurational entropy,[2] or molecular theories that describe changes in the magnitude of density fluctuations,[7, 14] have successfully described this phenomenon.

With regard to a possible mechanism responsible for aging, one might consider that after a sample is rapidly quenched below its T_g, there exists a distribution of free volume, regions of high and low fractional free volume, throughout the sample.[3, 11] During the aging process, at T_{age}, it is believed that free volume migrates via a vacancy diffusion mechanism.[13, 15-18] Different mechanisms associated with the internal annihilation of vacancies, [2, 7, 13, 19, 20] and the escape of free volume from the external interfaces,[9, 21] have been proposed. The latter mechanism, may be important for films in the micron-thickness, which are shown to age faster than their bulk analogs.[3, 10, 13, 18, 22] Models that account for a contraction of the "lattice," have also been proposed to describe time dependent changes in free volume associated with aging in the bulk.[23, 24] To date there still exists disagreement regarding the precise mechanisms that account aging in bulk polymers.

While phenomenon in bulk polymer systems has received signifcant attention in recent decades, considerably less is understood about thin films.[4, 9-11, 25, 26] The aging of ultra-thin films, with thicknesses ~100 nm and thinner, is shown to be slow compared to the bulk.[14, 18-20] The slow aging may be reconciled by accounting for a driving force determined by differences between T_{age} and the local values of T_g within the film, near the interfaces and the interior. In polymer nanocomposites, due largely to specific polymer-particle interfacial interactions, the aging rates are appreciably different from the neat homopolymers.[6, 27-30]

In this paper we show that the aging rates of star-shaped macromolecules, with functionalites, f, where $3< f \sim 16$, can be appreciably slower than their linear analogs. Tha aging of films in the thickness range 0.4 microns$< H <$ 2 microns were studied using variable angle spectroscopic ellipsometry. The aging rates decreased with decreasing M_n^{arm} and increasing f, for $f >3$. Because in this system the chemical structure of the molecules of interest is unchanged, only the topology is altered, it provides an ideal system to provide further understanding to the phenomenon of physical aging of polymeric materials.

2.2 EXPERIMENTAL SECTION

A series of star-shaped molecules, with the number of arms ranging from 3 to 16 were examined in this study. Linear PS, 4 and 8 arm star PS were purchased from Polymer Source Inc., whereas the 16 arm stars were synthesized by means of anionic polymerization using high vacuum techniques.[31, 32, 33] The materials used in this study are described in Appendix A.

One micron thick films of these polymers were prepared from filtered toluene solutions that were spin coated onto silicon wafers (Wafer World Inc.), possessing native oxide layers of 1.5 nm. The samples were subsequently annealed in vacuum for at least 24 hours at ~30°C above the T_g of bulk linear PS (LPS) to remove residual solvent. Spectroscopic ellipsometry was then used to measure the time dependent thickness changes exhibited by the samples after quenching below T_g to an aging temperature, T_{age}.

The glass transition temperatures of the films were first determined by monitoring the thickness of each film as it was cooled from a temperature, T, of approximately 150°C, at 1°C/min, using a variable angle spectrometric ellipsometer (M-2000, J.A. Woollam Co.) equipped with an Instec heating stage. The measurements performed at a fixed angle of 70°. The thickness, $H(T)$, and refractive index, $n(T)$, were determined by fitting the acquired ellipsometric angles Δ and Ψ to a Cauchy/SiO_x/Si model over the entire measured spectral range (wavelength range 400 - 1700 nm). During the experiments, the heating stage was purged using purified nitrogen gas, in order to maintain an inert atmosphere and prevent oxidation, as well as a liquid nitrogen pump to maintain the temperature and cooling rates. The T_g's were identified as the intersection of extrapolated linear fits through the glassy and rubbery regions of the data, H vs. T.[34]

After these measurements were completed, each film was heated to a temperature of ~40°C above the T_g where it was annealed for 30 min.; this removed the thermal history.[21] All samples were subsequently quenched to room temperature at a rate of ~85°C/min.; this quenching rate was consistent and reproducible. It is also noteworthy that due to the constant quenching rate (and depth) and the thermal expansion coefficient is approximately the same for all the materials, the internal stresses due to the thermal quench should be consistent in all samples.[35] The temperature was then rapidly increased to the desired aging temperature, T_{age}, where the sample thickness was measured. Each

data point was determined by averaging throughout an acquisition duration of 30 seconds; measurements were performed every 60 seconds. Each aging rate reported is an average of 3-5 aging tests of a particular sample; our results are entirely reproducible. Further details of the aging experiment and its reproducibility are discussed in Appendix B.

2.3 RESULTS AND DISCUSSION

The aging rate, β, of a bulk polymer may be determined by measuring of the time-dependence of the specific volume, $V(t_{age})$, by using the relation:

$$\beta = -1/V_\infty dV/d(\log t_{age}) \quad (2.1)$$

where V_∞ is the specific volume at equilibrium, and t_{age} is the aging time.[4] Generally, the time-dependence of $V(t)$ is sigmoidal on a semi-log scale: an initial plateau region, which may range from seconds to minutes depending on T_{age}, or more appropriately dependent on $\Delta T_{age} = T_{age} - T_g$, followed by a region where $V(t) \propto \log(t_{age})$.[6, 11] The time scale associated with this second regime may vary from hours to years, depending on the system and on the magnitude of ΔT_{age}. The final equilibrium region subsequently follows this so-called power-law regime.[5, 6, 9, 26] Other appropriate strategies for measuring aging in polymers includes time-dependent measurements of changes in the enthalpy,[1, 11, 25] and positron annihilation lifetime spectroscopy (PALS).[17, 36]

With regard to films, of particular interest in this study, the analogous equation for the aging rate is:

$$\beta = -1/H_\infty dH/d(\log t_{age}) \quad (2.2)$$

where H_∞ is the (theoretical) equilibrium film thickness.[21] In this case H_∞ was determined by linearly extrapolating the equilibrium expansion (rubbery) through the thickness at the annealing temperature to the aging temperature.[21] We are specifically interested in aging behavior in the intermediate regime, where $H(t) \propto \log(t_{age})$. An important precaution for aging studies is to ensure that the time-scale over which measurements of the intermediate time behavior are performed is not influenced by the initial nor terminal behavior.[6, 9, 11, 26] With regard to the initial plateau regime, it has been

shown that the aging time may treated as $t_{age} = t - t_0$, where t_0 is the duration of the initial plateau regime.[9, 11, 26] The initial plateau region occurs on the time-scale of seconds to minutes; the breadth of the plateau region increases with decreasing temperature.[9] It is most prominent at temperatures sufficiently far below T_g. Specifically, in the case of PS such a temperature range would be close to room temperature. We note that the trends in all our data, throughout our study, remain the same had we chosen $t_{age} = t$ (i.e.: $t_0=0$), because t_0 was very short; this is not uncommon in aging studies.[9, 11, 26]

In our study the thicknesses, $H(t_{age})$, of all films that underwent aging decreased linearly with $\log(t_{age})$. The data in Figure 2.1, showing a linear dependence of $H(t_{age})$ on $\log(t_{age})$, are typical of all our samples. Further precautions were taken to ensure that measurements were performed over a sufficiently long period of time such that the slope was truly representative of the actual aging rate.[7, 9, 14]

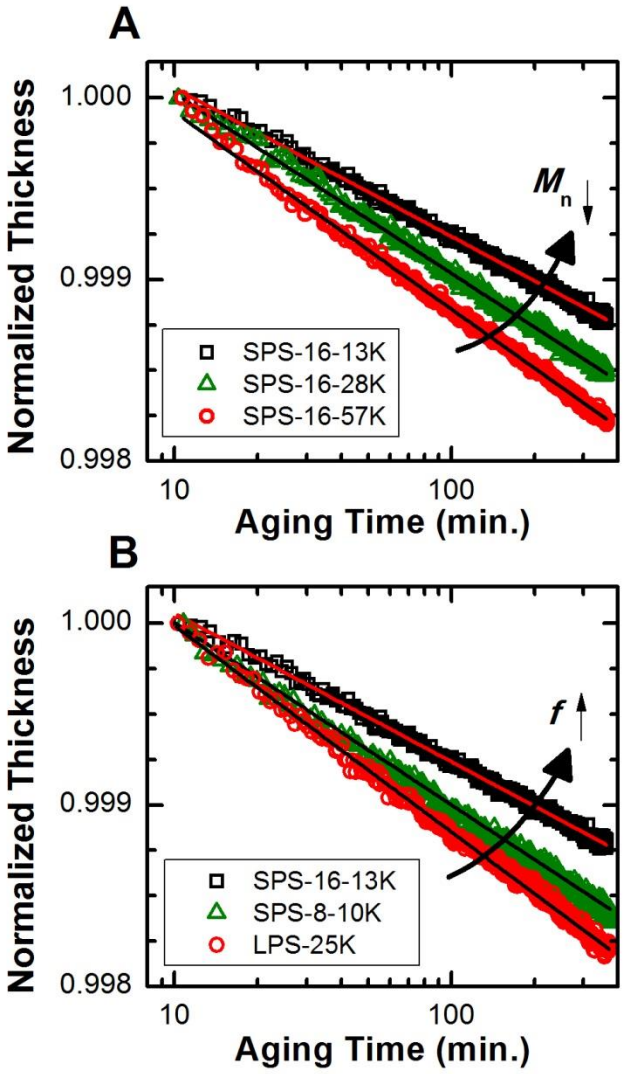

Figure 2.1 The time dependent thickness, at ΔT_A = -35°C, is shown here for a $H(T$=24°C) = 1.1 μm films. (A) For 3 different molecular weights: 13 kg/mol. (open squares), 28 kg/mol. (open triangles), and 52 kg/mol. (open circles), each of 16 arm star PS. (B) For 3 different functionalities: 16 arm (open squares), 8 arm (open triangles), and linear (open circles), each of molecular weight ~12 kg/mol.

It is evident from the data in Figure 2.1 that the aging rate, β, of 16-arm molecules decreases as the arm length, M_n^{arm}, decreases. Moreover, β decreases as the functionality, f, of the molecule increases. This dependence of β on f is shown more extensively in Figure 2.2, where β decreases with increasing f, for experiments conducted at ΔT_{age}=-5°C and -50°C. A dependence of the aging rate on ΔT_{age} is expected. The aging rate is well

known to exhibit a maximum as T_{age}-T_g increases, due to two competing effects: the driving force for aging increases as the magnitude of ΔT_{age} increases, yet the thermally activated relaxations decrease with decreasing k_BT (where k_B is the Boltzmann constant). In our specific case, we know from our experimental data that the maximum occurs at ΔT_{age}=-35°C.

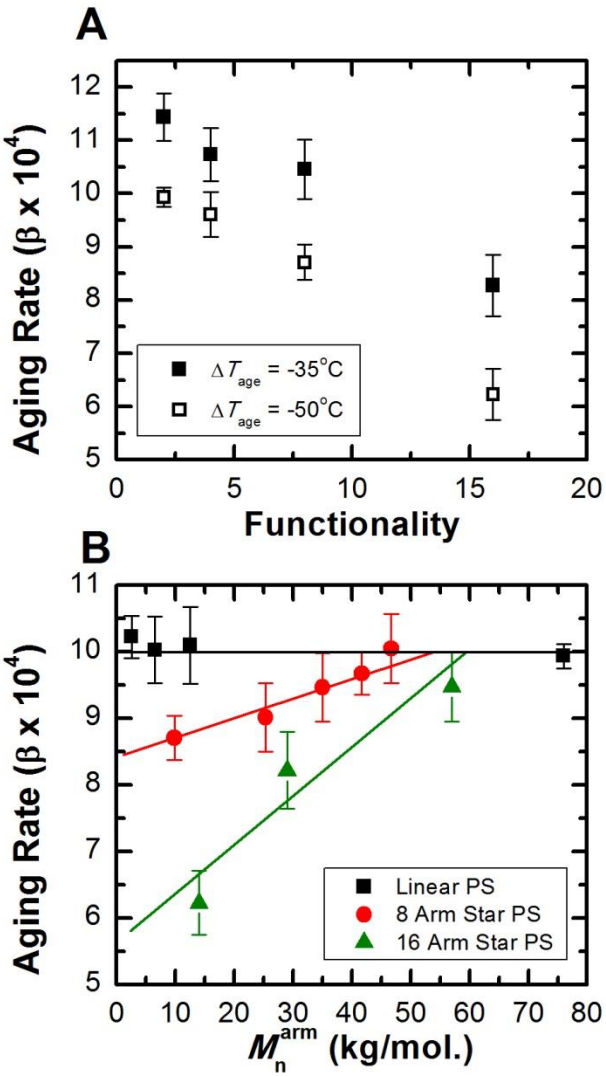

Figure 2.2 (A) A comparison of the aging rates of Star PS with approximately 10 kg/mol. arms, at ΔT_A= -35°C (filled squares) and ΔT_A= -50°C (open squares). (B) The aging rates with varying molecular weight of the arm for 8 arm star PS (filled circles) and 16 arm star PS (open circles) aged at ΔT_A= -50°C.

The physical aging rate of linear chains is independent of the molecular weight, and is faster than their star-shaped counterparts, as shown in Figure 2.2. The negligible influence of M_n on the aging rate of linear chains is consistent with the notion that the structural relaxations of polymer molecules responsible for aging involve a small, finite, number of monomer units.[4, 37-39] The data in Figure 2.2 also reveals that as the M_n^{arm} of the star-shaped molecules increases, the aging rate becomes independent of arm length for large M_n^{arm} and equal to that of linear chains. This data represents the first indication that molecular topology would influence the average physical aging of polymers.

With the foregoing, the role of macromolecular architecture on physical aging is now established. The differences between the physical aging rates could possibly be associated with differences between the amount of free volume, the free volume distribution, and the rates at which segmental relaxations accommodate structural changes throughout the systems. The glass transition temperature provides indirect insight into the free volume in the material. With regard to linear chains, the T_g decreases with decreasing M_n; the dependence is associated with a chain-end effect, where the fractional free volume (or configurational entropy) of short linear chains is larger than that of longer chains. The T_g is proportional $1/M_n$, following the well-known Fox-Flory relation while the aging rate, as mentioned earlier is independent of M_n.[40] The effect of architecture on T_g becomes apparent from the data in Figure 2.3, where T_g is plotted as a function of the number of chain ends (or number of arms per molecule) normalized by M_n.[41] As the number of arms/molecule, f, increases the dependence of T_g on M_n becomes appreciably stronger. A similar effect of f was observed by Qian *et. al.* with regard to 4 and 11 arm star polymers.[41] Star-shaped molecules, with sufficiently high f and low M_n^{arm}, show an increased frustration of packing in the bulk, which may be associated with the unusually strong dependence of average glass transition temperature on M_n.

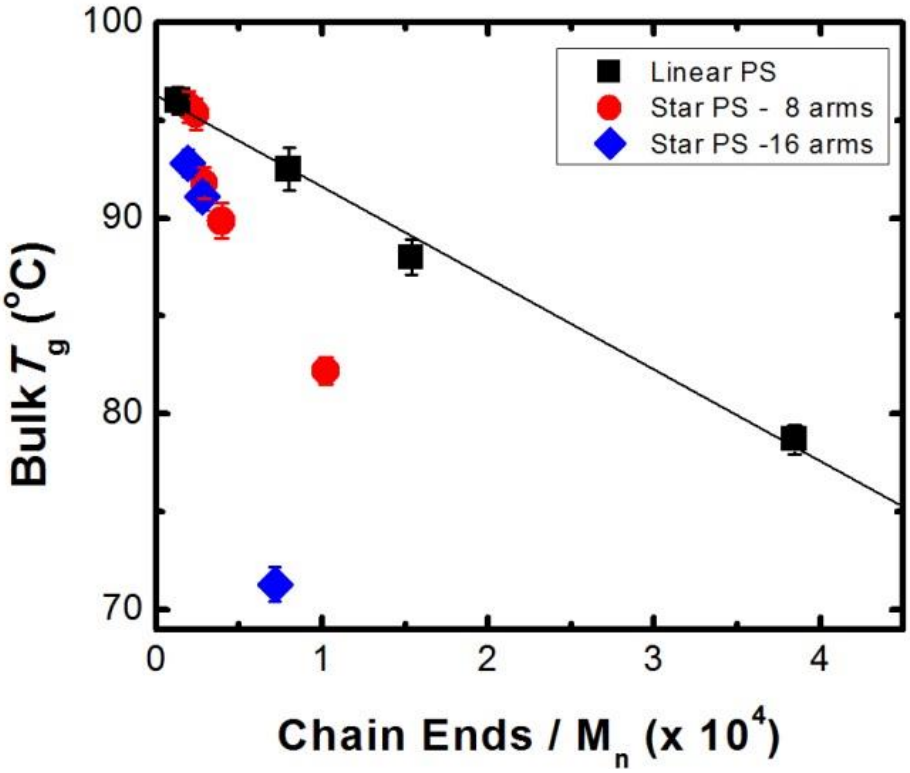

Figure 2.3 The bulk glass transition temperature as a function of chain ends per molecular weight for linear PS (filled squares), 8 arm star PS (filled circles) and 16 arm star PS (filled diamonds). For this case linear PS was assumed to be a 2 arm star and M_n is the total molecular weight of the molecule.

The slow aging behavior of star-shaped molecules may also be associated with differences in the "structure" at the free interfaces of the star and linear macromolecular systems. In the bulk, the aging rate is determined primarily by the diffusion and annihilation of free volume internally, accommodated by local chain segmental relaxations, or lattice contractions. It was previously demonstrated that the glass transition temperature at the free surface of SPS-8-10K and SPS-16-13K is higher than the interior of the film; in fact this effect extends tens of nanometers.[34, 42] More relevant to our study, the fractional free volume at the free surface is smaller than the interior due to the increased local T_g. In contrast, linear chain systems, in particular linear PS, possess lower free surface T_g's, T_g^{surf}, than the bulk, and an associated higher fractional free volume at the free surface than the interior of the film. We speculate that the smaller fractional free volume at the free surface of the star-shaped molecules restricts the rate at

which the free volume escapes from the free surface, compared to the case of linear chain systems. Hence, star-shaped molecules exhibit a lower average aging rate when the T_g^{surf} is larger than the bulk.[34]

We now speculate that the slow physical aging of star-shaped polymers may also be due in part to the following. Simulations reveal that the gradient in monomer density, from the vicinity of the core of the star-shaped molecule to the chain ends, increases and the effect increases as f increases.[43, 44] The local monomer packing would influence the stretching of the polymer chains close to the core of the molecule, thus increasing the local rigidity of the polymer chain. Hence the entropic penalty for relaxations would increase as M_n^{arm} decreases or as f increases, compared to linear chains. It also well known that the physical aging rate is a function of the rigidity of the polymer chain.[12] It follows that the rate of relaxations associated with free volume diffusion might also be slower for star-shaped polymers. It is also noteworthy that the core of the molecule also increases in size with increasing f. Although it is currently unclear as to how the size of the core may influence the physical aging rate, simulations and theory may play a key role in unraveling this effect.

2.4 CONCLUSIONS

In the film thickness regime between H=0.4 μm and 2 μm, the aging of linear chain polymers is rapid compared to the bulk and to ultra-thin films. With regard to stars, the aging rate is a function of M_n and f, particularly for larger f and smaller M_n. The entropic penalties associated with the relaxations of segments close to the core of a star-shaped molecule increases beyond that of linear chains; this may be responsible for slower relaxations responsible for a slower aging rate. The implications of these results are that changing the architecture of the molecule, and its chain length, without changing the chemical side-groups or backbone stiffness, can significantly impact aging, and hence the applications of polymers. The results suggest ways to develop new materials for membranes and other technologies that require thin polymer films by tuning the physical properties at the molecular level.

2.5 REFERENCES

1. Hodge, I. M. *Journal of Non-Crystalline Solids* **1994,** 169, (3), 211-266.
2. Chen, K.; Saltzman, E. J.; Schweizer, K. S., Molecular Theories of Segmental Dynamics and Mechanical Response in Deeply Supercooled Polymer Melts and Glasses. In *Annual Review of Condensed Matter Physics, Vol 1*, Annual Reviews: Palo Alto, 2010; Vol. 1, pp 277-300.
3. Kovacs, A. J. *Annals of the New York Academy of Sciences* **1981,** 371, (OCT), 38-66.
4. Struik, L. C. E., *Physical Aging in Amorphous polymers*. Elsevier Scientific Publishing Company: Amsterdam, 1978.
5. McKenna, G. B. *Journal of Physics-Condensed Matter* **2003,** 15, (11), S737-S763.
6. Priestley, R. D. *Soft Matter* **2009,** 5, (5), 919-926.
7. Chen, K.; Schweizer, K. S. *Physical Review Letters* **2007,** 98, (16).
8. Warren, M.; Rottler, J. *Physical Review E* **2007,** 76, (3).
9. Greiner, R.; Schwarzl, F. R. *Rheologica Acta* **1984,** 23, (4), 378-395.
10. Kovacs, A. J.; Aklonis, J. J.; Hutchinson, J. M.; Ramos, A. R. *Journal of Polymer Science Part B-Polymer Physics* **1979,** 17, (7), 1097-1162.
11. Hutchinson, J. M. *Progress in Polymer Science* **1995,** 20, (4), 703-760.
12. Levita, G.; Struik, L. C. E. *Polymer* **1983,** 24, (8), 1071-1074.
13. Thornton, A. W.; Hill, A. J. *Industrial & Engineering Chemistry Research* **2010,** 49, (23), 12119-12124.
14. Chen, K.; Schweizer, K. S. *Physical Review E* **2008,** 78, (3).
15. Curro, J. G.; Lagasse, R. R.; Simha, R. *Macromolecules* **1982,** 15, (6), 1621-1626.
16. Alfrey, T.; Goldfinger, G.; Mark, H. *Journal of Applied Physics* **1943,** 14, (12), 700-705.
17. Cangialosi, D.; Wubbenhorst, M.; Groenewold, J.; Mendes, E.; Schut, H.; van Veen, A.; Picken, S. J. *Physical Review B* **2004,** 70, (22).
18. Cangialosi, D.; Wubbenhorst, M.; Groenewold, J.; Mendes, E.; Picken, S. J. *Journal of Non-Crystalline Solids* **2005,** 351, (33-36), 2605-2610.
19. Angell, C. A.; Ngai, K. L.; McKenna, G. B.; McMillan, P. F.; Martin, S. W. *Journal of Applied Physics* **2000,** 88, (6), 3113-3157.
20. Chen, K.; Schweizer, K. S. *Journal of Chemical Physics* **2007,** 126, (1).
21. Baker, E. A.; Rittigstein, P.; Torkelson, J. M.; Roth, C. B. *Journal of Polymer Science Part B-Polymer Physics* **2009,** 47, (24), 2509-2519.
22. Cangialosi, D.; Boucher, V. M.; Alegria, A.; Colmenero, J. *Journal of Chemical Physics* **2011,** 135, (1).
23. McCaig, M. S.; Paul, D. R. *Polymer* **2000,** 41, (2), 629-637.
24. McCaig, M. S.; Paul, D. R.; Barlow, J. W. *Polymer* **2000,** 41, (2), 639-648.
25. Hodge, I. M. *Science* **1995,** 267, (5206), 1945-1947.
26. McKenna, G. B. *Computational Materials Science* **1995,** 4, (4), 349-360.
27. Rittigstein, P.; Torkelson, J. M. *Journal of Polymer Science Part B-Polymer Physics* **2006,** 44, (20), 2935-2943.
28. Boucher, V. M.; Cangialosi, D.; Alegria, A.; Colmenero, J. *Macromolecules* **2010,** 43, (18), 7594-7603.

29. Boucher, V. M.; Cangialosi, D.; Alegria, A.; Colmenero, J.; Gonzalez-Irun, J.; Liz-Marzan, L. M. *Soft Matter* **2010,** 6, (14), 3306-3317.
30. Boucher, V. M.; Cangialosi, D.; Alegria, A.; Colmenero, J.; Pastoriza-Santos, I.; Liz-Marzan, L. M. *Soft Matter* **2011,** 7, (7), 3607-3620.
31. Hadjichristidis, N.; Iatrou, H.; Pispas, S.; Pitsikalis, M. *Journal of Polymer Science Part a-Polymer Chemistry* **2000,** 38, (18), 3211-3234.
32. Uhrig, D.; Mays, J. W. *Journal of Polymer Science Part a-Polymer Chemistry* **2005,** 43, (24), 6179-6222.
33. Roovers, J.; Zhou, L. L.; Toporowski, P. M.; Vanderzwan, M.; Iatrou, H.; Hadjichristidis, N. *Macromolecules* **1993,** 26, (16), 4324-4331.
34. Glynos, E.; Frieberg, B.; Oh, H.; Liu, M.; Gidley, D. W.; Green, P. F. *Physical Review Letters* **2011,** 106, (12), 128301.
35. Gray, L. A. G.; Yoon, S. W.; Pahner, W. A.; Davidheiser, J. E.; Roth, C. B. *Macromolecules* **2012,** 45, (3), 1701-1709.
36. Rowe, B. W.; Pas, S. J.; Hill, A. J.; Suzuki, R.; Freeman, B. D.; Paul, D. R. *Polymer* **2009,** 50, (25), 6149-6156.
37. Robertson, R. E. *Journal of Applied Physics* **1978,** 49, (10), 5048-5054.
38. Robertson, R. E.; Simha, R.; Curro, J. G. *Macromolecules* **1984,** 17, (4), 911-919.
39. Huang, Y.; Paul, D. R. *Journal of Polymer Science Part B-Polymer Physics* **2007,** 45, (12), 1390-1398.
40. Fox, T. G.; Flory, P. J. *Journal of Applied Physics* **1950,** 21, (6), 581-591.
41. Qian, Z. Y.; Minnikanti, V. S.; Sauer, B. B.; Dee, G. T.; Archer, L. A. *Macromolecules* **2008,** 41, (13), 5007-5013.
42. Frieberg, B.; Glynos, E.; Green, P. F. *Submitted to Phys. Rev. Lett.* **2012**.
43. Likos, C. N.; Lowen, H.; Watzlawek, M.; Abbas, B.; Jucknischke, O.; Allgaier, J.; Richter, D. *Physical Review Letters* **1998,** 80, (20), 4450-4453.
44. Vlassopoulos, D.; Fytas, G.; Pakula, T.; Roovers, J. *Journal of Physics-Condensed Matter* **2001,** 13, (41), R855-R876.

CHAPTER 3
PHYSICAL AGING OF STAR-SHAPED MOLECULES: FROM LINEAR-LIKE BEHAVIOR TO SOFT COLLOIDS

3.1 INTRODUCTION

When an amorphous material is quenched below its glass transition temperature (T_g), it resides in a non-equilibrium state with excess specific volume, enthalpy and entropy compared to its equilibrium condition. Over time the resultant glass will undergo a series of structural relaxations[1-4] in order to return to equilibrium, a process that has been termed physical aging.[5-7] Structural relaxation leads to a time-dependence of many physical properties that will influence performance, such as: increased brittleness, enhanced modulus and reduced permeability. Thusly, there is a strong technological and scientific importance to understanding the underlying phenomenon behind this process.

The phenomenon of glassy structural relaxations has been a central problem in polymer physics for more than the last 50 years.[3-8] When a material is aged isothermally below its T_g, the ensuing time-dependent recovery of such thermodynamic properties is sigmoidal with respect to the logarithm of aging time, t_{age}.[8] The sigmoidal behavior can be thought of as three different regimes: the initial plateau, power law and equilibrium plateau regimes. It is from the intermediate power law regime in which the rate at which the material undergoes structural relaxations, physical aging rate, is calculated. It is well accepted that there is a non-monotonic dependence of the aging rate on the aging temperature, T_{age}, relative to its T_g. This difference is termed ΔT_A, and is depicted in Figure 1.1 of the introduction.

This non-monotonic behavior of the aging rate as a function of ΔT_A is the result of two competing mechanisms; the increased driving force for aging with increasing $|\Delta T_A|$, that can be defined as the distance of the material from equilibrium, and the decreasing thermal energy for the material to relax as the $|\Delta T_A|$ increases. At temperatures close to T_g, i.e. for small $|\Delta T_A|$, the aging rate will initially increase with increasing $|\Delta T_A|$ while at high enough $|\Delta T_A|$ the progressively slower structural relaxations of the material will dominate and the aging rate will decrease with further increase of $|\Delta T_A|$.

As the relaxation to equilibrium can take anywhere from hours to years,[8] a number of techniques have been employed in order to simulate and extrapolate the long term changes in physical properties, such as: stress relaxation experiments, volume,[9] dielectric strength[10] and enthalpy recovery[11] as well as fluorescence measurements.[4] Many different phenomenological models have been successfully employed to explain this complex process, such as time dependent changes in free volume from diffusion to interfaces and internal annihilation of vacancies,[10, 12-16] or even molecular theories incorporating configurationally entropy to describe changes in the magnitude of density fluctuations.[17, 18] While each model is successful in describing a specific set of data, there are numerous experiments that are seemingly contradictory at first glance. For example, while some studies demonstrate that enthalpy and volume recovery rates are different,[8, 19] others demonstrate there is no difference.[20] To this end, there are still many open questions as the physical phenomenon responsible for structural relaxation.

Many researchers have shown the aging behavior of a material strongly depends on its chemical structure.[9] This has been postulated to be due to the effect of chain chemical composition on its fractional free volume[21, 22] and its stiffness of the polymer chains for polymers such as polyimides and cellulose.[23] It can also be strongly dependent on β and γ relaxations such as in PMMA.[9] Recently we showed that changes in the macromolecular architecture can have a strong influence on the aging behavior.[24] In particular we demonstrated that the aging rates of star-shaped polymers are significantly slower than linear polymer of the same chemical composition. For linear PS molecules, it was found that there is no influence of the molecular weight on the physical aging rate. The aging rate of star-shaped polymers was shown to have a strong dependence on both

the degree of polymerization of the arm, N_{arm}, and/or the functionality, f, of the molecule; the aging rate decreased with both increasing f and/or decreasing N_{arm}.

In this chapter we address the more general question regarding the aging behavior of star-shaped polymers. We investigate if there is there a limit on the effect of functionality and the molecular weight as stars begin to exhibit a more colloid-like character. To address this, in this study we synthesized a wide range of star-shaped molecules with functionalities of up to 64 arms and N_{arm} ranging from about 80 to 1400. We show that the structural relaxation of the star-shaped molecules exhibit a limit to the reduction in aging rate as the functionality is further increased to 32 and 64 arms. We further show that the critical functionality in which the aging rate approaches a plateau inherently depends on N_{arm}. Additionally, when N_{arm} is sufficiently long and/or the f sufficiently small, the aging rate is equivalent to that of the linear polymer chain. Furthermore, we demonstrate that the influence of chain architecture depends strongly on the degree of undercooling, ΔT_A. At small $|\Delta T_A|$, the aging behavior is independent of chain architecture, while at large $|\Delta T_A|$ the differences with chain architecture are largest. The influence of chain architecture on the physical aging behavior of star-shaped molecules is discussed in terms of the competition between the departure from equilibrium and the glassy dynamics.

3.2 EXPERIMENTAL SECTION

3.2.1 Materials

The list of the polymers used in this study is displayed in Table 3.1. We synthesized the high functionality star-shaped PS (with $f \geq 8$) by means of anionic polymerization using high vacuum techniques.[25, 26] Excess of the living poly(styrenyl)lithium were reacted with the appropriate chlorosilane linking agent.[27] Sufficient time for the coupling reaction has to be allowed, and the excess arm material was removed by fractionation. The linear polystyrene (PS) molecules as well as some of the 8-arm star-shaped PS molecules (indicated in the table with a *) were purchased from Pressure Chemical and Polymer Source respectively.

Table 3.1 A list of the polymers used in this chapter.

Polymer	Functionality (f)[a]	M_n^{arm} (kg/mol)[c]	N_{arm}	PDI[d]
PS-4arm-4K (SPS-4-4K)*	4	4	38	1.03
PS-3arm-19K (SPS-3-19K)*	3	19	183	1.03
PS-8arm-10K (SPS-8-10K)*	8	10	96	1.03
PS-8arm-25K (SPS-8-25K)*	8	25	240	1.03
PS-8arm-35K (SPS-8-35K)*	8	35	337	1.02
PS-8arm-42K (SPS-8-42K)*	8	42	404	1.03
PS-8arm-47K (SPS-8-47K)*	8	47	452	1.03
PS-16arm-13K (SPS-16-13K)	16	13	125	1.02
PS-16arm-28K (SPS-16-28K)	16	28	269	1.02
PS-16arm-57K (SPS-16-57K)	16	57	548	1.01
PS-32arm-9K (SPS-32-9K)	32	9	87	1.03
PS-32arm-36K (SPS-32-36K)	32	36	346	1.03
PS-32arm-52K (SPS-32-52K)	32	52	500	1.01
PS-32arm-80K (SPS-32-80K)	32	80	769	1.01
PS-32arm-140K (SPS-32-140K)	32	140	1346	1.01
PS-64arm-9K (SPS-64-9K)	64	9	87	1.02
PS-64arm-36K (SPS-64-36K)	64	36	346	1.01
PS-64arm-52K (SPS-64-52K)	64	52	500	1.01
PS-64arm-80K (SPS-64-80K)	64	80	769	1.01
PS-64arm-140K (SPS-64-140K)	64	140	1346	1.01

[a]Functionality, f ,determined by the ratio $(M_w)_{star}/(M_n)_{arm}$. [b]From Low Angle Laser Light Scattering in THF at 25 ºC. [c]From membrane osmometry in toluene at 35 ºC. [d]From SEC in THF at 40 ºC calibrated with linear PS standards.*Purchased from Polymer Source Inc.

3.2.2 Sample preparation

Supported films, a micron in thickness, were spin-coated from a toluene solution of onto pre-cleaned silicon wafers (Wafer World Inc.) with a native oxide layer of 1.5 nm. The silicon wafers were cleaned by rinsing with ethanol and acetone followed by UV-ozone treatment for 3 minutes. The wafers were finally rinsed with toluene immediately prior to spin-coating. The samples were annealed 50K above their T_g for 48 hours. The polymer film thickness was measured using spectroscopic ellipsometry, SE (M-2000, J.A. Woollam Co.).

3.2.3 Glass Transition

The glass transition temperature, T_g, and thermal expansion coefficient of the supported films was measured by monitoring the change in film thickness upon cooling from 423K down to room temperature at a rate of 1K/min. using SE equipped with an Instec heating stage. The measurements were performed at a fixed angle of 70^o using a nitrogen purge gas; and liquid nitrogen was used in order to maintain the temperature and cooling rate. The thickness, $h(T)$, and refractive index, $n(T)$, were determined by fitting the ellipsometric angles Δ and Ψ to a Cauchy/SiO2/Si model over the wavelengths of 400-1700 nm. The glass transition temperature was determined by the intersection of extrapolated linear fits through the glassy and rubbery regions of the data.

3.2.4 Volume Recovery

The volume recovery experiments were conducted on 1 micron thick films using SE. The samples were heated to a temperature of 50K above their thermal T_g where it was annealed for 30 min. to remove any thermal history. It was then quenched at a rate of 85 K/min. to room temperature and then ramped back to the aging temperature, T_{age}, where the sample thickness, h, was monitored as a function of time. An acquisition time of 30 seconds was used to measure the thickness every 60 seconds. The experimental time of 360 minutes was used in this study, which has been reported to be sufficient to determine the average aging rate of the material within the experimental error.[28] The experiment was repeated a total of 3-5 times for each aging temperature in order to ensure that that the results were reproducible. The aging rate is then reported as the average of all of the aging tests.

3.2.5 Enthalpy Recovery

A TA Instruments Q200 differential scanning calorimeter (DSC) with a liquid nitrogen cooling system was used to perform the enthalpy recovery experiments. The experiments were conducted on approximately 5 mg of material, and a similar thermal procedure was used to mimic the ellipsometric (volume recovery) experiments. The samples were annealed at 40K above the calorimetric T_g for 30 minutes in order to remove any thermal history. The samples were then quenched at 50 K/min. to room temperature, and subsequently heated rapidly to the T_{age}. The sample was then kept at the aging temperature for a given amount of time, ranging from 1 minute to 12 hours, after which it is quenched to room temperature and then heated to above the T_g at 10K/min. It is on the last heating cycle that the heat flow is monitored and is always followed by a measurement without aging the sample in order to account for baseline drift. The enthalpy recovery can then be determined from the difference in area between the aged and unaged scans using a procedure widely used in the literature:

$$\Delta H = \frac{1}{m}\int_{T_a}^{T_b}\left(\dot{Q}_{aged} - \dot{Q}_{unaged}\right)dT \qquad (3.1)$$

where m is the heating rate (10 K/min.) and Q_{aged} and Q_{unaged} are the normalized DSC heat flows, in W/g, of the aged and unaged heating scans respectively. The absolute heat capacity of the polymers were measured using temperature modulated DSC, where the temperature was modulated with an amplitude of 0.5K and period of 40 seconds. The heat flow and heat capacity of the DSC were calibrated using indium and sapphire respectively.

3.3 RESULTS AND DISCUSSION

As it was mentioned in the introduction, as a polymeric material is quenched at a sufficiently rapid rate, the material will fall out of equilibrium and reside in a non-equilibrium state when the experimental time scale (cooling rate) is on the order of the relaxation time of the material. The material possesses an excess of thermodynamic properties such as enthalpy or specific volume, shown schematically in Figure 1.1.

In Figure 3.1 we plot the changes in thickness with aging time, for various star-shaped polystyrene (PS) molecules with the same N_{arm} ~ 100 and f =2 (linear), 16 and 64, as measured with ellipsometry. In this case, due to the isotropic nature of PS, and the

constraint of the film to the substrate, h is proportional to the volume. The volumetric aging rate is defined as:

$$\beta_{vol.} = \frac{1}{h_\infty} \frac{dh}{d\log(t_{age})} \tag{3.2}$$

where h_∞ is the specific volume at equilibrium and t_{age} is the aging time.[29] The data shown in Figure 3.1 demonstrates that the rate of change in film thickness at a constant temperature relative to T_g of the material is strongly dependent on the number of arms (functionality, f) of the star-shaped polymer; the aging rate decreases as f increases. It is important to point out that the aforementioned differences are purely an effect of the polymer architecture and not of the differences in the total degree of polymerization of the star-shaped polymer = $f\ N_{arm}$; linear PS have the same aging behavior independently of the degree of polymerization at a constant temperature relative to the T_g.[24]

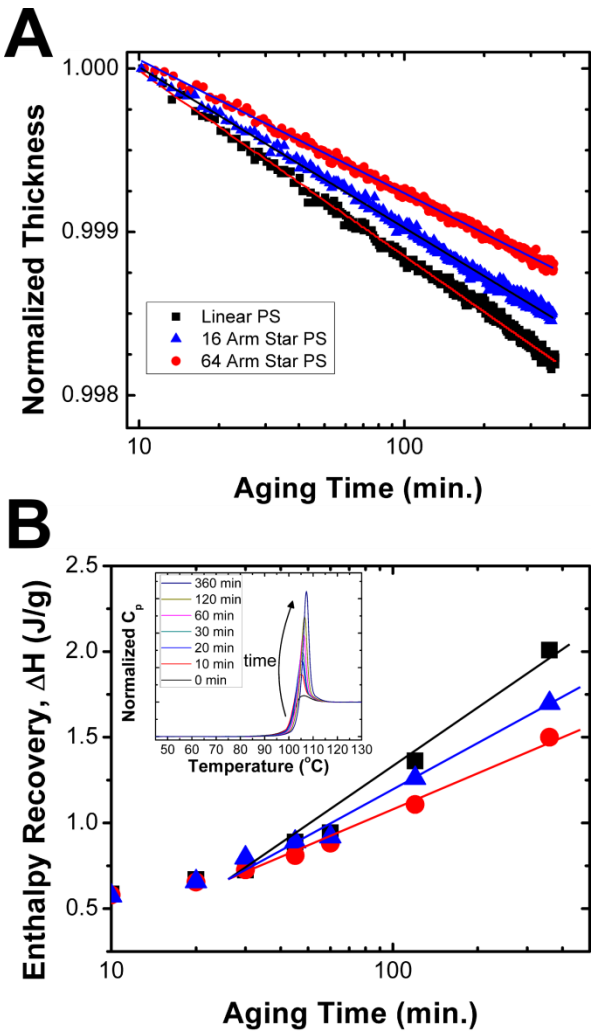

Figure 3.1 Aging experiments conducted at ΔT_A = -25K with molecules of a constant N_{arm} = 100. (A) The change in film thickness, normalized by the film thickness at 10 minutes, as a function of the aging time. The solid lines are guides to the eye that represent fittings to obtain the aging rate. (B) The enthalpy recovery as a function of the aging time. (inset) Normalized heat capacity measured as a function of temperature for various aging times ranging from 0 to 6 hours, for Linear PS N = 100, ΔT_A = -25K.

The structural relaxation rate of the star-shaped polymers, in terms of enthalpy recovery experiments, was also conducted using DSC. By measuring the enthalpy overshoot as a function of aging time, the amount of enthalpy recovery (that is a measure of the structural relaxation of a glassy material)[7] can be extracted and is shown in Figure 3.1. Typically enthalpy recovery tests utilize the Tool- Narayanaswamy-Moynihan (TNM) model in order to extract information about aging behavior,[30-32] but in order to

make a direct comparison with the volumetric aging studies we employ the following equation:

$$\beta_{enth.} = \frac{1}{H_0}\frac{dH}{d\log(t_{age})} \quad (3.3)$$

where H_0 is the initial enthalpy recovery at 30 min. after the quench. A similar analysis has been previously applied in the case of PS thin films[33, 34] as well as PS nanoparticles.[35, 36] As shown in Figure 3.1, the aging rate of star-shaped polymers, as measured from the enthalpy recovery measurements, decreases with increasing *f*, consistent with the data obtained by measuring the volume recovery (Figure 3.1). It is not surprising that the aging rate trends are qualitatively the same for both enthalpic and volumetric recovery measurements since it has previously been reported these two measurements exhibit similar trends with temperature for linear PS.[20]

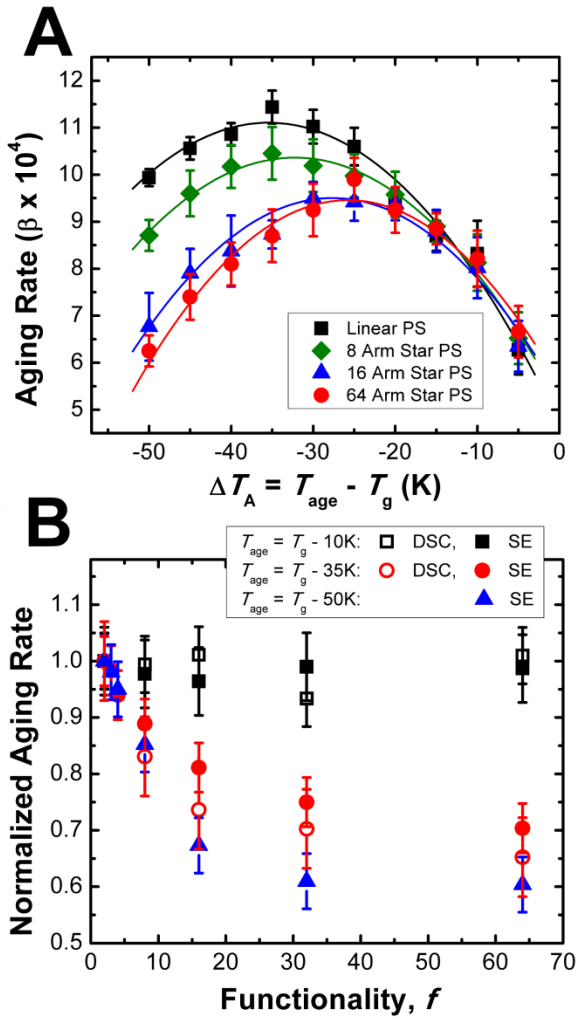

Figure 3.2 (A) The aging rate calculated from volumetric aging experiments as a function of aging temperature. (B) The aging rate, normalized by the aging rate of linear PS as a function of the number of arms, functionality at various temperatures. The closed symbols are determined from ellipsometry and the open symbols are calculated from DSC.

Figure 3.2 demonstrates the temperature dependence of the volumetric aging rate, calculated from equation 3.2, for star-shaped molecules with N_{arm} = 100 and different functionalities. The aging rate is plotted as the degree of undercooling, ΔT_A, which dictates the driving force for aging to be comparable, which will be discussed in more detail later in the chapter. For all the polymers a non-monotic ΔT_A-dependence on the aging rates is observed. This non-monotonic behavior has been previously reported,[9] and has been explained in terms of two competing effects; an increasing driving force for aging as $|\Delta T_A|$ increases and a decreasing segmental mobility as $|\Delta T_A|$ increases. As the

temperature is initially decreased, the increasing driving force for aging enhances the average rate that the system will age. Nevertheless when the temperature is further decreased, the progressively slower segmental mobility dominates and the average aging rate begins to decrease, resulting in a maximum in the aging rate.

A direct comparison between enthalpic and volumetric recovery experiments can be made by normalizing the aging rates for the different samples by the corresponding aging rate of linear PS. Figure 3.2 plots the normalized aging rates as a function of functionality for different ΔT_A's. At temperatures close to the T_g (small $|\Delta T_A|$), the aging rate is independent of chain architecture while at temperature well below T_g (larger $|\Delta T_A|$) the aging rates exhibits a strong functionality dependence.

The departure from equilibrium (which is the driving force for aging) at a given ΔT_A can be estimated from the thermal expansion coefficients. This is based on the assumption that the equilibrium volume is simply the extrapolation of the rubbery thermal expansion into the glassy state,[5, 8, 9, 29] and the departure of equilibrium, δ, can be estimated as $\delta = h_0/(h_0-h_\infty)$. δ (and hence he driving force for aging) are independent of chain architecture. It's important to point out that the thermal expansion coefficient, as measured by ellipsometry, in both the rubbery and glassy regimes is independent of chain architecture, consistent with previous work.[37] The fact that the thermal expansion coefficient is independent of f can explain that at small ΔT_A the aging rate is independent of chain architecture; at small $|\Delta T_A|$ the driving force for aging dominates the average aging rate.

Having demonstrated that a low $|\Delta T_A|$ the aging rates between different linear and star-shaped polymers are similar due to same driving force for aging, we now turn our attention to large $|\Delta T_A|$, where there is a significant effect of architecture on the aging rate. As we have already discussed, for larger $|\Delta T_A|$ the aging behavior is governed by the glassy segmental relaxations of the material. Recall that the competition between increasing driving force for aging and decreasing glassy dynamics with increasing $|\Delta T_A|$ results in a maximum on the aging rate-$|\Delta T_A|$ behavior. Figure 3.2 show that the aging rate decreases with increasing functionality for $\Delta T_A < -20\ ^oC$. The depression in the aging rate with f increases with decreasing ΔT_A; for $\Delta T_A = -50\ ^oC$ star-shaped polymers with $f \geq 32$ appear to have an aging rate that is about 50% slower than that of the linear

polymers. Our data indicate that the structural dynamics of star-shaped polymers are significantly different from their linear counterparts and become slower with increasing *f*. This effect of architecture on the polymer's structural dynamics can be understood in terms of the effect of the star-shaped polymer architecture on the conformation properties and the monomer density in these systems. In the case of star-shaped molecules, there is a gradient in monomer density from the core of the molecule to the outer end of the chains. As the functionality is increased, for a constant N_{arm}, the "crowding" effect of monomers near the core of the molecule is increased. The chains can no longer follow the conformations of an "ideal chain", they stretch in order to accommodate the excess chains. The stretched conformation of the arms and the resultant increase in the monomer density leads to a restriction of the motions with the polymer chains. Therefore, at low aging temperatures where the segmental motions dominate the average physical aging rate there is a much stronger influence of chain architecture. This behavior is seen consistently in both enthalpy recovery and volumetric aging experiments.

While the aging rate is indicative of how fast the material will recover to equilibrium, it does not describe the entire structural relaxation process. In order to fully understand the influence of chain architecture on the structural recovery behavior, one must also account for the amount of time for the material to equilibrate. It has been demostrated that the aging behavior can be described in terms of a stretched exponential with time which assumes a distribution in polymer dynamics, i.e. the KAHR based model.[33, 35, 36, 38] From the KAHR model, one can measure a relaxation time, defined as the time that the material needs to reach equilibrium,[38, 39] at a given temperature below T_g.

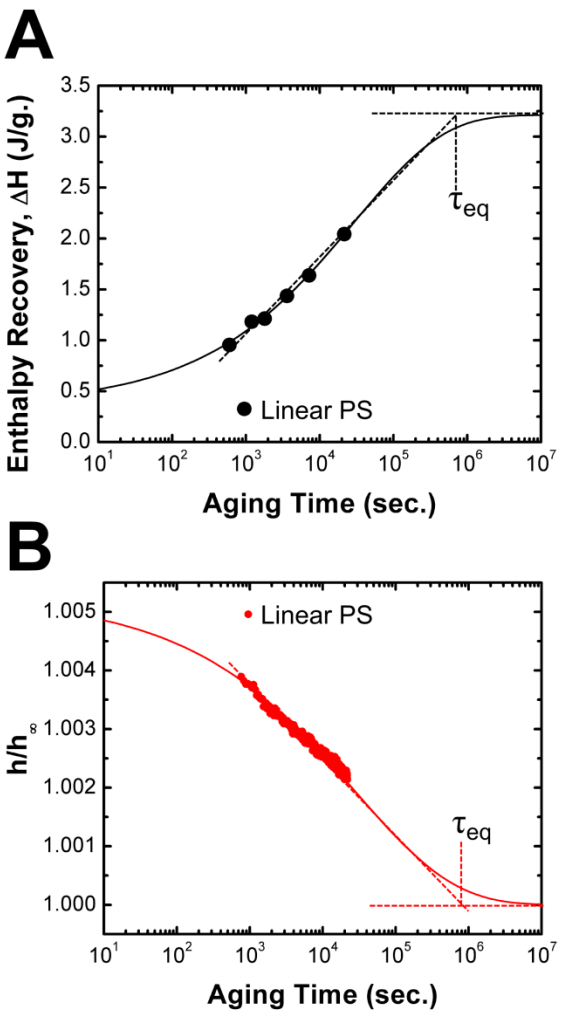

Figure 3.3 The time dependence of (A) enthalpy recovery and (B) volume recovery of linear PS-25 kg/mol. aged at 10K below the T_g. The solid lines represent fittings to a stretched exponential and the dashed lines represent the linear extrapolation to equilibrium used to estimate the equilibration time.

A stretched exponential based on the KAHR model was fit to the volume recovery data for different aging times (Figure 3.3). However in order to extract the equilibration time, τ_{eq}, a linear fit was conducted in order to extrapolate the approximate time to reach equilibrium, as is shown in Figure 3.3, and in a similar manner that has been employed recently in the literature.[39] In order to do so, one must also determine the equilibrium thickness of the polymer film. The equilibrium film thickness was estimated by linearly extrapolating the film thickness of the rubbery state to the aging temperature using the thermal expansion coefficient and the thickness at the annealing temperature,

schematically shown in Figure 1.1. By extrapolating the data to the equilibrium thickness, one can effectively estimate τ_{eq}, from the ellipsometry measurements.

Similarly, the equilibration time can be determined for the DSC measurements of aging. The data can be extrapolated to the equilibrium value; although in this case the equilibrium value is determined using a method outline by Koh *et al.*[38] The equilibrium values were estimated using the absolute heat capacity measured by modulated DSC to accurately determine the equilibrium enthalpy recovery as seen in equation 3.

$$\Delta H_\infty = \int_{T_{f0}}^{T_{age}} \Delta C_p \, dT \tag{3.4}$$

where ΔC_p is the theoretical change in C_p at T_{f0}, which depends on the aging temperature and was extracted from the absolute heat capacity from temperature modulated DSC. As a point of reference, it was found to be 0.29 J/(g K) at T_g (373K) for linear PS, consistent with literature results.

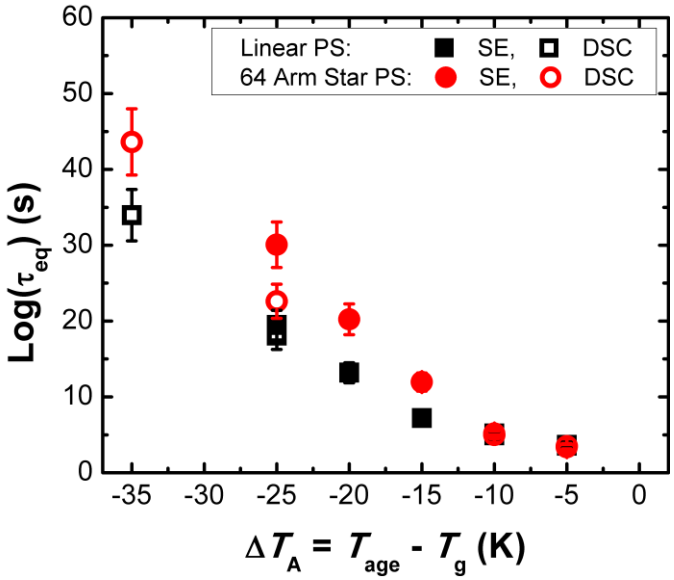

Figure 3.4 The temperature dependence of the equilibration time measured by ellipsometry (closed symbols) and DSC (open symbols).

The τ_{eq} values as a function of ΔT_A for both DSC and ellipsometry are shown in Figure 3.4 . Although there is a difference between the absolute values obtained from the two techniques, which has previously been reported in the literature,[40] the trends remain the same. At high temperatures, there is little to no difference in the equilibration time for the linear PS compared to the star PS. For low temperatures, the star-shaped molecules

exhibit orders of magnitude longer aging times compared to their linear analogs. It is clear from these results that the equilibration time is longer for the star-shaped molecules at large undercoolings (lower aging temperatures) consistent with the aging rate results.

A number of recent works have described the physical aging process in bulk polymers, polymer nanocomposites and polymer thin films in terms of a free volume diffusion model.[12, 14-16, 21, 22, 41-52] We have also employed this model to our data, (data not shown here) and the free volume diffusion coefficient decreases with increasing functionality, consistent with with the data shown in Figure 3.4. It has also been demonstrated that the diffusion of free volume through an amorphous glass inherently depends on the glassy dynamics of polymer.[5, 7, 14, 16, 34, 35, 49, 53] To this end, if the aging process is thought of in terms of escape of free volume, the diffusion of free volume is slower in star-shaped molecules and decreases with increasing functionality due to the restriction of the segmental motions near the core of the molecule for high *f*.

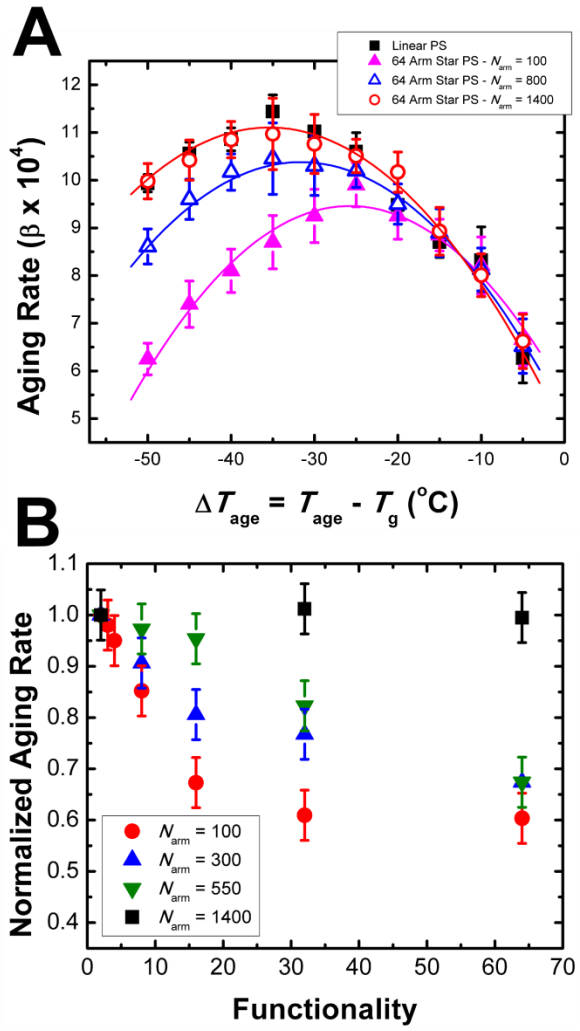

Figure 3.5 (A) The aging rate calculated from volumetric aging experiments as a function of aging temperature, for the 64 arm stars of varying degrees of polymerization. The aging rate of linear polystyrene is shown as black squares for reference. (B) The aging rate, normalized by the aging rate of linear PS as a function of the number of arms, functionality at various degrees of polymerization. The aging rates were determined from ellipsometry and were conducted at ΔT_A = -50K.

Up to this point, our discussion on the effect of functionality on the aging behavior of star-shaped polymer was for star-shaped polymers where the N_{arm} was constant at 100 and only f was varied from 2 to 64. To this end, one would anticipate that by increasing N_{arm} for a fixed f, the aging rate of the system should increase and reach the values of linear chains for large enough N_{arm}. To this end, Figure 3.5 plots the aging rate-ΔT_A dependence of star-shaped polymers with f = 64 and N_{arm} from 100 to 1344. It is clear that as N_{arm} is increased to 1344 the aging behavior of the system gradually returns

to that of linear polystyrene. This is further exemplified in Figure 3.5B, where the influence of functionality was investigated at different N_{arm} (100, 300, 550, and 1344). As N_{arm} increases, at a constant functionality, the fraction of the arms that can attain ideal conformations, and have an aging behavior akin to a linear chain, increases. It is important to point out that as Figure 3.5 indicates the critical number of arms necessary to see deviations from linear-like aging behavior increases with increasing degree of polymerization. In a similar fashion, the critical N_{arm}, below which a star-shaped polymer of functionality *f*, will have a different aging behavior than a linear, decreased with increasing *f*.

3.4 CONCLUSIONS

In conclusion, we have demonstrated that there is a strong influence of the chain architecture on the glassy dynamics as it was shown in terms of effect of the molecular characteristics of a star-shaped polymer (functionality and degree of polymerization of each arm) on its aging behavior. Our data show that star-shaped molecules provide a model system in which the structural relaxation process can be significantly changed without changes the chemical structure of the molecule. The temperature dependence of the physical aging behavior, and thereby the time dependence of physical properties, can be explained and even tailored through precise control of the molecular architecture of polymeric materials.

3.5 REFERENCES

1. Weeks, E. R.; Crocker, J. C.; Levitt, A. C.; Schofield, A.; Weitz, D. A. *Science* **2000,** 287, (5453), 627-631.
2. Torre, R.; Bartolini, P.; Righini, R. *Nature* **2004,** 428, (6980), 296-299.
3. Hodge, I. M. *Science* **1995,** 267, (5206), 1945-1947.
4. Priestley, R. D.; Ellison, C. J.; Broadbelt, L. J.; Torkelson, J. M. *Science* **2005,** 309, (5733), 456-459.
5. Struik, L. C. E., *Physical Aging in Amorphous polymers*. Elsevier Scientific Publishing Company: Amsterdam, 1978.
6. McKenna, G. B. *Journal of Physics-Condensed Matter* **2003,** 15, (11), S737-S763.
7. Kovacs, A. J.; Aklonis, J. J.; Hutchinson, J. M.; Ramos, A. R. *Journal of Polymer Science Part B-Polymer Physics* **1979,** 17, (7), 1097-1162.
8. Hutchinson, J. M. *Progress in Polymer Science* **1995,** 20, (4), 703-760.
9. Greiner, R.; Schwarzl, F. R. *Rheologica Acta* **1984,** 23, (4), 378-395.
10. Cangialosi, D.; Wubbenhorst, M.; Groenewold, J.; Mendes, E.; Picken, S. J. *Journal of Non-Crystalline Solids* **2005,** 351, (33-36), 2605-2610.
11. Hodge, I. M. *Journal of Non-Crystalline Solids* **1994,** 169, (3), 211-266.
12. Cangialosi, D.; Boucher, V. M.; Alegria, A.; Colmenero, J. *Journal of Chemical Physics* **2011,** 135, (1), 014901.
13. Cangialosi, D.; Wubbenhorst, M.; Groenewold, J.; Mendes, E.; Schut, H.; van Veen, A.; Picken, S. J. *Physical Review B* **2004,** 70, (22), 224213.
14. Curro, J. G.; Lagasse, R. R.; Simha, R. *Macromolecules* **1982,** 15, (6), 1621-1626.
15. McCaig, M. S.; Paul, D. R.; Barlow, J. W. *Polymer* **2000,** 41, (2), 639-648.
16. Thornton, A. W.; Hill, A. J. *Industrial & Engineering Chemistry Research* **2010,** 49, (23), 12119-12124.
17. Chen, K.; Schweizer, K. S. *Physical Review Letters* **2007,** 98, (16).
18. Chen, K.; Schweizer, K. S. *Physical Review E* **2008,** 78, (3).
19. Petrie, S. E. B. *Journal of Polymer Science Part a-2-Polymer Physics* **1972,** 10, (7), 1255-1272.
20. Hadac, J.; Slobodian, P.; Riha, P.; Saha, P.; Rychwalski, R. W.; Emri, I.; Kubat, J. *Journal of Non-Crystalline Solids* **2007,** 353, (28), 2681-2691.
21. Huang, Y.; Wang, X.; Paul, D. R. *Journal of Membrane Science* **2006,** 277, (1-2), 219-229.
22. Rowe, B. W.; Pas, S. J.; Hill, A. J.; Suzuki, R.; Freeman, B. D.; Paul, D. R. *Polymer* **2009,** 50, (25), 6149-6156.
23. Levita, G.; Struik, L. C. E. *Polymer* **1983,** 24, (8), 1071-1074.
24. Frieberg, B.; Glynos, E.; Sakellariou, G.; Green, P. F. *Acs Macro Letters* **2012,** 1, (5), 636-640.
25. Hadjichristidis, N.; Iatrou, H.; Pispas, S.; Pitsikalis, M. *Journal of Polymer Science Part a-Polymer Chemistry* **2000,** 38, (18), 3211-3234.
26. Uhrig, D.; Mays, J. W. *Journal of Polymer Science Part a-Polymer Chemistry* **2005,** 43, (24), 6179-6222.
27. Roovers, J.; Zhou, L. L.; Toporowski, P. M.; Vanderzwan, M.; Iatrou, H.; Hadjichristidis, N. *Macromolecules* **1993,** 26, (16), 4324-4331.

28. Pye, J. E.; Rohald, K. A.; Baker, E. A.; Roth, C. B. *Macromolecules* **2010,** 43, (19), 8296-8303.
29. Baker, E. A.; Rittigstein, P.; Torkelson, J. M.; Roth, C. B. *Journal of Polymer Science Part B-Polymer Physics* **2009,** 47, (24), 2509-2519.
30. Tool, A. Q. *Journal of the American Ceramic Society* **1946,** 29, (9), 240-253.
31. Moynihan, C. T.; Macedo, P. B.; Montrose, C. J.; Gupta, P. K.; Debolt, M. A.; Dill, J. F.; Dom, B. E.; Drake, P. W.; Easteal, A. J.; Elterman, P. B.; Moeller, R. P.; Sasabe, H.; Wilder, J. A. *Annals of the New York Academy of Sciences* **1976,** 279, (OCT15), 15-35.
32. Narayana.Os. *Journal of the American Ceramic Society* **1971,** 54, (10), 491-&.
33. Koh, Y. P.; Simon, S. L. *Journal of Polymer Science Part B-Polymer Physics* **2008,** 46, (24), 2741-2753.
34. Boucher, V. M.; Cangialosi, D.; Alegria, A.; Colmenero, J. *Macromolecules* **2012,** 45, (12), 5296-5306.
35. Guo, Y. L.; Zhang, C. A.; Lai, C.; Priestley, R. D.; D'Acunzi, M.; Fytas, G. *Acs Nano* **2011,** 5, (7), 5365-5373.
36. Zhang, C.; Guo, Y. L.; Priestley, R. D. *Journal of Polymer Science Part B-Polymer Physics* **2013,** 51, (7), 574-586.
37. Qian, Z. Y.; Minnikanti, V. S.; Sauer, B. B.; Dee, G. T.; Archer, L. A. *Macromolecules* **2008,** 41, (13), 5007-5013.
38. Koh, Y. P.; Simon, S. L. *Macromolecules* **2013,** 46, (14), 5815-5821.
39. Cangialosi, D.; Boucher, V. M.; Alegria, A.; Colmenero, J. *Physical Review Letters* **2013,** 111, (9).
40. Simon, S. L.; Sobieski, J. W.; Plazek, D. J. *Polymer* **2001,** 42, (6), 2555-2567.
41. Boucher, V. M.; Cangialosi, D.; Alegria, A.; Colmenero, J. *Macromolecules* **2010,** 43, (18), 7594-7603.
42. Boucher, V. M.; Cangialosi, D.; Alegría, A.; Colmenero, J. *Thermochimica Acta* **2014,** 575, (0), 233-237.
43. Boucher, V. M.; Cangialosi, D.; Alegria, A.; Colmenero, J.; Gonzalez-Irun, J.; Liz-Marzan, L. M. *Soft Matter* **2010,** 6, (14), 3306-3317.
44. Boucher, V. M.; Cangialosi, D.; Alegria, A.; Colmenero, J.; Gonzalez-Irun, J.; Liz-Marzan, L. M. *Journal of Non-Crystalline Solids* **2011,** 357, (2), 605-609.
45. Boucher, V. M.; Cangialosi, D.; Alegria, A.; Colmenero, J.; Pastoriza-Santos, I.; Liz-Marzan, L. M. *Soft Matter* **2011,** 7, (7), 3607-3620.
46. Huang, Y.; Paul, D. R. *Polymer* **2004,** 45, (25), 8377-8393.
47. Napolitano, S.; Cangialosi, D. *Macromolecules* **2013,** 46, (19), 8051-8053.
48. Napolitano, S.; Capponi, S.; Vanroy, B. *European Physical Journal E* **2013,** 36, (6).
49. Robertson, R. E.; Simha, R.; Curro, J. G. *Macromolecules* **1984,** 17, (4), 911-919.
50. Tang, Q.; Hu, W. *Physical Chemistry Chemical Physics* **2013,** 15, (47), 20679-20690.
51. Alfrey, T.; Goldfinger, G.; Mark, H. *Journal of Applied Physics* **1943,** 14, (12), 700-705.
52. Simha, R.; Curro, J. G.; Robertson, R. E. *Polymer Engineering and Science* **1984,** 24, (14), 1071-1078.

53. Priestley, R. D.; Broadbelt, L. J.; Torkelson, J. M. *Macromolecules* **2005,** 38, (3), 654-657.

CHAPTER 4

CORRELATION BETWEEN GLASSY DYNAMICS AND PHYSICAL AGING

4.1 INTRODUCTION

When an amorphous material is quenched below its glass transition temperature (T_g), it resides in a non-equilibrium state with excess specific volume, enthalpy and entropy compared to its equilibrium condition. Over time the resultant glass will undergo a series of structural relaxations in order to relax towards equilibrium, a process that has been termed physical aging. This phenomenon has been of interest to polymer scientists for more than one half of a century.[1-6] This behavior has important implications for the reliability polymers used for applications, from pharmaceuticals and gas separation membranes to insulation, where they must maintain certain physical properties for durations from days to decades.

The time dependent change of a thermodynamic property, such as the specific volume, that underlies aging is characterized by sigmoidal behavior with respect to the logarithm of aging time, t_{age}.[1] The initial plateau is strongly dependent on the experimental conditions; the subsequent intermediate regime is characterized by a power law dependence on t_{age}. The final regime, which may occur on time-scales from hours to years, or even centuries, is the so-called equilibrium plateau regime. The aging rate is extracted from the time dependent change of an appropriate thermodynamic property in the intermediate regime. It is known that for linear chain polymer systems the temperature dependence of the aging rate is non-monotonic, that depends on the aging temperature, T_{age}, relative to T_g, $\Delta T_A = T_{age} - T_g$. The aging rate exhibits a maximum in aging rate at a threshold departure from T_g, ΔT_{th}. This maximum is due to two competing

mechanisms. The driving force for return to equilibrium increases with increasing $|\Delta T_A|$. However with decreasing T_{age}, increasing departure, the loss of thermal energy, $k_B T$, reduces the relaxation rates, thereby reducing the rate of recovery.

A number of different models have been applied over the years in order to account for the structural relaxation behavior in the glassy state. A number of models have relied on the observation that the volume contraction is related to a characteristic relaxation time of the material in the glassy state, such as the Kovacs,[7] Struik,[5] or KAHR[2] based models. In which it is assumed in the glassy state that there is a distribution of relaxation times that Hutchinson[1] suggested could represent a distribution of free volume. A number of other models, first suggested by Alfrey et al.[8] and later extended by Curro, Lagasse and Simha,[9] explain the volume recovery through a vacancy diffusion mechanism. In this case it is assumed that free volume in the glassy material can transport through a vacancy diffusion mechanism, which can later annihilate at a free surface, an external interface or through a lattice contraction mechanism. A combination of either external annihilation and lattice contraction[10-12] or a time dependent length scale[13] has been employed to account for the thickness dependence in free standing polymer films. However, in order to account for the experimental results in bulk material, it is assumed that the vacancies must annihilate at an internal interface.[14-16] It was suggested recently that such internal interfaces can be found in terms of fluctuations in density. Recent molecular dynamics simulations of glass forming liquids, have demonstrated that although there are large scale fluctuations in elastic properties of a glass quenched from the melt state, there are no long range fluctuations in the density.[17] Therefore, to date there are many open questions as to the physical mechanism responsible for the structural relaxations in the glassy state.

Although there are numbers of direct studies that have experimentally shown the influence of the departure from equilibrium on the average physical aging rate, there is very little experimental evidence to connect the glassy dynamics, relaxation rates, to the physical aging rate.[18] A number of studies have attempted to connect the segmental relaxations above T_g to the glassy dynamics, as outlined in a recent review.[18] Other studies have demonstrated a connection through time-temperature superposition.[19] The connection between glassy dynamics and physical aging has also been demonstrated

through simulations.[20] In a recent study, a connection was made between the reductions in the strength of the β-relaxation in poly methyl methacrylate (PMMA) nanocomposites and reduced aging rates.[21] However a number of polymers such as polystyrene do not show evidence of strong evidence of a β-relaxation and PMMA and other polymers still observe physical aging below the β-transition temperature, it is unclear what the connection is between aging and a β-relaxation. To this end, there is still a lack of direct experimental evidence providing a connection between glassy dynamics and the physical aging rate of polymers; and is a subject in need of further investigation.

These relaxation times, which may occur on time-scales from hours to years depending on the depth of quench and dimensions of the sample,[1] have been investigated using various techniques that probe time-dependent changes in thermodynamic properties: volume relaxation experiments,[22] measurements of dielectric strength[15] and enthalpy recovery,[23] as well as fluorescence measurements.[4] Different phenomenological, and statistical mechanical, models based on various mechanisms, have been proposed; they each describe the phenomenon with varying degrees of success.[9, 11, 13, 15, 16, 24,25, 26 1, 27, 28] Because of its technological and scientific importance, regarding the longevity and stability of polymers in the glassy state, this continues to be an active area of research.

Several studies have shown the aging behavior of materials depend on their chemical structures, which influences, chain stiffness and the fractional free volume.[22,29, 30 31] The aging rate has also been suggested to be influenced by sub-T_g relaxations, such as on β and γ relaxations in PMMA.[22] While for linear chain polymers the aging rate is independent of molecular weight, the rates for star-shaped polymers are significantly slower than their linear chain polymer analogs.[32]

An important question surrounding glassy structural relaxation polymeric materials is the physical mechanism responsible for this process. In order to investigate this, we studied the aging of star-shaped molecules with functionalities, $f \leq 64$ arms, each with a comparable degree of polymerization per arm, $N_{arm} \sim 100$. When aging occurs at temperatures close to T_g, the physical aging rates, β, are independent of f; however for increasing ΔT_A, dependence on f is significant. The threshold distance ΔT_{th} from T_g that the rates exhibit a maxima, decreases with increasing f. These observations are reconciled

in terms of changes in the in glassy dynamics of the macromolecules, as measured using inelastic neutron scattering.

4.2 EXPERIMENTAL SECTION

4.2.1 Materials

We synthesized the high functionality star-shaped PS (with $f \geq 8$) by means of anionic polymerization using high vacuum techniques.[33, 34 35] The linear polystyrene (PS) molecules and 3, 4 and 8-arm star-shaped PS molecules were purchased from Pressure Chemical and Polymer Source, respectively.

4.2.2 Sample Preparation

Supported films, each one micron in thickness, were spin-coated from toluene solutions onto pre-cleaned silicon wafers (Wafer World Inc.) with a native oxide layer of 1.5 nm. Prior to spin coating the silicon wafers were cleaned by rinsing with ethanol and acetone followed by UV-ozone treatment for 3 minutes. The wafers were then rinsed with toluene immediately prior to spin-coating. The samples were then annealed 50K above their T_g's for 48 hours. The polymer film thicknesses were measured using variable angle spectroscopic ellipsometry, VASE (M-2000, J.A. Woollam Co.).

4.2.3 Spectroscopic Ellipsometry

The glass transition temperature and thermal expansion coefficient of each supported film was extracted from data obtained from measurements of the change in film thickness during cooling from 423K down to room temperature, at a rate of 1K/min. using the VASE instrument equipped with an Instec heating stage. During the measurements, which were performed at a fixed angle of 70^o, the samples were under a nitrogen purge gas environment; liquid nitrogen was used in order to maintain the temperature and cooling rate. The thickness, $h(T)$, and refractive index, $n(T)$, were determined by fitting the ellipsometric angles Δ and Ψ to a Cauchy/SiO2/Si model over the wavelengths of 400-1700 nm. The glass transition temperature was determined by the intersection of extrapolated linear fits through the glassy and rubbery regions of the data.[36, 37] The thermal expansion coefficients of the glassy and rubbery states were determined by normalizing the slope from the linear fit by $h(T$=30K).

The physical aging experiments were conducted on the films using VASE. Each sample was first heated to a temperature of 50K above their T_g's and annealed for 30 minutes to remove any thermal history. It was then quenched at a rate of 85 K/min. to room temperature and then ramped to the aging temperature, T_{age}, where the sample thickness, *h*, was monitored as a function of time. An acquisition time of 30 seconds was used to measure the thickness every 60 seconds. The experimental time of 360 minutes was used in this study, which has been reported to be sufficient to determine the average aging rate of the material within the experimental error.[38] Each experiment was repeated for a total of 3-5 times at each aging temperature in order to ensure that that the results were reproducible. The aging rate was then reported as the average of all of the aging tests.

4.2.4 Incoherent Neutron Scattering

Incoherent neutron scattering (INS) measurements were performed on the high-flux backscatter spectrometer (HFBS) at the NG2 beam line at the NIST Center for Neutron Research. The HFBS has a resolution of 0.85 μeV which means that the motions that it picks up are faster than 200 MHz (10 ns). The scattering cross section of hydrogen atoms is approximately 20 times larger than that of carbon (polymer backbone) or oxygen (dendritic core) and more than 40 times larger than that of silicon (dendritic core) and aluminum (canister). Therefore, the signal obtained from incoherent scattering is from the atomic scale motions of hydrogen atoms. The polymer powder was wrapped tightly in aluminum foil and then pressed firmly to the walls of the aluminum canister. The canister was then sealed within an argon atmosphere. The spectrometer operates with a monochromatic neutron beam with a wavelength of 6.271Å over a *Q* range of 0.25-1.75 $Å^{-1}$. The INS experiments were conducted using fixed window scans (FWS) in order to investigate elastic scattering.

The FWS experiments were performed with the Doppler turned off; therefore the incident and scattered neutron energies were fixed and equal, thereby enabling measurement of the elastically scattered neutrons. These measurements were performed while ramping the temperature at a rate of 1 K/min., from 30 K to 450K. The elastic scattering intensity was recorded as a function of *Q* by averaging over the signal in bins of 1K.

The mean square displacement, ‹μ^2›, of the hydrogen atoms were approximated using the Debye-Waller approximation:

$$I_{inc}(Q) \propto e^{-(1/3)Q^2\left\langle \mu^2 \right\rangle} \tag{4.1}$$

where Q is the momentum transfer vector. Although the dynamics of polymers are inherently anharmonic, the Debye-Waller approximation can be applied to the range of 0.09 Å^{-2} < Q^2 < 1Å^{-2}, as has previously been done in the literature,[39-44] in order to obtain an approximation of the ‹μ^2› in the glassy state.

4.3 RESULTS AND DISCUSSION

The changes in film thickness as measured by ellipsometry are plotted in Figure 4.1 as a function of aging time for star-shaped molecules with N_{arm} ~ 100 and varying functionalities. The aging rate is defined as:

$$\beta_{vol.} = \frac{1}{h_\infty}\frac{dh}{d\log(t_{age})} \tag{4.2}$$

where h_∞ is the film thickness at equilibrium and t_{age} is the aging time.[45] The data shown in Figure 4.1 demonstrates that the aging rate at a constant temperature relative to T_g of the material is strongly dependent on the functionality of the molecule; the aging rate decreases as f increases. It was previously demonstrated that the physical aging behavior is independent of the total molecular weight for linear macromolecules at a constant temperature relative to T_g.[32]

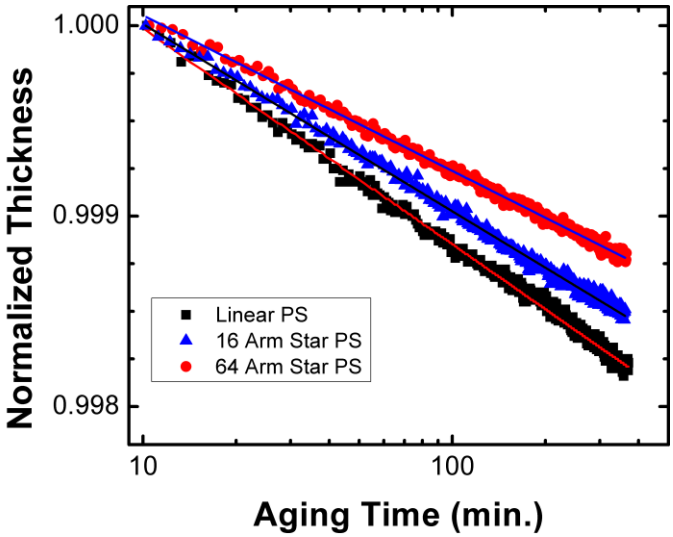

Figure 4.1 Aging experiments conducted at ΔT_A = -25K with molecules of a constant N_{arm} = 100; the change in film thickness, normalized by the film thickness at 10 minutes, as a function of the aging time. The solid lines represent fittings to obtain the aging rate.

The aging rates plotted in Figure 4.2 were calculated using equation 4.2, for the molecules used in this study. These rates are plotted as a function of ΔT_A, where a non-monotonic dependence on ΔT_A is observed, as explained in the introduction. At temperatures close to the T_g (small $|\Delta T_A|$), the aging rate is independent of chain architecture while for temperature well below T_g (larger $|\Delta T_A|$) the aging rates exhibit a strong dependence on functionality. We understand these influences of chain architecture in terms of the competing effects that give rise to the maximum in structural relaxation rate.

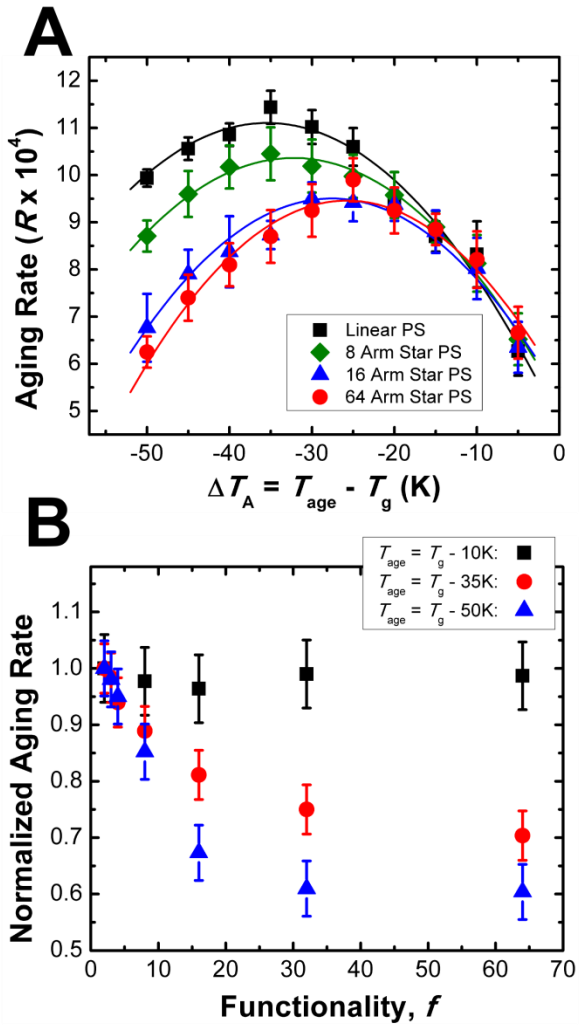

Figure 4.2 (A) The aging rate calculated from volumetric aging experiments as a function of aging temperature. (B) The aging rate, normalized by the aging rate of linear PS as a function of the number of arms, functionality at various temperatures. The closed symbols are determined from ellipsometry and the open symbols are calculated from DSC.

The departure from equilibrium at a given ΔT_A, which is the driving force for aging, may be estimated from the thermal expansion coefficients as measured using ellipsometry (Figure 4.3). This is based on the assumption that the equilibrium volume is simply the extrapolation of the rubbery thermal expansion into the glassy state,[1, 5, 22, 45] and the departure of equilibrium, δ, is $\delta = h_0/(h_0-h_\infty)$. The departure δ is plotted as a function of f in Figure 4.3, for different aging temperatures. δ, and hence the driving force for aging, appear to be independent of chain architecture. It is important to emphasize that the thermal expansion coefficient, as measured by ellipsometry, in both the rubbery

and glassy regimes is independent of chain architecture, consistent with previous work.[46] Moreover, though the thermal expansion coefficients were measured upon cooling at 1 K/min. the same trends were observed when measuring at different cooling rates, ranging from 0.1 to 10 K/min. The fact that the driving force for aging appears to be independent of f can explain that at small $|\Delta T_A|$ the aging rate is independent of chain architecture.

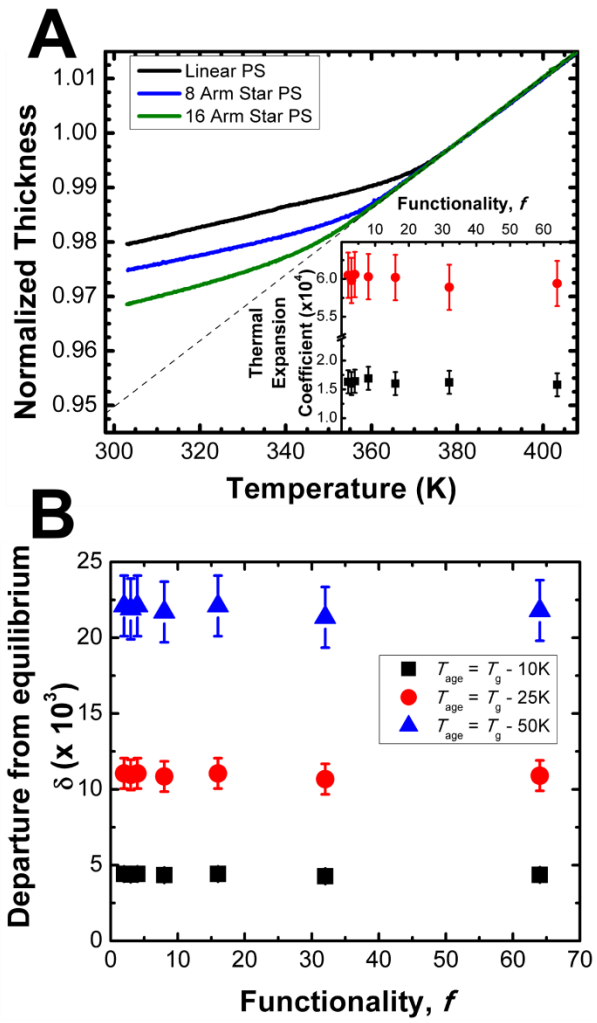

Figure 4.3 (A) The temperature dependence of the film thickness for the star shaped molecules. The inset shows the thermal expansion coefficient, calculated from the slope of the thickness curves as a function of the functionality. (B) The departure from equilibrium at 3 different aging temperatures.

In order to understand the influence of chain architecture on the physical aging rate in the low temperature regime, we need to turn our attention to the mechanism for formation of a glass. It has been well reported in the literature that an amorphous material

in the glass state maintains heterogeneity in dynamics which is especially prominent as temperature approaches the glass transition.[47-51] The notion presides that as temperature decreases there is a growth of clusters of cooperatively rearranging regions (CRR).[50] These CRRs observe two different characteristic times scales representing slow and fast moving regions. The size of these regions, and therefore the difference between time scales grow with decreasing temperature. This divergence as temperature approaches T_g leads to the breakdown of the Stokes-Einstein relation.[48, 51] It is the faster moving "mobile" regions that account for the diffusive motion in the material, and the slower moving "immobile" regions that account for the structural relaxation of the material. It is also the "immobile" clusters that are also responsible for the mechanical strength of the material. The dynamic heterogeneity observed in melts that is often associated with the heterogeneity in free volume in polymer glasses. However a recent simulation demonstrated that while there is a large scale distribution in local compliance of the material, no large scale fluctuations in the free volume were observed.[17] It is those same heterogeneities in elastic properties that may also be responsible for the structural relaxation behavior in the material. The local elastic properties of the material can be associated with atomic vibrations of the atoms, according to the Debye-Waller factor, $\kappa = 3k_BT/\langle\mu^2\rangle$,[52] where the harmonic force constant, κ, is a measure of the resistance to atomic vibrations. The mean square displacement of atomic vibrations, $\langle\mu^2\rangle$, can readily be measured using incoherent neutron scattering.

The temperature dependence of the $\langle\mu^2\rangle$ for linear PS and star-shaped molecules of varying functionality were determined and are shown in Figure 4.4. It is evident that the $\langle\mu^2\rangle$ is smaller for the star-shaped molecules than for linear PS. It is also apparent that they observe different temperature dependences. In order to understand this, we employ an analysis that has been used in order to directly compare the different molecules through a harmonic force constant. At temperatures below 250K, a similar analysis has been employed to other polymeric systems.[53-55] Here we assume that the motions hydrogen atoms are harmonically oscillating in a potential well. We note that at high temperatures this assumption would not hold, but it has been shown previously that for PS and other polymers this assumption is reasonable at temperatures less than 250K. This assumption is consistent with a linear increase in the $\langle\mu^2\rangle$ as a function of temperature and

therefore the harmonic force constant is proportional to the inverse of the slope of such an increase as is depicted in Figure 4.4. The resistance to displacement, stiffness, can be quantified in terms a harmonic force constant: $\kappa = 3k_BT/\langle\mu^2\rangle$. Therefore, slope of the increase in $\langle\mu^2\rangle$ is inversely proportional to κ. The linear chain PS molecules exhibited the largest increase with temperature within this temperature range, consequently it has the lowest force constant, κ = 1.2 N/m. The harmonic force constant was found to gradually increase with functionality up to 2.1 N/m for the 64 arm star.

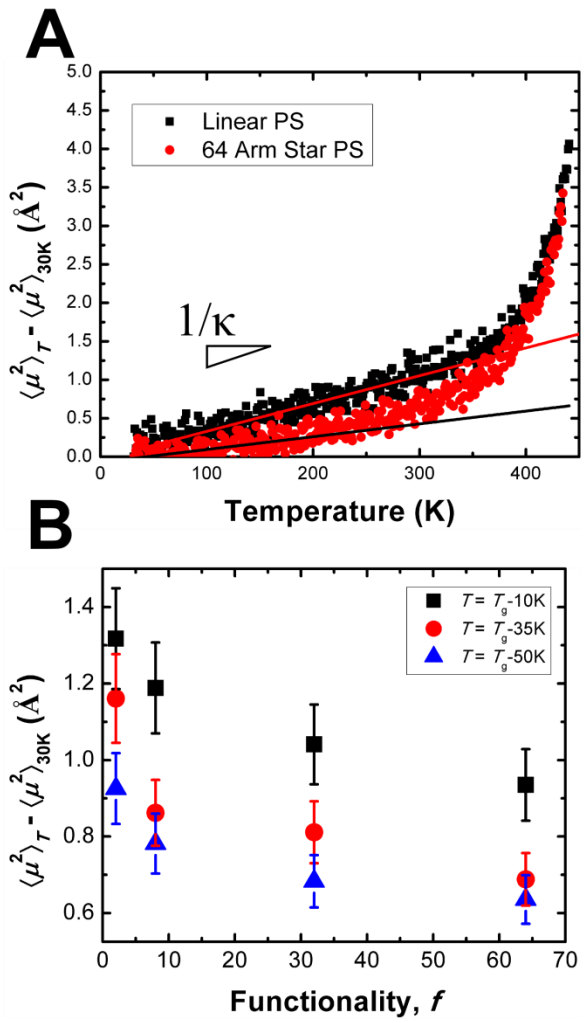

Figure 4.4 (A) The $\langle\mu^2\rangle$ as a function of temperature for linear PS (black squares) and the 64 arm star PS (red circles). The solid lines represent fittings to harmonic force constant from T=30-250K. (B) The $\langle\mu^2\rangle$ as a function of the number of arms for a constant at 3 different temperatures relative to T_g.

The $\langle\mu^2\rangle$ is shown as a function of *f* at several temperatures in which the aging experiments were conducted. It was observed that there was a monotonic decrease in the

mean square displacements, or equivalently the increase of the force constants, with increasing functionality. The polymer chains are connected to a branch point and the atomic displacements of star-shaped polymers are hindered due to this loss of entropy, due to packing constraints imposed by the branching point. This effect will monotonically increase with increasing *f*. Linear chain polymer monomers have a higher degree of entropy. It is also apparent that there is a strong correlation in the trends with aging rates shown in Figure 4.2 and the $\langle\mu^2\rangle$ depicted in Figure 4.4. It is clear, nevertheless, from these measurements that the slower physical aging is connected to/correlated with the restricted atomic vibrations and enhanced local elastic properties of the star-shaped molecules. This correlation is further shown, by comparing the harmonic force constant with the physical aging rate measured at the lowest temperature, which should be the most dependent on the restriction of segmental motions. In order to further this correlation, three different 64 arm stars are also shown, with varying molecular weights of the arm ranging from 9 kg/mol. to 80 kg/mol. If the argument holds, as the molecular weight of the arm is increased, the restriction of the segmental motions should be less significant. It is shown in Figure 4.5 that there is a strong correlation between the harmonic force constant and the physical aging rate measured at ΔT_A = -50K.

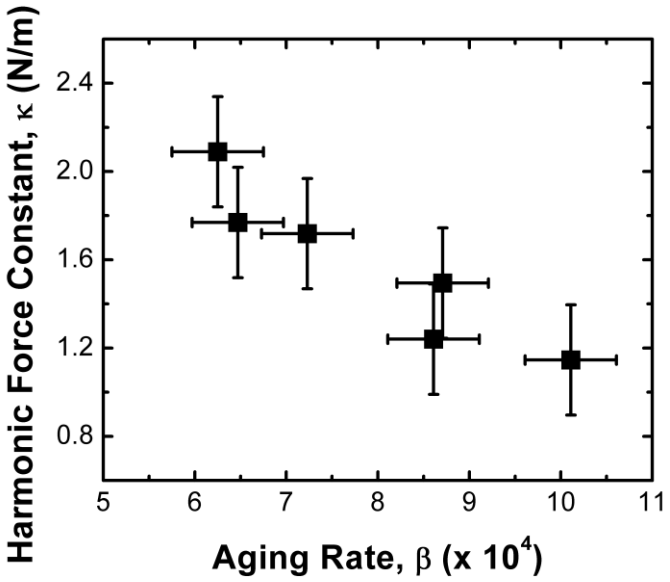

Figure 4.5 The harmonic force constant estimated from the $\langle\mu^2\rangle$ between 30 and 250 K plotted as a function of the average aging rate measured at ΔT_A = -50K, where the influence of the restriction of segmental motions dominates the physical aging rate.

Now that we have discussed how the competing effects governing the non-monotonic temperature behavior of the physical aging rate with regards to chain architecture, we turn our attention to the position of the maximum aging rate, ΔT_{th}. With regards to the ΔT_{th} value, the maximum in aging rate shifts to lower ΔT_{th} values with increasing *f*, as seen in Figure 4.2. As the driving force for aging is independent of chain architecture and the only factor that changes with architecture is the glassy dynamics, which is shown in Figure 4.4. As seen from the INS experiments, as the functionality is increased the temperature dependence of the $\langle \mu^2 \rangle$ is decreased (inverse of the harmonic force constant). Therefore the influence of chain architecture on the temperature dependence of the glassy dynamics causes the maximum in aging rate to shift to higher temperatures. This implies that as the number of arms is increased the reduction in glassy segmental relaxations influences the average physical aging rate to higher temperatures.

4.4 CONCLUSIONS

In conclusion the structural relaxations of star-shaped polymers with comparable N_{arm} and functionalities up to 64 exhibits significantly lower aging rates than their linear analogs. The physical aging rate at low temperatures was demonstrated experimentally to be connected to glassy segmental dynamics which were measured to be significantly slower for star-shaped molecules by incoherent neutron scattering. It was also demonstrated that the temperature dependence of the glassy dynamics, encompassed within the inverse of the harmonic force constant, was twice as large for the linear chain polymer; thus resulting in a shift in the maximum of the aging rate to higher temperatures for star-shaped molecules.

4.5 REFERENCES

1. Hutchinson, J. M. *Progress in Polymer Science* **1995,** 20, (4), 703-760.
2. Kovacs, A. J.; Aklonis, J. J.; Hutchinson, J. M.; Ramos, A. R. *Journal of Polymer Science Part B-Polymer Physics* **1979,** 17, (7), 1097-1162.
3. Hodge, I. M. *Science* **1995,** 267, (5206), 1945-1947.
4. Priestley, R. D.; Ellison, C. J.; Broadbelt, L. J.; Torkelson, J. M. *Science* **2005,** 309, (5733), 456-459.
5. Struik, L. C. E., *Physical Aging in Amorphous polymers*. Elsevier Scientific Publishing Company: Amsterdam, 1978.
6. McKenna, G. B. *Journal of Physics-Condensed Matter* **2003,** 15, (11), S737-S763.
7. Kovacs, A. J. *Annals of the New York Academy of Sciences* **1981,** 371, (OCT), 38-66.
8. Alfrey, T.; Goldfinger, G.; Mark, H. *Journal of Applied Physics* **1943,** 14, (12), 700-705.
9. Curro, J. G.; Lagasse, R. R.; Simha, R. *Macromolecules* **1982,** 15, (6), 1621-1626.
10. McCaig, M. S.; Paul, D. R. *Polymer* **2000,** 41, (2), 629-637.
11. McCaig, M. S.; Paul, D. R.; Barlow, J. W. *Polymer* **2000,** 41, (2), 639-648.
12. Huang, Y.; Paul, D. R. *Polymer* **2004,** 45, (25), 8377-8393.
13. Thornton, A. W.; Hill, A. J. *Industrial & Engineering Chemistry Research* **2010,** 49, (23), 12119-12124.
14. Boucher, V. M.; Cangialosi, D.; Alegria, A.; Colmenero, J. *Macromolecules* **2012,** 45, (12), 5296-5306.
15. Cangialosi, D.; Wubbenhorst, M.; Groenewold, J.; Mendes, E.; Picken, S. J. *Journal of Non-Crystalline Solids* **2005,** 351, (33-36), 2605-2610.
16. Cangialosi, D.; Wubbenhorst, M.; Groenewold, J.; Mendes, E.; Schut, H.; van Veen, A.; Picken, S. J. *Physical Review B* **2004,** 70, (22), 224213.
17. Riggleman, R. A.; Douglas, J. F.; de Pablo, J. J. *Soft Matter* **2010,** 6, (2), 292.
18. Cangialosi, D.; Boucher, V. M.; Alegria, A.; Colmenero, J. *Soft Matter* **2013,** 9, (36), 8619-8630.
19. Lee, A.; Lichtenhan, J. D. *Macromolecules* **1998,** 31, (15), 4970-4974.
20. Pryamitsyn, V.; Ganesan, V. *Macromolecules* **2010,** 43, (13), 5851-5862.
21. Priestley, R. D.; Rittigstein, P.; Broadbelt, L. J.; Fukao, K.; Torkelson, J. M. *Journal of Physics-Condensed Matter* **2007,** 19, (20).
22. Greiner, R.; Schwarzl, F. R. *Rheologica Acta* **1984,** 23, (4), 378-395.
23. Hodge, I. M. *Journal of Non-Crystalline Solids* **1994,** 169, (3), 211-266.
24. Cangialosi, D.; Boucher, V. M.; Alegria, A.; Colmenero, J. *Journal of Chemical Physics* **2011,** 135, (1), 014901.
25. Chen, K.; Schweizer, K. S. *Physical Review Letters* **2007,** 98, (16).
26. Chen, K.; Schweizer, K. S. *Physical Review E* **2008,** 78, (3).
27. Petrie, S. E. B. *Journal of Polymer Science Part a-2-Polymer Physics* **1972,** 10, (7), 1255-1272.
28. Hadac, J.; Slobodian, P.; Riha, P.; Saha, P.; Rychwalski, R. W.; Emri, I.; Kubat, J. *Journal of Non-Crystalline Solids* **2007,** 353, (28), 2681-2691.

29. Huang, Y.; Wang, X.; Paul, D. R. *Journal of Membrane Science* **2006,** 277, (1-2), 219-229.
30. Rowe, B. W.; Pas, S. J.; Hill, A. J.; Suzuki, R.; Freeman, B. D.; Paul, D. R. *Polymer* **2009,** 50, (25), 6149-6156.
31. Levita, G.; Struik, L. C. E. *Polymer* **1983,** 24, (8), 1071-1074.
32. Frieberg, B.; Glynos, E.; Sakellariou, G.; Green, P. F. *Acs Macro Letters* **2012,** 1, (5), 636-640.
33. Hadjichristidis, N.; Iatrou, H.; Pispas, S.; Pitsikalis, M. *Journal of Polymer Science Part a-Polymer Chemistry* **2000,** 38, (18), 3211-3234.
34. Uhrig, D.; Mays, J. W. *Journal of Polymer Science Part a-Polymer Chemistry* **2005,** 43, (24), 6179-6222.
35. Roovers, J.; Zhou, L. L.; Toporowski, P. M.; Vanderzwan, M.; Iatrou, H.; Hadjichristidis, N. *Macromolecules* **1993,** 26, (16), 4324-4331.
36. Kawana, S.; Jones, R. A. L. *Physical Review E* **2001,** 63, (2).
37. Forrest, J. A.; DalnokiVeress, K.; Dutcher, J. R. *Physical Review E* **1997,** 56, (5), 5705-5716.
38. Pye, J. E.; Rohald, K. A.; Baker, E. A.; Roth, C. B. *Macromolecules* **2010,** 43, (19), 8296-8303.
39. Angell, C. A.; Ngai, K. L.; McKenna, G. B.; McMillan, P. F.; Martin, S. W. *Journal of Applied Physics* **2000,** 88, (6), 3113-3157.
40. Colmenero, J.; Arbe, A. *Physical Review B* **1998,** 57, (21), 13508-13513.
41. Frick, B.; Richter, D. *Science* **1995,** 267, (5206), 1939-1945.
42. Soles, C. L.; Douglas, J. F.; Wu, W. L. *Journal of Polymer Science Part B-Polymer Physics* **2004,** 42, (17), 3218-3234.
43. Soles, C. L.; Douglas, J. F.; Wu, W. L.; Dimeo, R. M. *Physical Review Letters* **2002,** 88, (3).
44. Soles, C. L.; Douglas, J. F.; Wu, W. L.; Peng, H. G.; Gidley, D. W. *Macromolecules* **2004,** 37, (8), 2890-2900.
45. Baker, E. A.; Rittigstein, P.; Torkelson, J. M.; Roth, C. B. *Journal of Polymer Science Part B-Polymer Physics* **2009,** 47, (24), 2509-2519.
46. Qian, Z. Y.; Minnikanti, V. S.; Sauer, B. B.; Dee, G. T.; Archer, L. A. *Macromolecules* **2008,** 41, (13), 5007-5013.
47. Long, D.; Lequeux, F. *European Physical Journal E* **2001,** 4, (3), 371-387.
48. Ediger, M. D. *Annual Review of Physical Chemistry* **2000,** 51, 99-128.
49. Berthier, L.; Biroli, G. *Reviews of Modern Physics* **2011,** 83, (2), 587-645.
50. Adam, G.; Gibbs, J. H. *Journal of Chemical Physics* **1965,** 43, (1), 139-&.
51. Starr, F. W.; Douglas, J. F.; Sastry, S. *Journal of Chemical Physics* **2013,** 138, (12).
52. Zaccai, G. *Science* **2000,** 288, (5471), 1604-1607.
53. Soles, C.; Douglas, J.; Wu, W. l.; Dimeo, R. *Physical Review Letters* **2002,** 88, (3).
54. Soles, C. L.; Douglas, J. F.; Wu, W.-L. *Journal of Polymer Science Part B: Polymer Physics* **2004,** 42, (17), 3218-3234.
55. Kropka, J. M.; Sakai, V. G.; Green, P. F. *Nano Letters* **2008,** 8, (4), 1061-1065.

CHAPTER 5
STRUCTURAL RELAXATIONS OF THIN POLYMER FILMS

Reprinted with permission from:

Frieberg, B.; Glynos, E.; Green, P.F.; *Phys. Rev. Lett.* **2012**, 108, 268304-1 – 268304-4.

5.1 INTRODUCTION

When a liquid is quenched at a sufficiently rapid rate to a temperature T below its glass transition temperature, T_g, it forms a glass. Some systems, such as atactic polymers, by virtue of their molecular structure, form glasses upon solidification, regardless of quenching rates. In this non-ergodic state, at $T<T_g$, the material possesses excess thermodynamic properties. At such a temperature, the glass structurally relaxes toward equilibrium, accompanied by time dependent changes in physical properties.[1-4] This phenomenon, known as physical aging, has been studied in material systems for decades. The long-term structural stability of glasses, regardless of chemical structure, is important for their functionality and reliability in different technologies.

The driving force for physical aging depends on the difference between T_g and the temperature T_{age}, $\Delta T_A=T_{age}-T_g$, at which the sample is held during aging. The aging rate, β, is zero when $\Delta T_A\approx 0$ and increases with increasing magnitude of ΔT_A; it exhibits a maximum before approaching zero again as ΔT_A is increased further.[5-7] The maximum is believed to be due to a competition between the increasing driving force for aging, ΔT_A, with decreasing temperature and the thermally activated molecular relaxations that

accommodate the recovery of the system, which decrease with decreasing aging temperature, T_{age}.[8]

While the phenomenon of aging has been studied in the bulk for decades,[1, 4, 7, 9] there has recently been a keen interest in thin polymer films, for both scientific and technological reasons.[2, 6, 10] The challenge associated with thin films is that the interfaces (substrates or free surface) influence the local monomer segmental packing density, and configurational entropies.[11-15] A natural consequence of such effects associated with monomer-interface interactions is that the average T_g of polymer thin films is a function of its thickness H; this thickness dependence is well documented by experiment,[16-18] theory and simulations.[11-15, 19] For thin supported films of linear chains on a non-wetting substrate, e.g. polystyrene (PS) on silicon oxide (PS/SiO_x), [18-21] the average glass transition temperature of a film of thickness H, $T_g(H)$, decreases with decreasing H ($\Delta T_g < 0$).[16, 18, 20-23] Conversely, when the monomer-substrate interactions are strong, such as poly(methyl methacrylate) (PMMA) on SiO_x substrates, due to hydrogen-bonding between the polymer and the SiO_x, the average $T_g(H)$ increases with decreasing H ($\Delta T_g>0$).[11-15, 18, 22-24]

It was evident from the work of Kawana and Jones, who examined the PS/SiO_x system, which due to the existence of a low T_g surface layer, T_g^{surf}, the aging of the interior of the film would occur at a different rate than the free surface.[6, 8, 10, 25] Priestley *et. al*. subsequently showed that in the $PMMA/SiO_x$ thin film system, the aging rate decreased by factors of 2 and 15, at the free surface and substrate, respectively.[2] These measurements were performed at a single aging temperature, where $\Delta T_A \sim -80°C$. The slow aging of the film was reconciled by considering that near the free surface the driving force is lower than the bulk because $(T_g^{surf} - T_{age}) < (T_g(H) - T_{age})$. Additionally, the reduction of the aging rate at the substrate stems from the reduced cooperative segmental mobility at the substrate.[2] Through a more extensive study of the PS/SiO_x system, over a wide range of aging temperatures, Pye *et. al.* showed that the physical aging rate of PS films of H=30 nm was slow, for all temperatures, relative to the bulk.[6] They interpreted their observations by assuming that the relevant parameters are a mobile surface layer of characteristic thickness, H_{FS}, that does not age, and that the remainder of the film exhibits the bulk aging rate. The existence of a liquid-like surface layer, with the remaining

sample possessing a bulk T_g, has been used to explain the thickness dependent behavior of T_g.[26, 27]

The differences between the chemical structures and associated differences between the monomer-interface interactions are responsible for the differences of the values of T_g^{surf} and $T_g(H)$ for PS/SiO_x and for PMMA/SiO_x. Therefore, in light of the foregoing discussion, it is not immediately obvious how to reconcile the fact that both PS/SiO_x and PMMA/SiO_x thin films age slowly compared to thicker films and to the bulk.

Recently it was shown that for star-shaped polystyrene, changes only in the functionality, f, (number of arms) and the degree of polymerization, N_{arm}, of the macromolecule, would lead to increases or decreases in T_g^{surf}, relative to the bulk.[28, 29] The magnitudes of the changes in $T_g(H)$ with H for these star-shaped macromolecules are the same as those exhibited linear chain PS and PMMA macromolecules on the same substrates. It follows that the behavior of the star-shaped polymer systems provides an opportunity to examine how changes in the local T_g affect the aging of thin films, in the absence of the added complication of differences in chemical structure. Through a study involving a range of values of T_{age}, and samples of different f and N_{arm}, we show that by accounting for the continuous depth dependence of the T_g of thin films the slow physical aging behavior of all these systems could be rationalized in terms of a universal picture. Our study also reveals that the aging rate of star-shaped macromolecules is slow compared to their linear PS analogs. This is noteworthy because it is now apparent that the aging rate in materials may be controlled by changes in the architecture and size of the macromolecule.

5.2 EXPERIMENTAL SECTION

5.2.1 Materials

The physical aging of linear and star-shaped polystyrene (PS) macromolecular thin films of thicknesses 50nm < H < 1000 nm supported by SiO_x substrates were examined using *in situ* spectroscopic ellipsometry (SE). Linear PS of molecular weight of 152 kg/mol. (LPS-152K) and star-shaped PS, possessing eight arms each of molecular

weight M_{arm}= 10 kg/mol. and M_{arm} =25 kg/mol. were studied. The (SPS-8-10K and SPS-8-25K) was purchased from Polymer Source Inc. This particular star-shaped polymer was chosen because it exhibits a surface T_g that is appreciably higher than the bulk, and is well characterized.[28] Moreover, its average T_g increases with decreasing H. In contrast average T_g's the linear chain PS decrease with decreasing H.

5.2.2 Sample Preparation

The films were prepared by spin casting filtered (through 0.2 μm Teflon Millipore filters) polymer/toluene solutions onto SiO_x wafers ($\langle 100 \rangle$ oriented silicon wafers, purchased from Wafer World Inc.), possessing a native oxide layer of 1.5 nm. Each sample was annealed in vacuum for at least 24 hours at ~30°C above the T_g of bulk LPS-152K to remove any residual solvent.

5.2.3 Sample Characterization

The temperature dependence of the thickness, H, and refractive index, n, of all the films was determined by fitting the acquired ellipsometric angles Δ and Ψ to a Cauchy/SiO_x/Si model over the entire measured spectral range (wavelength range 400 - 1700 nm) using a variable angle spectroscopic ellipsometer (M-2000, J.A. Woollam Co.). The ellipsometer was equipped with an Instec heating stage. In all experiments, measurements were taken while the samples were cooled from temperatures of approximately 150°C at 1°C/min. The T_g of each film was determined from the H vs. T data, as described in prior publications.[28]

After the T_g measurements were performed on a sample, all subsequent aging experiments were completed *without moving the sample in the chambe*r, in order to ensure that the same spot on the film was being measured at each T_{age}. The films were then heated to 40°C above the average T_g for 30 min.; this removed all thermal history. The sample was then quenched to room temperature (at ~85°C/min.), while its thickness and refractive index were continuously monitored. The temperature of each sample was then rapidly ramped to the desired aging temperature. Its thickness was determined by averaging over an acquisition time of 30 seconds, while taking measurements every 60 seconds throughout the duration of the experiment (360 minutes). Each physical aging

rate that is reported is the result of an average of 3-5 aging tests. This ensured the reliability of the reported values.

5.3 RESULTS AND DISCUSSION

The physical aging of linear and star-shaped polystyrene (PS) macromolecular thin films of various thicknesses, H, where 50 nm < H < 1 micron, supported by silicon oxide substrates, were examined using *in situ* spectroscopic ellipsometry (SE) by monitoring the change in H at a constant $T_{age}<T_g$, with time. Linear PS of molecular weight of M_w=152 kg/mol. (LPS-152K) and two 8-arm star-shaped PS macromolecules: one with M_{arm}= 10 kg/mol. (SPS-8-10K) and the other with 25 kg/mol. (SPS-8-25K), were investigated. The SPS-8-10K polymer was chosen because its T_g^{surf} and T_g^{subst} are appreciably higher than the bulk.[28] Recall, in contrast, that for linear chain PS, supported by the same substrates, T_g^{surf} is appreciably lower than the bulk and its T_g^{subst} is comparable to the bulk. The T_g^{surf} of the SPS-8-25K sample is comparable to its bulk value whereas its T_g^{subst} is slightly higher than the bulk. In short, we investigate the behavior of three systems of the same chemical structure, but different architecture, and consequently very different interfacial and bulk T_g's.

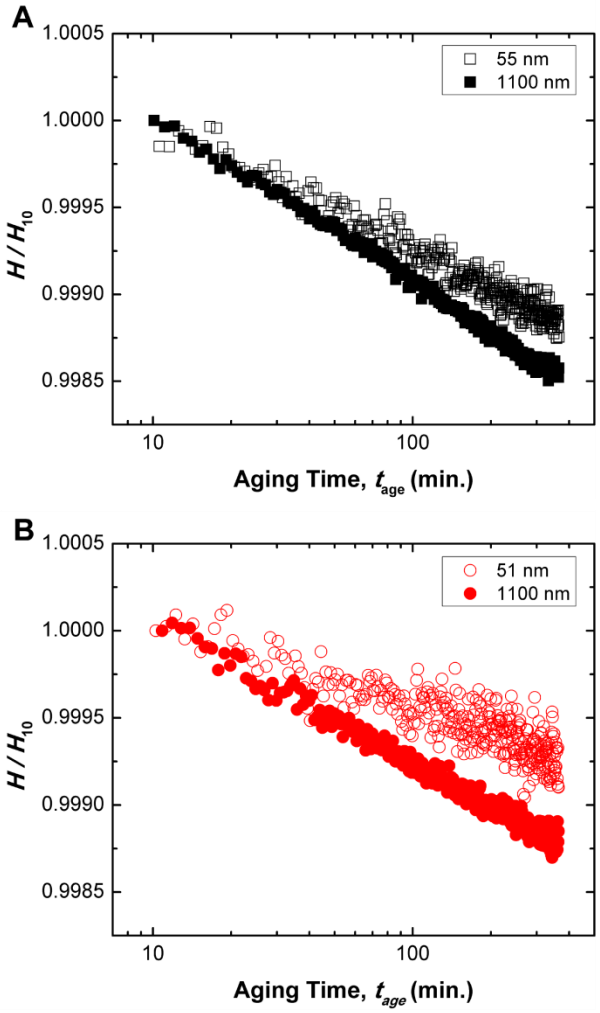

Figure 5.1 H(t)/H(tage=10 minutes) is plotted as a function of aging time, for films ((A) LPS-152K and (B) SPS-8-10K) of two different thicknesses. Measurements were performed at Tg-Tage=-50°C.

Ellipsometry measurements of the normalized thickness, $H(t_{age})/H(t_{age}=10)$, dependencies on time, t_{age}, for LPS-152K and SPS-8-10K films and for two different thicknesses are shown in Figure 5.1. The thinner film (initial thicknesses H_0~50 nm) exhibits a weaker dependence on time than the thicker (H_0~1100 nm) film. Note that in this figure, $t_{age} = t - t_0$ is plotted instead of t, since during the initial stage of any aging experiment the thickness is constant in this so-called initial plateau regime.[10] The width of the plateau region increases with decreasing T_{age}.[7, 30] The physical aging rate exhibits a logarithmic dependence on time and is well described by:

$$\beta = (-1/H_\infty)\, dH(t_{age}) / d(\log t_{age}) \qquad (5.1)$$

where H_∞ is the "equilibrium" film thickness.[5] We note that the aging rate of the LPS-152K system is consistent with the data previously described by Pye *et. al.*, who also studied the aging of linear PS.[6]

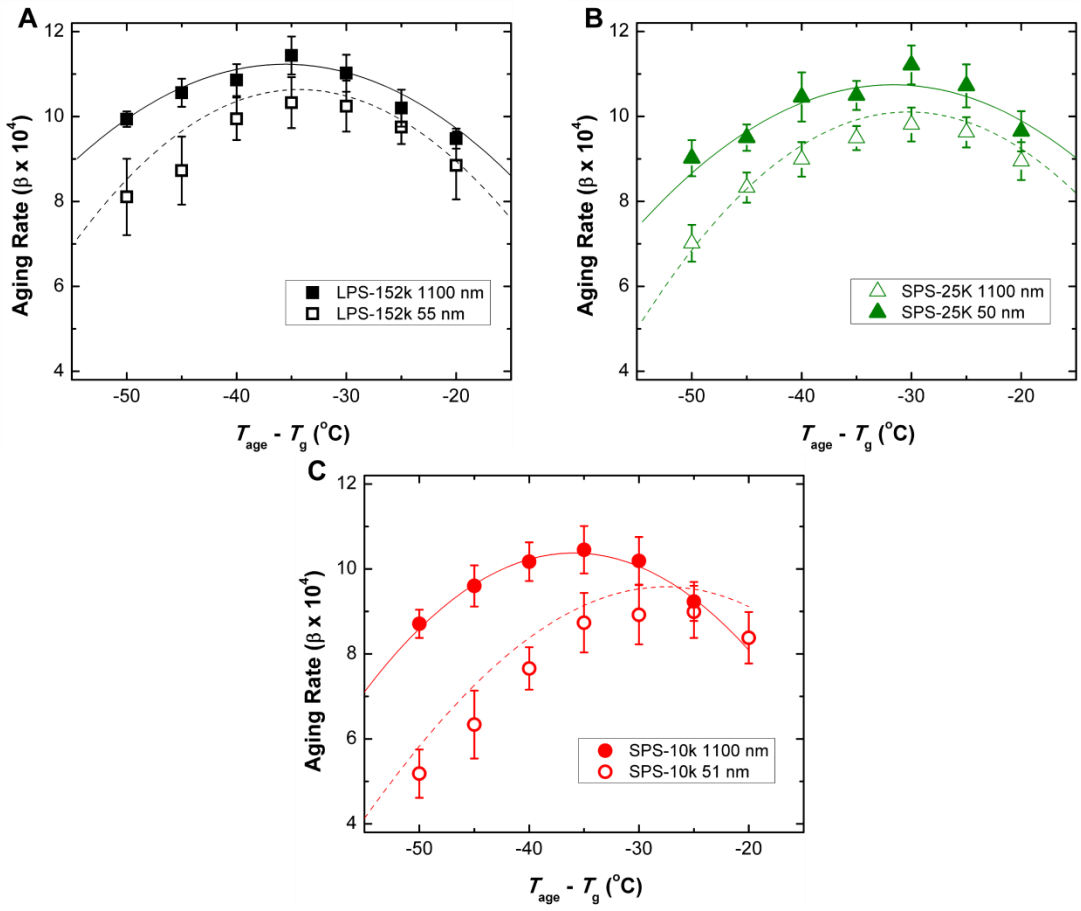

Figure 5.2 The physical aging rates at different T_{age} relative to the average T_g of the film for: (A) LinearPS-152K, (B) StarPS-8arms-25K and (C) StarPS-8 arms-10K. The filled symbols are for a 1.1 micron thick film and open symbols for a 50 nm thin film. The solid lines represent quadratic fits to the 1.1 micron film. The broken lines were calculated using the gradient model, described in the text.

The physical aging rates, calculated using equation 1, are plotted in Figure 5.2 as a function of $\Delta T_A = T_{age} - T_g$. It is evident from these data that the physical aging rates of the thinner (51± 1 nm) films is slower than those of thick films, for all three systems. Additionally, it is evident from Figure 5.3, where data for different thicknesses are included, that the aging rates of the star-shaped macromolecules exhibit stronger

thickness dependencies than their linear chain analogs. The differences between the physical aging behavior of the linear and star-shaped macromolecules cannot be reconciled entirely in terms of T_g^{surf} and $T_g(H)$. The aging rates may however be reconciled in terms of a model that accounts for the changes in the local T_g as a function of depth, $L_g(x)$, of the films. Knowledge of the $L_g(x)$ profile for a polymer film would enable calculation of the *local* aging rate, $\beta(x)$. As discussed below, $L_g(x)$ may be computed from experimentally measured thickness dependence of $T_g(H)$.[18] From the $L_g(x)$ profile, the average aging rate, β, for a film of thickness H can be extracted; this will be compared directly with the experimental data in Figure 5.2 for the thinner films (H~50 nm), with no additional fitting parameters.

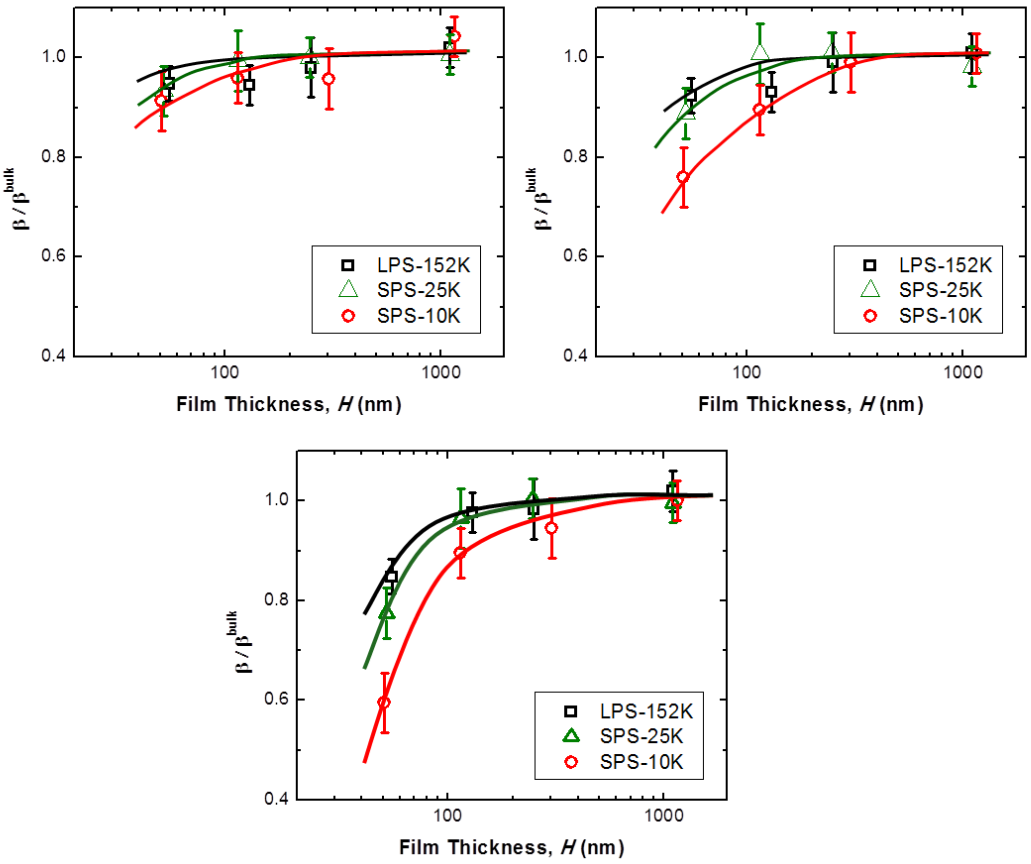

Figure 5.3 The physical aging rate normalized by the bulk physical aging rate as a function of thickness at (A) 30, (B) 40 and (C) 50°C below the average Tg of the film for: LinearPS-152K (open squares), StarPS-8arms-25K (open triangles) and StarPS-8arms--10K (open circles).

We first proceed by fitting the experimental data for the thick film, H~1 micron, using an empirical quadratic equation: $\beta(\Delta T_A)=a(\Delta T_A)^2+b(\Delta T_A)+c$, where $\Delta T_A=T_{age}-T_g(H)$; $T_g(H)$ is identically T_g^{film}. The solid lines, drawn through the thick film data (filled symbols) in Figure 5.2, were computed using this equation. The connection between $T_g(H)$ and $L_g(x)$ is determined by considering the film to be composed of a large number of layers, each located a distance x away from the free surface. Each layer is characterized by a single T_g, $L_g(x)$; in the limit of an infinitesimal layer thickness $L_g(x)$ is treated as a smooth and continuous function. So the average T_g of a film may be defined such that

$$T_g(H) = \int_0^H L_g(x)dx / \int_0^H dx \qquad (5.2)$$

Experimentally it is well established that for thin films the thickness dependence of T_g scales inversely as $1/H$.[16, 17, 20, 26] This is also supported by theory.[14, 15, 19] Models based on dynamic percolation also lead to the same conclusion.[12, 13] Consequently, following Kim et al. the following relation for $T_g(H)$, is used:[18]

$$1/T_g(H) = \xi/T_g^{\infty} \cdot 1/H + 1/T_g^{\infty} \qquad (5.3)$$

where ξ is a measure of the influence of the interfacial interactions influence T_g^{surf}. Physically, ξ is a length scale that characterizes the distance from the free surface to the interior of the film where the half the bulk glass transition temperature, T_g^{∞}, is recovered. This parameter is not temperature dependent. Kim *et. al.* showed that for the non-wetting case, such as for PS on SiO_x that $T_g^{surf}<T_g^{\infty}$ and that $T_g^{\infty}\approx T_g^{subst}$. It follows from equations 2 and 3 that $L_g(x) = T_g^{\infty} \cdot x(2\xi + x)/(\xi + x)^2$.[18] Using the published experimental data for $T_g(H)$ for the samples whose aging behavior is described in Figure 5.3, $L_g(x)$ was calculated and plotted in Figure 5.4.[28, 29] Details describing these calculations are provided in Appendix C. It is evident that $L_g(x)$ of the linear chain system is smallest near the free surface and increases with x before reaching a plateau at T_g^{∞}=99°C, a value dictated by our experimental data. The value of $L_g(x\approx0)$ was also determined from our published data.[28, 29] The plateau in the figure is expected, based on all the available experimental data for the T_g of linear chain PS. The dependence of $L_g(x)$ for the SPS-8-25K sample is similar to that of the linear chains in the vicinity of the free surface; however $L_g(x)$ increases at the substrate. The situation involving SPS-8-10K is

different; $L_g(x)$ is highest at both interfaces, as shown experimentally, and is independent of thickness in the middle of the film. This is in agreement with the experimentally determined local T_g's of this sample, measured using variable energy positron annihilation lifetime spectroscopy (PALS), at the free surface, and atomic force microscopy, at the substrate interface.[28, 29] The PALS data are plotted in the inset of Figure 5.4; the agreement between the calculations of the model and experimental data is good. Additional results, calculated, using equation 5.2, as a function of H are compared with experimental data in Appendix C.

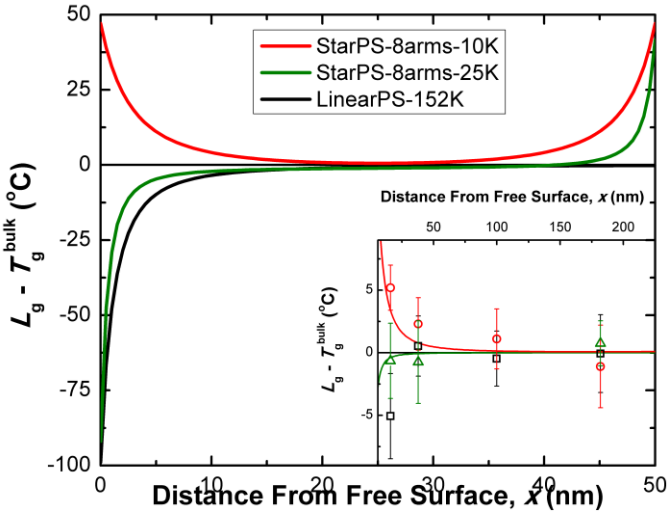

Figure 5.4 The distribution in local Tg (Lg) throughout a 50 nm supported film for LPS-152K (black, squares), SPS-8-25K (green, triangles) and SPS-8-10K (red, circles) according to a gradient Tg model. The inset shows the same Lg for a 350nm film, with the PALS results overlaid.

The next step is to calculate the local aging rate, $\beta(x)$, for each sample, based on $L_g(x)$; this enables calculation of the average aging rates of the H~50 nm samples and therefore a direct comparison with the experimental data in Figure 5.2. With the use of the empirical fitting parameters, a, b and c, from the quadratic equation, and replacing T_{age}-T_g with T_{age}-$L_g(x)$, the local aging rates for LPS-152K and SPS-8-10K were calculated and plotted in Figure 5.5. For the linear PS system, the aging rate at the free surface is zero, because $T_{age} > T_g^{surf}$. Interestingly, for specific T_{age}, $\beta(x)$ exhibits a maximum for depths close to the interfaces. This may be rationalized in terms of the gradient in the local T_g close to the interfaces and, moreover, the non-monotonic

dependence of aging rate on T_{age}. Since $\beta(T_{age})$ is in general not monotonic, then the assumption of an exponential decay in aging rate is not always appropriate.[6]

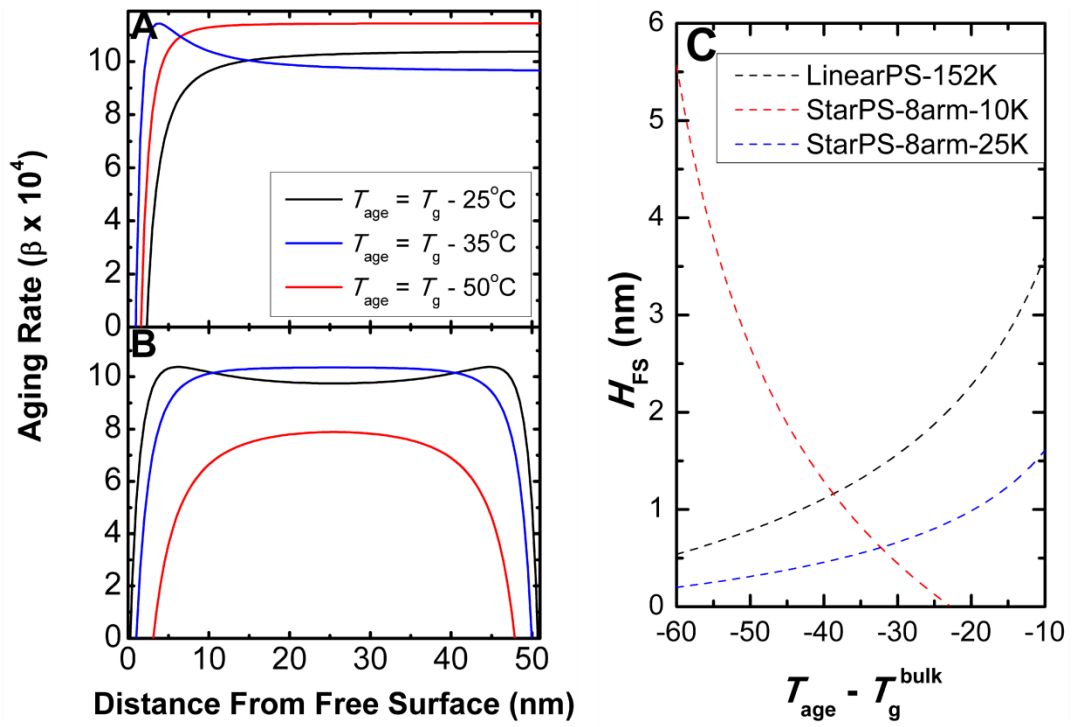

Figure 5.5 The distribution in local physical aging rate throughout a 50 nm supported film of T_g-25°C (black), T_g -35°C (blue) and Tg-50°C (red) for (A) LinearPS-152K and (B) StarPS-8arms-10K. (C) The thickness of the free surface layer that does not age for: LinearPS-152K (black), StarPS-8arms-10K (red) and StarPS-8arms-25K (blue).

It is also apparent from the data in Figure 5.5 that the depth within the film at which the aging rate reaches zero, H_{FS}, is dependent on temperature. In the case of linear PS and SPS-8-25K, H_{FS} is a measure of the mobile free surface layer thickness. This layer does not age since $T_{age} > L_g(x)$. H_{FS} is shown to increase with increasing temperature, Figure 5.5. It is important to note that one consequence of using the 2-layer model is that H_{FS} is predicted to increase with decreasing temperature. This is not only in contrast to our findings; it is also not in agreement with recent studies by Paeng and Ediger on linear chain systems.[6, 31-33] In the case of SPS-8-10K, $\beta(x)$ reaches zero at both interfaces. This is of course not because $T_{age} > L_g(x)$, but due to the fact that $L_g(x) >> T_{age}$. Since $L_g(x)$ is significantly larger than T_{age}, $\beta(x)$ is essentially zero due to the

reduced cooperative segmental mobility of the adsorbed layer, in line with a physical argument by Priestley *et. al.*[2]

Finally, we now reconcile these results with the experimental data in Figure 5.2. Specifically, we calculate the average physical aging rates from the data in Figure 5.5 and compare them to the experimental data in Figure 5.2, for the H~50 nm films. To this end we consider a sample composed of infinitesimally thin films, each exhibiting a specific aging rate. With this, the average physical aging rate for a film, $\beta(H, T_{age})$ may be defined:

$$\beta\left(H, T_{age}\right) = \int_0^H \beta\left(T_{age} - L_g(x)\right)dx / \int_0^H dx \qquad (5.4)$$

The broken lines drawn through the data in Figure 5.2 were computed using the above equation; the agreement is very good. Clearly, the physical aging of the star and linear macromolecular thin films is extremely well described by the model that accounts solely for local changes in the *glass transition temperature*, $L_g(x)$, of the film. It is apparent from this assessment that it is imperative to account for both the local T_{age}-$L_g(x)$ and the bulk T_{age}-T_g. It is noteworthy that our analysis reveals that the characteristic length scale over which interfaces can influence the average aging rate may be as small as a few nanometers or as large as few hundreds of nanometers, depending on T_{age}-$L_g(x)$, or the bulk T_{age}-T_g, Figure 5.3.[2, 6]

5.4 CONCLUSIONS

In conclusion, we showed that the average physical aging rate of supported polystyrene films of varying architectures is significantly slower than the bulk. Regions of the films in proximity to interfaces age at substantially different rates. This difference in aging rate of thin films is reconciled in terms of differences between local glass transition temperatures, $L_g(x)$, and T_{age}. Additionally, it was demonstrated that the aging rates of the star-shaped macromolecules depends on the functionality and arm length of the macromolecule. The star-shaped macromolecules of sufficiently high functionality, and low M_{arm}, age more slowly than their linear chain analogs because they possess higher interfacial T_g's; in other words T_{age}-T_g(bulk) < T_{age}-T_g(interface). To this end, we have shown that the aging rates of thin films may be reconciled in terms of a universal

picture that accounts for differences between T_{age} and the local glass transition temperature, $L_g(x)$. The results of this study indicate that the physical aging rates of thin polymer films may be tailored by controlling the molecular architecture. The macromolecular/interfacial interactions are sensitive to the architecture of the molecule, due primarily to entropic effects.

5.5 REFERENCES

1. Struik, L. C. E., *Physical Aging in Amorphous polymers*. Elsevier Scientific Publishing Company: Amsterdam, 1978.
2. Priestley, R. D.; Ellison, C. J.; Broadbelt, L. J.; Torkelson, J. M. *Science* **2005,** 309, (5733), 456-459.
3. Hodge, I. M. *Science* **1995,** 267, (5206), 1945-1947.
4. Hutchinson, J. M. *Progress in Polymer Science* **1995,** 20, (4), 703-760.
5. Baker, E. A.; Rittigstein, P.; Torkelson, J. M.; Roth, C. B. *Journal of Polymer Science Part B-Polymer Physics* **2009,** 47, (24), 2509-2519.
6. Pye, J. E.; Rohald, K. A.; Baker, E. A.; Roth, C. B. *Macromolecules* **2010,** 43, (19), 8296-8303.
7. Greiner, R.; Schwarzl, F. R. *Rheologica Acta* **1984,** 23, (4), 378-395.
8. Priestley, R. D.; Broadbelt, L. J.; Torkelson, J. M. *Macromolecules* **2005,** 38, (3), 654-657.
9. Kovacs, A. J.; Aklonis, J. J.; Hutchinson, J. M.; Ramos, A. R. *Journal of Polymer Science Part B-Polymer Physics* **1979,** 17, (7), 1097-1162.
10. Priestley, R. D. *Soft Matter* **2009,** 5, (5), 919-926.
11. Baschnagel, J.; Varnik, F. *Journal of Physics-Condensed Matter* **2005,** 17, (32), R851-R953.
12. Lipson, J. E. G.; Milner, S. T. *European Physical Journal B* **2009,** 72, (1), 133-137.
13. Long, D.; Lequeux, F. *European Physical Journal E* **2001,** 4, (3), 371-387.
14. Mittal, J.; Shah, P.; Truskett, T. M. *Journal of Physical Chemistry B* **2004,** 108, (51), 19769-19779.
15. Truskett, T. M.; Ganesan, V. *Journal of Chemical Physics* **2003,** 119, (4), 1897-1900.
16. Keddie, J. L.; Jones, R. A. L.; Cory, R. A. *Europhysics Letters* **1994,** 27, (1), 59-64.
17. Forrest, J. A.; Dalnoki-Veress, K. *Advances in Colloid and Interface Science* **2001,** 94, (1-3), 167-196.
18. Kim, J. H.; Jang, J.; Zin, W. C. *Langmuir* **2001,** 17, (9), 2703-2710.
19. Morita, H.; Tanaka, K.; Kajiyama, T.; Nishi, T.; Doi, M. *Macromolecules* **2006,** 39, (18), 6233-6237.
20. Keddie, J. L.; Jones, R. A. L.; Cory, R. A. *Faraday Discussions* **1994,** 98, 219-230.
21. Ellison, C. J.; Torkelson, J. M. *Nature Materials* **2003,** 2, (10), 695-700.
22. Pham, J. Q.; Green, P. F. *Journal of Chemical Physics* **2002,** 116, (13), 5801-5806.
23. Pham, J. Q.; Green, P. F. *Macromolecules* **2003,** 36, (5), 1665-1669.
24. vanZanten, J. H.; Wallace, W. E.; Wu, W. L. *Physical Review E* **1996,** 53, (3), R2053-R2056.
25. Kawana, S.; Jones, R. A. L. *European Physical Journal E* **2003,** 10, (3), 223-230.
26. Forrest, J. A.; Mattsson, J. *Physical Review E* **2000,** 61, (1), R53-R56.
27. Mattsson, J.; Forrest, J. A.; Borjesson, L. *Physical Review E* **2000,** 62, (4), 5187-5200.

28. Glynos, E.; Frieberg, B.; Oh, H.; Liu, M.; Gidley, D. W.; Green, P. F. *Physical Review Letters* **2011,** 106, (12), 128301.
29. Glynos, E.; Frieberg, B.; Green, P. F. *Physical Review Letters* **2011,** 107, (11), 118303.
30. Boucher, V. M.; Cangialosi, D.; Alegria, A.; Colmenero, J.; Gonzalez-Irun, J.; Liz-Marzan, L. M. *Soft Matter* **2010,** 6, (14), 3306-3317.
31. Paeng, K.; Swallen, S. F.; Ediger, M. D. *Journal of the American Chemical Society* **2011,** 133, (22), 8444-8447.
32. Paeng, K.; Ediger, M. D. *Macromolecules* **2011,** 44, (17), 7034-7042.
33. Ilton, M.; Qi, D.; Forrest, J. A. *Macromolecules* **2009,** 42, (18), 6851-6854.

CHAPTER 6
SURFACE LAYER DYNAMICS IN MISCIBLE POLYMER BLENDS

Reprinted with permission from:

Frieberg, B.; Kim, J.; Narayanan, S.; Green, P.F.; *ACS Macro. Lett.* **2013**, 2, 388-392.

6.1 INTRODUCTION

In A/B polymer/polymer mixtures the free surface composition is, in the absence of unusual entropic effects, dominated by the lower cohesive energy density component; this contributes to decreasing the overall free energy of the system.[1, 2] Much is understood about the phase behavior of these systems, including phenomena such as surface directed spinodal decomposition, dating back nearly 20 years.[3-7] The preferential surface segregation by one component can change the shape of the coexistence curve; thus, the phase and wetting transition temperatures also become dependent on film thickness. Near the phase boundary a wetting transition would occur, wherein the wetting layer becomes very large.[8-10] In this paper we are particularly interested in the surface dynamics of compatible A/B polymer/polymer mixtures at temperatures far from the phase boundaries. Indeed, apart from open scientific questions related to dynamic phenomena at surfaces, this topic is of particular interest because most polymeric systems of practical interest are mixtures. The design of smart coatings and surfaces, used for different practical applications, from medicine and biology to microelectronics and sensors, would benefit from further insight into the structure and dynamics at interfaces.

There are quantitative differences between the chain dynamics at free surfaces and the bulk. For single component, linear chain, homopolymer systems the glass transition temperature, T_g,[11-14] at the free surface is lower than the bulk; the surface dynamics[15-17] are fast compared to the bulk. Moreover the effective chain entanglements, in highly entangled melts, are lower at the free surface, further contributing to enhancements of the free surface translational dynamics. A long chain in a highly entangled polymer melt undergoes slithering motions within the confines of a virtual tube, defined by its intersections with neighboring chains.[18-20] The longest relaxation time, τ_{Rep}, of the dynamics of a polymer chain of degree of polymerization N in this highly entangled melt is dictated by a molecular friction factor, ζ, manifesting the "drag" that the chain experiences due to local inter- and intra-molecular interactions: $\tau_{\mathrm{Re}p} \propto (\zeta / T) N_e^{-2`} N^3$; N_e is the average degree of polymerization between entanglements and T is the absolute temperature.[18] When the chains are short and unentangled, the relaxation time of a chain is $\tau_{\mathrm{Ro}} \propto \zeta N/T$.

In the A/B polymer/polymer mixtures virtually nothing is understood about the dynamics of chains at the free surface in relation to the bulk. This kind of information may uniquely be extracted from X-ray photon correlation spectroscopy (XPCS) measurements. Herein, XPCS is used to examine the surface dynamics of a miscible blend of deuterated polystyrene (dPS) and poly(vinyl methyl ether) (PVME). The dynamics of capillary waves are probed at the free surface of PS/PVME blends of varying thickness. These dynamics manifest the behavior of PVME chains in different environments in the mixture. We show that the PVME chains exist in in two local environments of distinct composition: a rapid process associated with a PVME-rich environment at the free surface, and a second slower dynamic process, two orders of magnitude slower, associated with the other population of PVME in the bulk, composed of a higher PS composition. The dynamics of these chains in the bulk and at the free surface manifest from the influence of film thickness constraints.

6.2 EXPERIMENTAL SECTION

6.2.1 Materials

In this study we investigated blends of deuterated polystyrene (dPS), M_n=10,900 (M_w/M_n = 1.05) and poly(vinyl methyl ether) (PVME), M_n=24,400 (M_w/M_n = 1.08) purchased from Polymer Source Inc. Thin films of thickness, H, ranging from 30 nm to 600 nm of the polymer blends (75% dPS, 25% PVME) were prepared by spin-coating from a toluene solution onto pre-cleaned silicon substrates with a native oxide layer of approximately 1.5 nm, measured by variable angle spectroscopic ellipsometry (VASE, J.A. Woollam M-2000). The substrates were rinsed in ethanol, acetone and toluene prior to being UV-cleaned for 3 minutes. The polymer solutions were immediately spin-coated following the cleaning procedure. The samples were then immediately transferred to a vacuum oven where the samples were annealed at room temperature for 24 hours under vacuum and then 18 hours at 65°C (T_g+30°C). The samples were then kept in a desiccator until they were measured by XPCS or VASE.

6.2.2 Differential Scanning Calorimetry (DSC)

The glass transition of ~5-10 mg of the pure polymers as well as the blend, were measured by DSC (TA Instruments Q200). Each sample was first heated to 150°C at a rate of 10°C/min. to erase previous thermal history. The samples were then quenched to -100°C at 50°C/min. using a liquid nitrogen cooling system. A second heating scan from -100°C to 150°C was then immediately carried out at 10°C/min. The T_g was determined from the temperature corresponding to half the complete change in heat capacity on the second heating scan. All DSC measurements were completed in a nitrogen atmosphere.

6.2.3 X-Ray Photon Correlation Spectroscopy (XPCS)

The free surface dynamics of supported polymer films were investigated using XPCS. The XPCS experiments were performed at beam line 8-ID-I at the Advanced Photon Source (APS) at Argonne National Laboratory. Details of the XPCS experiment are described elsewhere.[1] We used an incident angle of 0.14°, less than the critical angle of 0.16° of the PS/PVME system; which was determined by x-ray reflectivity with incident x-ray energy of 7.5 keV. This limits the penetration of the x-ray beam to less

than 10 nm from the free surface.[1] A fast x-ray reflectivity measurement was performed on the same spot as the dynamics measurement in order to ensure that the sample was not damaged during measurement by an induced surface roughness. In addition the observed intensity did not change more than 5% during a dynamics measurement.

6.2.4 Variable Angle Spectroscopic Ellipsometry (VASE)

The same sample structure (polymer blend on pre-cleaned silicon) was used with VASE in order to determine the wetting layer thickness. For these measurements, the ellipsometric angles Ψ and Δ are collected over the entire spectral range (375 – 1700 nm). The optical constants were obtained from a 200 nm film of each of the pure polymer components by fitting Ψ and Δ to a Cauchy model. For the blend films, first a Cauchy layer was used in order to obtain an estimate for the film thickness. Then, a three layer effective medium approximation (EMA) model was then used to model the blend films, where the optical constants of PS and PVME were fixed, but the weight fraction of PS in each layer and the layer thickness were allowed to vary. This allowed for obtaining a lower mean squared error (MSE) than fitting to a Cauchy layer for the entire film. The sum of all three EMA layers was verified to be approximately the same as the estimate found from the Cauchy model. Similarly a gradient model was applied, where the optical constants were allowed to follow a simple linear and exponential gradient from the interface to the interior, but the MSE was found to increase compared to the three layer model.

6.3 RESULTS AND DISCUSSION

The free surface dynamics of supported polymer films were investigated using XPCS through monitoring the scattering of X-rays from surface capillary waves. The XPCS experiments were performed at beam line 8-ID-I at the Advanced Photon Source (APS) at Argonne National Lab. Details of the XPCS experiment are described elsewhere.[21] The XPCS measurements of the dynamics of the dPS/PVME polymer blends reveal the existence of two distinct relaxations. Plotted in Figure 6.1, for various q-vectors, are the intensity autocorrelation functions, $g_2(q,t)$:

$g_2(q,t)=1+A\,|\,f(q,t)\,|^2$ (6.1)

for two temperatures 80°C and 90°C. [22] In this equation *A* represents the speckle contrast; the intermediate scattering function is:

$$f(q,t) = r\exp[-(t/\tau_1)] + (1-r)\exp[-(t/\tau_2)], \quad (6.2)$$

where r is the fraction of exponential decay from the shorter relaxation, and τ_1 and τ_2 are the shorter and longer relaxation times, respectively. The data in Figure 6.1reveal that τ_1 is approximately two orders of magnitude shorter than τ_2. Note that in single component homopolymer films, only a single dominant relaxation is observed, reflecting the dynamics of a single component.[21, 23] If the two modes were at similar time scales, only one stretched exponential would have been observed. Therefore, the two relaxations reflect that the capillary waves at the free surface represent temperature fluctuations of two very distinct modes.

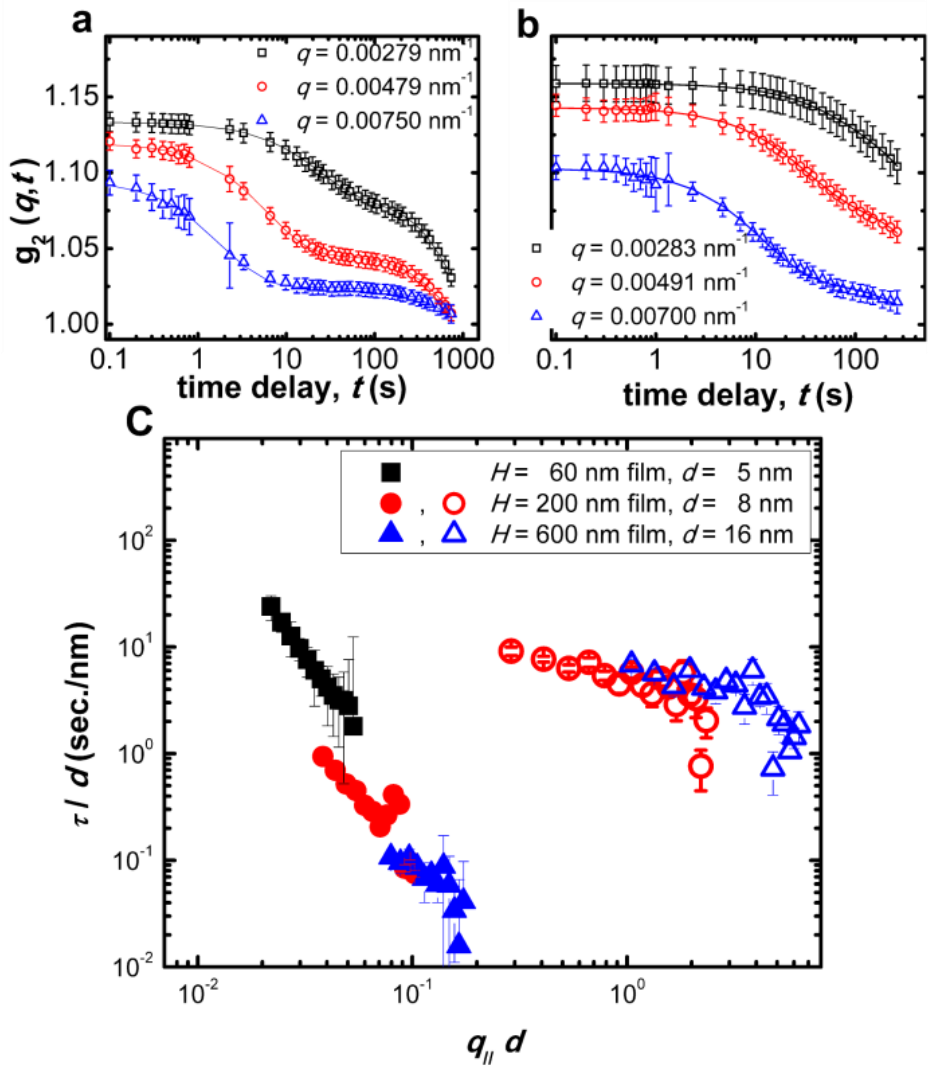

Figure 6.1 Measured autocorrelation function, g2(q,t), of dPS/PVME film at 3 different q vectors at T= 90°C for (a) a 200 nm film and (b) a 60 nm film. Solid lines are the fittings to KWW equation, assuming that two relaxations (τ1 & τ2) exist (equation 2 in the main text). (c) Relaxation time/surface segregated layer thickness as a function of q-vector x surface segregated layer thickness at the free surface of dPS/PVME blend films for τ1 (closed symbols) and τ2 (open symbols) for various film thicknesses.

We propose that the two relaxation processes revealed by the data in Figure 6.1 represent the dynamics of two separate populations of chains, one undergoing translational motion in one environment and the other exhibiting ballistic, and caged, behavior of chains in a different environment. This is further demonstrated in Figure 6.1 where the relaxation time as a function of *q*-vector dependence also shows a two order of

magnitude increase for the 2nd relaxation. In this plot, the relaxation time is shown as the ratio of τ/d vs. the product of $q_{//}\, d$ where d is the thickness of the film. When calculating the viscosity of the free surface, d is the thickness of the wetting layer. It has previously been demonstrated by hydrodynamic theory[21, 24] that the ratio of τ/d is proportional to the viscosity, η, over the surface tension, γ, (η/γ) as shown in equation 3:

$$\tau = \frac{2\,\eta\,(cosh^2(q_{//}\ d) + q_{//}^2 d^2)}{\gamma q_{//}\,(\sinh(q_{//}\,d)\cosh(q_{//}\,d) - q_{//}\,d)}. \qquad (6.3)$$

The information in Figure 6.1 reveals the existence of two apparent relaxations, suggestive of polymer chains undergoing dynamics in two different environments. It is important to note that the PVME and PS chains are miscible at the temperatures where the experiments were conducted. For the materials used in our experiments, the lower critical solution temperature (LCST) is above 200°C;[25, 26] much higher than the experimental temperatures, 90 and 100°C. Further the T_g of PVME is -35°C and that of the PS component is 91°C measured by Differential Scanning Calorimetry (DSC). PVME possesses a much lower surface energy than PS, 22 and 32 mN/m respectively (at 150°C), and is well documented to reside at the free surface at concentrations in excess of its bulk.[27, 28] Tentatively, we propose that the faster relaxation, representing a center of mass diffusive motion of the polymer chains, would be associated with the faster PVME chains in a PVME rich environment at the free surface. The second, slower relaxation would be associated with the dynamics of bulk PVME chains in an environment containing a higher local concentration of PS and associated with a higher local T_g.

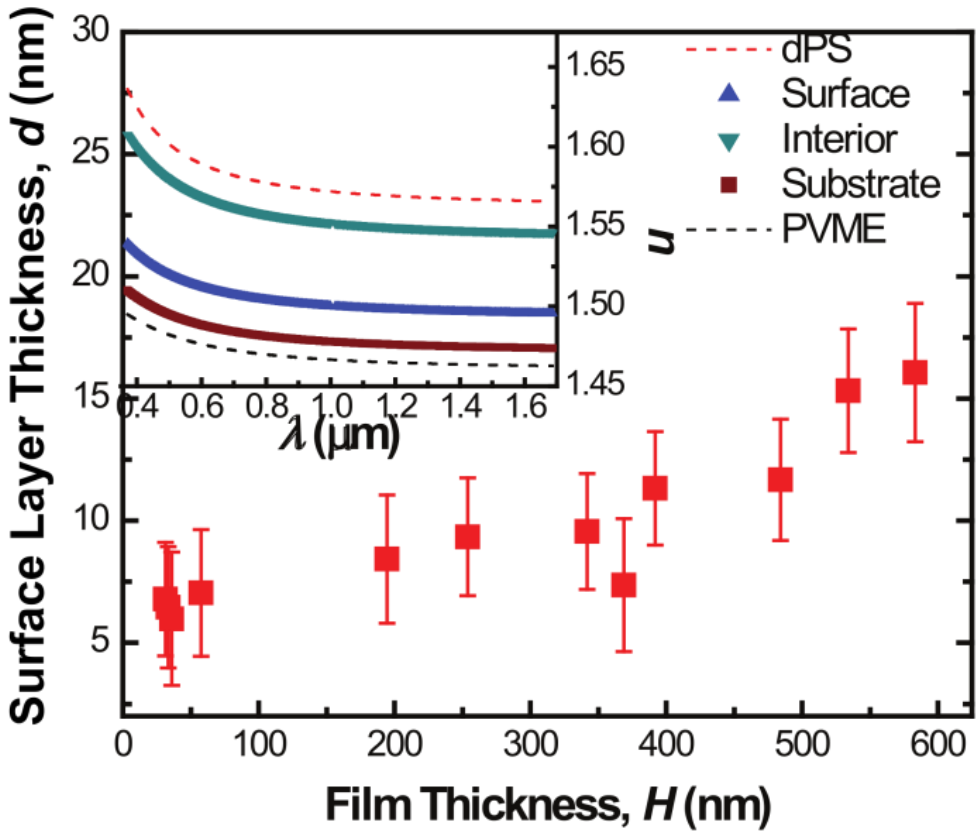

Figure 6.2 The thickness of the free surface segregated layer was measured by ellipsometry as a function of total film thickness. (Inset) The refractive index is shown as a function of wavelength for the three layers in a 200 nm film; free surface layer (blue triangles), interior (cyan inverted triangles), and substrate layers (maroon squares). The dashed lines represent the refractive index of the pure PS (red) and PVME (black) components.

We now examine the conjecture regarding the PVME composition in the free surface region, using spectroscopic ellipsometry.[29] We begin with the simplest model, a three-layer model, which assumes the existence of a thin layer mixture at the free surface and at the substrate; these layers are reasonably assumed to be PVME rich in comparison to the bulk.[30] The optical constants of the materials were determined from ellipsometric analyses of pure 200 nm thick PS and PVME layers; these constants are distinct. The refractive indices of the pure polymers, as well as those measured for the three layers, are plotted in the inset of Figure 6.2 for a 200 nm blend film, for different wavelengths. In the blended films, both the composition and thicknesses of the layers were modeled and are shown in Figure 6.2. For thick films (films thicker than 200 nm) the composition of

the free surface layer was found to be approximately 70% PVME, while the bulk is ~ 25%; the margin of error is approximately ±15%. Such a concentration is consistent with previous studies using techniques such as X-ray photoelectron spectroscopy (XPS)[27, 28] and variable angle spectroscopic ellipsometry (VASE).[29] The thickness of the surface segregated layer is found to increase as a function of total film thickness until thicknesses greater than 600nm. This suggests that the surface segregated layer composition remains constant, and increases in thickness, with increasing total film thickness. Our data are consistent with those reported in the literature, the compositions at the free surface,[28] and the thickness dependence.[31]

The information provided by our ellipsometric measurements is consistent with our conjecture that the two relaxations are associated with the dynamics of PVME chains in two different environments. The first is associated with center of mass dynamics in a highly enriched PVME environment near the free surface of the film. On the other hand, the slower, caged dynamics is consistent with the behavior of the latter population of chains in a higher PS concentration with a higher local T_g. Because, the measurement temperatures are close to average T_g of this region, $T < 1.2T_g$ (T_g = 41°C), the dynamics follow that of caged motion.[32, 33] While at the free surface, the dynamics of the PVME chains in the nearly pure environment are expected to follow center of mass, translational diffusion, which is observed.

These observations are now discussed within the context of bulk dynamics of polymer/polymer mixtures. In a compatible A/B mixture the A and B chains experience different average local compositional environments, which have important consequences on their dynamics. Specifically the monomer-monomer mixing of the dissimilar A/B segments is not random, due to the connectivity between monomers that constitute each chain.[20, 34] Hence the local environment of a monomer is characterized by a self-concentration that is different from the average macroscopic concentration of the bulk; the length scale is on the order of the Kuhn step length, at least close to the glass transition.[19, 35] Natural consequences of the chain connectivity and local concentration fluctuations include the fact that the dynamics of each component of blend exhibits different temperature dependences. Moreover they each experience a different, and distinct, local glass transition T_g^{eff}. In fact, the relaxation rates of the chains in the

mixtures are slower than in the pure components at the same temperature. Consequently the relaxation rates of the individual components are significantly different, particularly when there is a significant difference in the T_g's of the pure components. In short the effective friction factors ζ_{eff}, manifest, in part a unique local compositional environment, coupled with its own intra-molecular contributions are distinct.

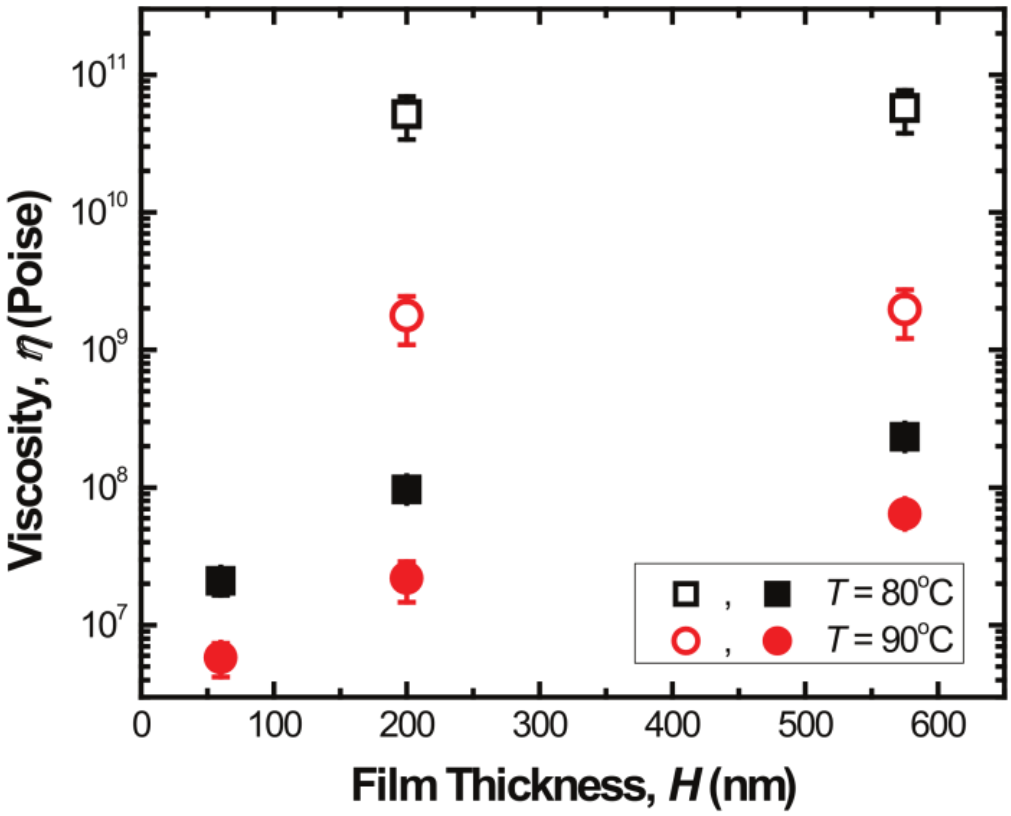

Figure 6.3 Viscosity changes as a function of total film thickness. The viscosities were measured at 80°C (squares) and 90°C (circles). The viscosity calculated from relaxation 1 is shown as the closed symbols and relaxation 2 is shown as the open symbols.

Using hydrodynamic theory (described by equation 3) and the thickness of each of the polymer layers, one can calculate the viscosity of each of the layers assuming that the faster relaxation is associated with the surface segregated layer and the latter with the polystyrene rich, interior, film. The fits, are plotted as solid lines in Figure 6.1, describe the data nicely for both the first and second relaxations. In addition the viscosities extracted from the data are plotted in Figure 6.3. First we will discuss the thickness dependence of the viscosity calculated from the 2nd relaxation. The viscosity could only

be calculated for the thicker films, because when the film was 60 nm thick, the relaxation time is longer than could be measured using XPCS. However the autocorrelation functions do not exhibit plateaus at values of unity, indicating there is another slower relaxation. Such a relaxation is shown in Figure 6.1. This relaxation is consistent with the results of others who have reported that in pure homopolymer systems (such as polystyrene thin films) the viscosities measured from capillary waves at the free surface using XPCS are independent of film thickness and are comparable in magnitude to the zero-shear viscosities measured using rheology.[21, 23] Interestingly, there is significant thickness dependence on the viscosity of the surface segregated layer. For this analysis, the thickness of the film was taken to be the thickness of the surface segregated layer measured by ellipsometry. Note further that if the thickness of the entire film were to be used, there would still be a thickness dependent viscosity.

The viscosity of the surface segregated layer decreases by almost an order of magnitude between film thicknesses of 600nm and 60nm. When the mixture is 60 nm thick, the surface segregated layer is on the order of R_g of the PVME molecules ($R_g^{PVME} \approx$ 5.7 nm).[36] Therefore, when thickness of the surface segregated layer is comparable to the size of the polymer chain, the number of inter chain entanglements is reduced; the local friction coefficient experienced by the PVME chains is also expected to be reduced. It has also been previously demonstrated that in bilayers of polymers, the dynamics of the top layer are significantly influenced by the modulus of the bottom layer.[37] Therefore, when the film is thin, the interfacial segregation of PVME to the oxide substrate will influence the elastic properties of the bulk layer and therefore influence the viscosity measured at the free surface.

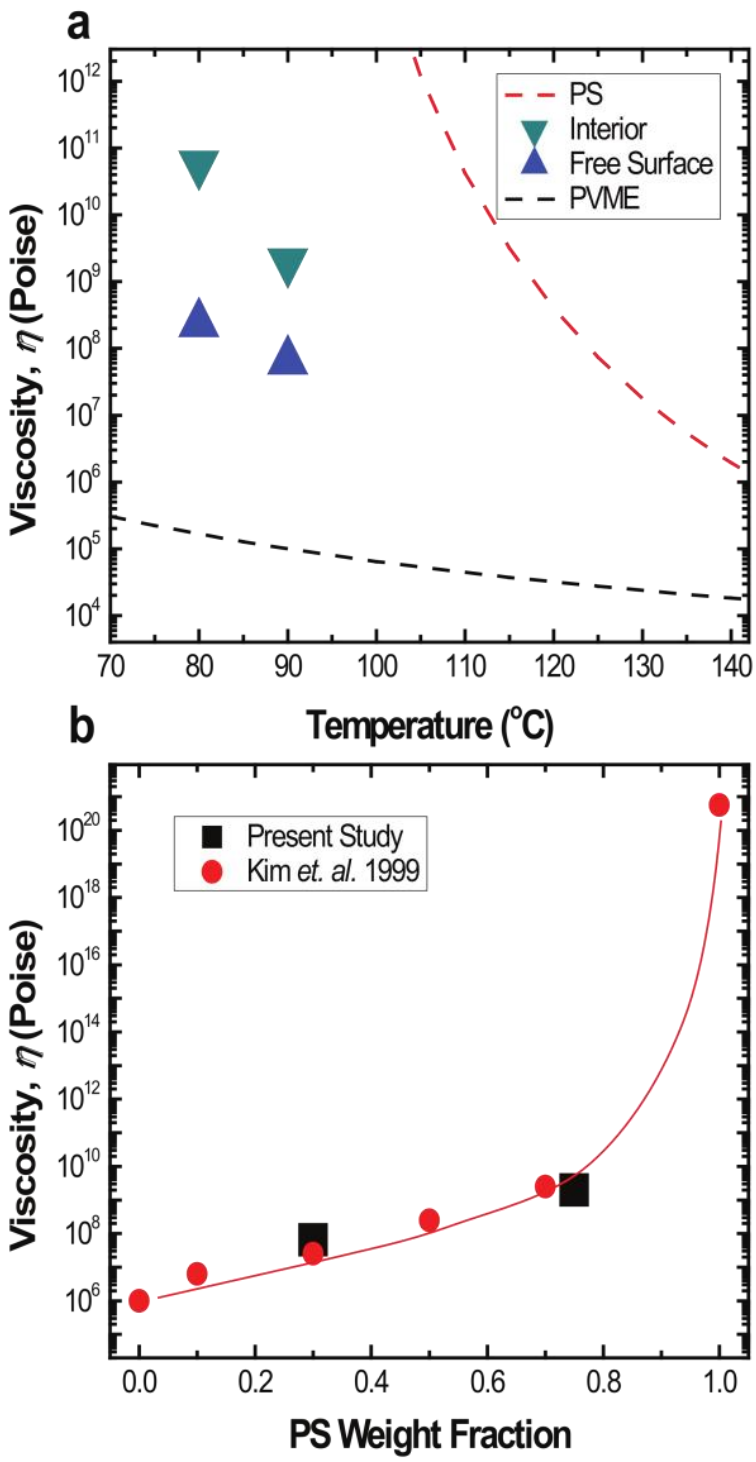

Figure 6.4 (a) The viscosity as a function of temperature calculated from relaxation 1 (Free Surface) and relaxation 2 (Interior). The temperature dependence of the viscosity for each of the pure components are reproduced from refs [38, 39]. (b) Viscosity as a function of composition for the free surface (30% PS) and interior (75% PS) as it compares to bulk viscosity values reproduced from refs [38, 39]. The symbol size is indicative of the error.

In order to understand how the viscosity of these layers compare to those measured for the bulk, the data in Figure 6.4 should be considered. The viscosities of the 600 nm film at the free surface (1^{st} relaxation), for the interior (2^{nd} relaxation) and the zero-shear viscosities of the pure PVME and PS measured by rheology are plotted.[38, 39] It is clear that all of the measured viscosities fall between that of the pure components, demonstrating that neither the free surface or interior of the film is composed of a pure component. It is noteworthy, however, that the viscosity measured for the free surface, using XPCS, is consistent with what one would suspect from a 70% PVME material. Moreover, the viscosity we extracted for interior is approximately what one would expect from a blend with 25% PVME; these data are plotted in Figure 6.4.

6.4 CONCLUSIONS

With the use of XPCS we studied the PVME chain dynamics at the surfaces of miscible thin film blends of PS and PVME of various film thicknesses. The intensity autocorrelation functions provided evidence of dynamics of PVME from two separate environments: (1) rapid center of mass dynamics of PVME chains in an environment rich in PVME at the free surface; (2) PVME chains exhibiting caged, ballistic, dynamics in an environment with a higher PS concentration and higher local T_g in the interior of the film. The latter dynamics were approximately two orders of magnitude slower. The viscosities extracted from the XPCS data for the two different environments are consistent with bulk viscosity values of samples of the same compositions when the film is thick. When the surface layer is on the order of R_g of the polymer chains the viscosity is depressed. These results reveal for the first time that insights into the surface viscosities of liquid/liquid mixtures strongly manifest the local composition of the mixture.

6.5 REFERENCES

1. Nakanishi, H.; Pincus, P. *Journal of Chemical Physics* **1983,** 79, (2), 997-1003.
2. Schmidt, I.; Binder, K. *Journal De Physique* **1985,** 46, (10), 1631-1644.
3. Bank, M.; Thies, C.; Leffingw.J. *Journal of Polymer Science Part a-2-Polymer Physics* **1972,** 10, (6), 1097-&.
4. Coleman, M. M.; Graf, J. F.; Painter, P. C., *Specific interactions and the Miscibility of Polymer Blends*. Technomic Publishing: Lancaster, PA, 1991.
5. Coleman, M. M.; Painter, P. C. *Progress in Polymer Science* **1995,** 20, (1), 1-59.
6. Dudowicz, J.; Freed, K. F. *Macromolecules* **1991,** 24, (18), 5076-5095.
7. Dudowicz, J.; Freed, K. F. *Macromolecules* **1991,** 24, (18), 5112-5123.
8. Das, S. K. P., S.; Horbach, J. and Binder, K. *Physical Review E.* **2006,** 73.
9. Binder, K. *Acta Polymerica* **1995,** 46, (3), 204-225.
10. Binder, K. *Journal of Non-Equilibrium Thermodynamics* **1998,** 23, (1), 1-44.
11. Keddie, J. L.; Jones, R. A. L.; Cory, R. A. *Faraday Discussions* **1994,** 98, (Polymers at Surfaces and Interfaces), 219-30.
12. Ellison, C. J.; Torkelson, J. M. *Nature Materials* **2003,** 2, (10), 695-700.
13. Glynos, E.; Frieberg, B.; Oh, H.; Liu, M.; Gidley, D. W.; Green, P. F. *Physical Review Letters* **2011,** 106, (12), 128301.
14. Frieberg, B.; Glynos, E.; Green, P. F. *Physical Review Letters* **2012,** 108, (26), 268304.
15. Koga, T.; Li, C.; Endoh, M. K.; Koo, J.; Rafailovich, M.; Narayanan, S.; Lee, D. R.; Lurio, L. B.; Sinha, S. K. *Physical Review Letters* **2010,** 104, (6).
16. Fakhraai, Z.; Forrest, J. A. *Science* **2008,** 319, (5863), 600-604.
17. Qi, D.; Fakhraai, Z.; Forrest, J. A. *Physical Review Letters* **2008,** 101, (9).
18. Doi, M.; Edwards, S. F., *The Theory of Polymer Dynamics*. Oxford University Press: New York, 1988.
19. Lodge, T. P.; McLeish, T. C. B. *Macromolecules* **2000,** 33, (14), 5278-5284.
20. Lorthioir, C.; Alegria, A.; Colmenero, J. *Physical Review E* **2003,** 68, (3).
21. Kim, H.; Ruhm, A.; Lurio, L. B.; Basu, J. K.; Lal, J.; Lumma, D.; Mochrie, S. G. J.; Sinha, S. K. *Physical Review Letters* **2003,** 90, (6).
22. Falus, P.; Borthwick, M. A.; Narayanan, S.; Sandy, A. R.; Mochrie, S. G. J. *Physical Review Letters* **2006,** 97, (6), 066102.
23. Wang, S. F.; Jiang, Z.; Narayanan, S.; Foster, M. D. *Macromolecules* **2012,** 45, (15), 6210-6219.
24. Jackle, J. *Journal of Physics-Condensed Matter* **1998,** 10, (32), 7121-7131.
25. Ubrich, J. M.; Larbi, F. B.; Halary, J. L.; Monnerie, L.; Bauer, B. J.; Han, C. C. *Macromolecules* **1986,** 19, (3), 810-815.
26. Nishi, T.; Kwei, T. K. *Polymer* **1975,** 16, (4), 285-290.
27. Bhatia, Q. S.; Pan, D. H.; Koberstein, J. T. *Macromolecules* **1988,** 21, (7), 2166-2175.
28. Pan, D. H. K.; Prest, W. M. *Journal of Applied Physics* **1985,** 58, (8), 2861-2870.
29. Thomas, K. R.; Clarke, N.; Poetes, R.; Morariu, M.; Steiner, U. *Soft Matter* **2010,** 6, (15), 3517-3523.

30. Karim, A.; Slawecki, T. M.; Kumar, S. K.; Douglas, J. F.; Satija, S. K.; Han, C. C.; Russell, T. P.; Liu, Y.; Overney, R.; Sokolov, O.; Rafailovich, M. H. *Macromolecules* **1998,** 31, (3), 857-862.
31. Jones, R. L.; Indrakanti, A.; Briber, R. M.; Muller, M.; Kumar, S. K. *Macromolecules* **2004,** 37, (18), 6676-6679.
32. Caronna, C.; Chushkin, Y.; Madsen, A.; Cupane, A. *Physical Review Letters* **2008,** 100, (5), 055702.
33. Debenedetti, P. G.; Stillinger, F. H. *Nature* **2001,** 410, (6825), 259-267.
34. Leroy, E.; Alegria, A.; Colmenero, J. *Macromolecules* **2003,** 36, (19), 7280-7288.
35. Colmenero, J.; Arbe, A. *Soft Matter* **2007,** 3, (12), 1474-1485.
36. Manson, J. A.; Arquette, G. J. *Makromolekulare Chemie* **1960,** 37, (3), 187-197.
37. Evans, C. M.; Narayanan, S.; Jiang, Z.; Torkelson, J. M. *Physical Review Letters* **2012,** 109, (3).
38. Green, P. F.; Adolf, D. B.; Gilliom, L. R. *Macromolecules* **1991,** 24, (11), 3377-3382.
39. Kim, J. K.; Son, H. W. *Polymer* **1999,** 40, (24), 6789-6801.

CHAPTER 7
SURFACE DYNAMICS OF MISCIBLE POLYMER BLEND NANOCOMPOSITES

7.1 INTRODUCTION

The design and function of polymer surfaces have significant scientific and practical implications in diverse areas, from medicine and biology to microelectronics and microfluidics. Fundamental questions regarding connections between the structure and dynamics of macromolecules at interfaces are of interest to various interdisciplinary research communities. The local structure, organization of segments, of polymeric molecules in the vicinity of an interface, free surface or otherwise, differs from the bulk, due largely to local competing entropic and enthalpic interactions. The consequences of such interactions can be significant, as they are often responsible for changes in average physical materials properties such as glass transition temperatures,[1, 2] adhesion,[3] and various transport properties, from segmental dynamics[4] to electronic carrier transport,[5] measured by different techniques. Polymer nanocomposites (PNCs) represent an important class of materials in which polymer/nanoparticle interfacial interactions play an important role toward dictating the overall phase behavior and physical properties.[6, 7] In PNCs, the properties of the polymer host are modified appreciably with the addition of small quantities, even less than a few percent, of nanoparticles (*e.g.*: quantum dots,

fullerenes, metallic nanoparticles *etc*.). Based on the functionality of the nanoparticle and that of the polymer, diverse physical properties may be achieved.

The dynamics of polymer chains in bulk PNCs have been investigated by a number of authors and a reasonable understanding exists. For example, it has been shown that the addition of polystyrene (PS) nanoparticles to a PS host has the effect of reducing the viscosity of the polymer by approximately a factor of two.[8] On the other hand the addition of silica and other inorganic nanoparticles to polymers has the effect of increasing the viscosity of melts and enhancing the mechanical properties of the material in the solid state.[7] The addition of fullerenes to polymethyl methacrylate (PMMA) has been shown, through a series of rheological measurements, to increase the longest relaxation time, or equivalently, the viscosity of the PMMA chains.[9] Quasi-elastic neutron scattering (QENS) studies revealed that the effect of the C_{60} nanoparticles on the dynamics occurred on a local scale; at short nanosecond time scales, an increase of the local friction factor of the chain was due to intermittent attractive polymer-segment/nanoparticle interactions.[10] Hence the longest relaxation time of the polymer, τ_R, and therefore the viscosity increased. More recently we demonstrated that the PS chain relaxations could be influenced significantly with the addition of polystyrene brush-coated nanoparticles to PS polymer hosts.[11] Control of the volume fraction of NPs, the brush length of the grafted PS chains relative to the host chain length, enabled the relaxation times to increase, or decrease, by up to an order of magnitude.

Miscible A/B polymer/polymer blends are compositionally heterogeneous due to effects associated with self-concentrations, due to monomer connectivity, and to thermally induced composition fluctuations. The A and B type chains each experience a different local composition. Moreover they each experience a distinct local T_g and temperature dependent dynamics that is similar to their pure components, as revealed by broadband dielectric spectroscopy[12, 13] and molecular tracer diffusion measurements.[14] While these techniques provide information about the dynamics of individual components, techniques such as rheology[14, 15] and X-ray photon correlation spectroscopy (XPCS)[16] provide information about relaxations that enable determination of the viscosity of blends.

Of particular interest in the paper is the manner in which nanoparticles influence the surface dynamics, or surface viscosity, of a polymer nanocomposite composed of a miscible polymer/polymer blend and brush-coated nanoparticles. By way of context we note that in miscible A/B polymer/polymer systems the free surface composition is generally dominated by the lower cohesive energy density component, in comparison to its bulk concentration; this reduces the overall free energy of the system.[17, 18] While, notably, much is understood about surface directed spinodal decomposition and wetting transitions in miscible blends, dating back nearly 20 years, only very recently were reliable and direct measurements of the free surface dynamics of polymer mixtures achieved.[16] X-ray photon correlation spectroscopy (XPCS) was used to show that in a miscible blend of PS and poly vinyl methyl ether (PVME),[16] the surface relaxations of the blends were characterized by two separate time-scales: a rapid process associated with a PVME-rich environment, and a second dynamic process, two orders of magnitude slower, associated with polymer chains in a local compositional environment appreciably richer in PS. In this paper we report the effect of PS brush coated gold nanoparticles on the surface dynamics of the PVME chains in a PS/PVME/PS-Au nanocomposite measured by XPCS. Our primary finding is that in the nanocomposite, the dynamics are shown, remarkably, to be nearly an order magnitude faster than those of the neat PS/PVME blend, suggesting that the surface properties of the nanocomposite remain significantly more fluid than the neat blend. The dynamics of the surface are otherwise similar to those in the neat blend; the polymer chain relaxations manifest the influence of two significantly different average compositional environments.

7.2 EXPERIMENTAL SECTION

7.2.1 Materials

In this study we investigated blends of deuterated polystyrene (dPS), M_n=10,900 g/mol. (M_w/M_n = 1. 09) and poly(vinyl methyl ether) (PVME), M_n=24,400 g/mol. (M_w/M_n = 1.2) purchased from Polymer Source Inc. The polymers were blended in a ratio of 75 wt. % dPS and 25 wt. % PVME. Polystyrene grafted gold nanoparticles were also incorporated into the polymer blends at 4 wt. % Au.

7.2.2 Sample Preparation & Storage

Two types of thin films were prepared and examined for this study. In the first, thin films of the polymer blends (75% dPS, 25% PVME) were prepared by spin-coating from a toluene solution onto pre-cleaned silicon substrates with a native oxide layer of approximately 1.5 nm, measured by variable angle spectroscopic ellipsometry (VASE, J.A. Woollam M-2000). The substrates were cleaned by washing with ethanol, acetone and toluene and were then treated with UV-Ozone. The substrates were rinsed in ethanol, acetone and toluene prior to being UV-cleaned for 3 minutes. The polymer solutions were immediately spin-coated following the cleaning procedure. The samples were then immediately transferred to a vacuum oven where the samples were annealed at room temperature for 24 hours under vacuum and then 18 hours at 65°C (T_g+30°C). The samples were then kept in a desiccator cabinet until they were measured by XPCS or VASE. After the measurements were completed, the samples were verified to be smooth and continuous by optical microscopy and atomic force microscopy in order to confirm the films did not dewet from the substrate. The second class of thin films was polymer nanocomposites (PNCs). PNC films were prepared by adding 4 wt. % (~0.2 vol. %) Au NPs to the polymer solution prior to spin-coating.

7.2.3 Nanoparticle Synthesis

Gold nanoparticles (Au NPs) were synthesized using the two-phase arrested precipitation method reported by Brust *et al*.[19] Thiol-terminated polystyrene molecules (PS-SH) of number-average molecular weight M_n = 1100 g/mol. (M_w/M_n = 1.12), purchased from Polymer Source, Inc., were then grafted onto the surfaces of the nanoparticles. We will refer to the surfaces grafted chains as a brush layer, throughout this article. The newly synthesized particles were cleaned at least 10 times using methanol and toluene to remove excess ligands and salts in the solution. Information from thermogravimetric analyses (TGA, TA 2960) of the samples, together with the weight fractions and densities of the gold and the ligands, was used to estimate the grafting densities, σ, of the nanoparticles.

7.2.4 Nanoparticle Characterization

The diameters of the NP cores, D_{core}, and the grafted brush thicknesses, h_{brush}, were determined from scanning transmission electron microscopy (STEM, JEOL 2010F),

high angle annular dark field (HAADF) operated at 200 kV, images of the samples. The average particle sizes were determined by measuring the diameters of groups more than 300 NPs in each image. Two sets of brush-coated nanoparticles were prepared: (1) Au(5)-PS is a nanoparticle of D_{core} = 5.1 ± 1.2 nm, N = 10, σ = 2.1 chains/nm^2; and (2) Au(2)-PS is a nanoparticle of D_{core} = 2.2 ± 0.45 nm, N = 10 and σ = 1.9 chains/nm^2.

7.2.5 Nanoparticle Distribution

The film morphology and distributions of nanoparticles in these PNCs were determined using a combination of STEM and dynamic secondary ion mass spectrometry (DSIMS). The samples examined using STEM were prepared first by spin-coating solutions onto glass slides and then floating the film from the slide using deionized water. These films were then transferred onto Si_3N_4 grids and subsequently dried by vacuum annealing at 65°C for 16 hours. DSIMS measurements, performed at University of California Santa Barbara by Tom Mates, using a Physical Electronics 6650 Quadropole instrument, were used to determine the depth profile of Au within the PS films.

7.2.6 Calorimetry Measurements

The glass transition of ~5-10 mg of the pure polymers as well as the blend, were measured by differential scanning calorimetry (DSC, TA Instruments Q200). Each sample was first heated to 150°C at a rate of 10°C/min. to erase previous thermal history. The samples were then quenched to -100°C at 50°C/min. using a liquid nitrogen cooling system. A second heating scan from -100°C to 150°C was then immediately carried out at 10°C/min. The T_g was determined from the temperature corresponding to half the complete change in heat capacity on the second heating scan. All DSC measurements were completed in a nitrogen atmosphere. It is important to note that the PVME and PS chains are miscible at the temperatures (80°C and 90°C) where the experiments were conducted. For the materials used in our experiments, the lower critical solution temperature (LCST) is above 200°C.[20, 21] Further the T_g of PVME is -35°C and that of the PS component is 91°C. PVME possesses a much lower surface energy than PS, 32 and 22 mN/m respectively (at 150°C), and resides at the free surface at concentrations in excess of its bulk.[22, 23]

7.2.7 XPCS Measurements

The free surface dynamics of supported polymer films were investigated using XPCS. The XPCS experiments were performed at beam line 8-ID-I at the Advanced Photon Source (APS) at Argonne National Laboratory. Details of the XPCS experiment are described elsewhere.[24] We used an incident angle of 0.14°, less than the critical angle of 0.16° of the PS/PVME system; which was determined by x-ray reflectivity with incident x-ray energy of 7.5 keV. This limits the penetration of the x-ray beam to less than 10 nm from the free surface.[24] A fast x-ray reflectivity measurement was performed on the same spot as the dynamics measurement in order to ensure that the sample was not damaged during measurement by an induced surface roughness. In addition the observed intensity did not change more than 5% during a dynamics measurement.

7.2.8 VASE Measurements

The same sample structure (polymer blend on pre-cleaned silicon) was used with variable angle spectroscopic ellipsometry (VASE, J.A. Woollam M-2000) in order to determine the wetting layer thickness. For these measurements, the ellipsometric angles Ψ and Δ are collected over the entire spectral range (375 – 1700 nm). The optical constants were obtained from a 200 nm film of each of the pure polymer components by fitting Ψ and Δ to a Cauchy model. For the blend films, first a Cauchy layer was used in order to obtain an estimate for the film thickness. Then, a three layer effective medium approximation (EMA) model was then used to model the blend films, where the optical constants of PS and PVME were fixed, but the weight fraction of PS in each layer and the layer thickness were allowed to vary. This allowed for obtaining a lower mean squared error (MSE) than fitting to a Cauchy layer for the entire film. The sum of all three EMA layers was verified to be approximately the same as the estimate found from the Cauchy model. Similarly a gradient model was applied, where the optical constants were allowed to follow a simple linear and exponential gradient from the interface to the interior, but the MSE was found to increase compared to the three layer model.

7.3 RESULTS AND DISCUSSION

In this study we investigated the surface dynamics of supported thin films consisting of a miscible blend of 75% deuterated PS (dPS) and 25% PVME containing 4

wt. % Au nanoparticles (NPs) of different sizes (2 and 5nm diameter). The XPCS measurements of the dynamics of the dPS/PVME/brush-coated gold NPs polymer nanocomposites reveal the existence of two distinct relaxations. Details of the XPCS experiment are described elsewhere as well as in the methods section.[24] Plotted in Figure 7.1, for various q-vectors, are the intermediate scattering functions, $f(q,t)$, determined from the intensity autocorrelation functions, $g_2(q,t)$:

$$g_2(q,t)=1+A\left|f(q,t)\right|^2 \qquad (7.1)$$

for experiments performed at 90°C. [25] In this equation A represents the speckle contrast and the intermediate scattering function is:

$$f(q,t) = r\exp[-(t/\tau_1)] + (1-r)\exp[-(t/\tau_2)], \qquad (7.2)$$

where r is the fraction of the contribution to the exponential decay from the shorter relaxation; and τ_1 and τ_2 are the shorter and longer relaxation times, respectively.

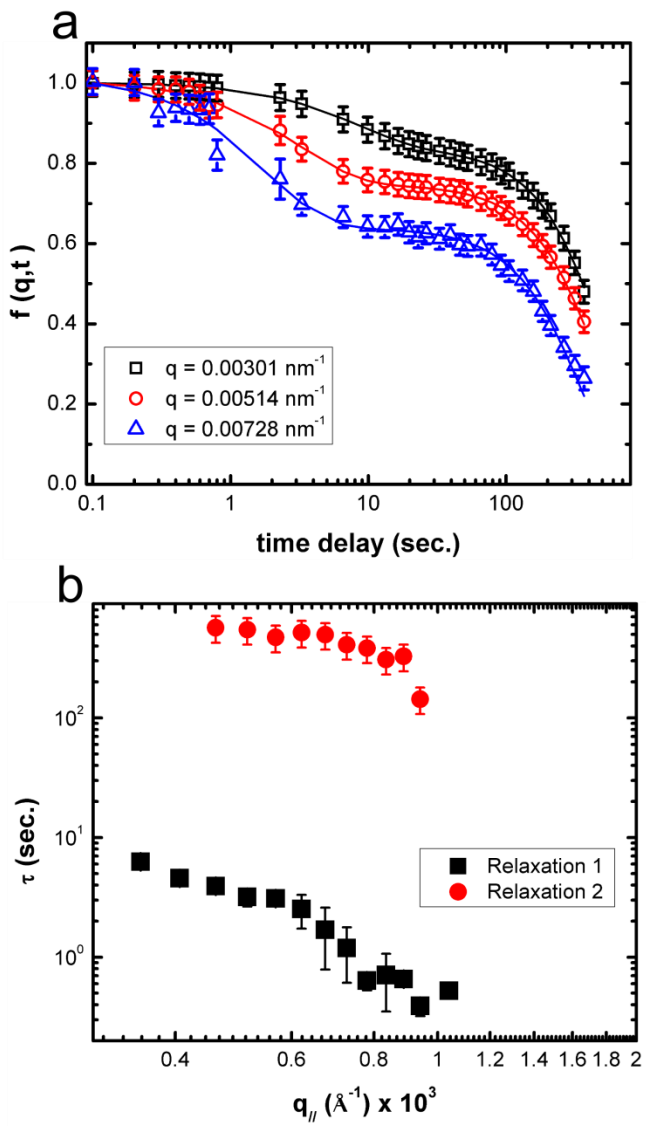

Figure 7.1 (a) Measured intermediate scattering function $f(q,t)$ of dPS11k/PVME with 4 wt% 2nm Au NPs for 3 different q-vectors at T= 90°C. Solid lines are the fittings to a simple exponential, assuming that two relaxations (τ_1 & τ_2) exist (eq. 2 in the main text). (b) Relaxation time (τ) as a function of q-vector ($q_{//}$) at T=90°C (circles). The black squares represent the relaxation time of the faster relaxation and the red circles the slower relaxation.

As discussed in our previous publication, these two relaxation processes represent the dynamics of chains undergoing translational motion in one environment with a high PVME concentration and the other exhibiting significantly slower chain relaxations in a different environment, with a higher PS concentration. This point is further illustrated in

Figure 7.1 where the relaxation time is plotted as a function of *q*-vector; a 2 order of magnitude difference between the two relaxation processes is evident.

Because the scattering signal of polymer thin films from XPCS measurements conducted below the critical angle of external reflection are dominated by the relaxation modes of thermally induced surface capillary waves, the viscosity of the surface layer may be extracted based on the following. According to hydrodynamic theory the ratio τ/d is proportional to η/γ, where η is the viscosity γ is the surface tension, such that:

$$\tau = \frac{2\,\eta\,(cosh^2(q_{//}\,d) + q_{//}^2 d^2)}{\gamma q_{//}\,(\sinh(q_{//}\,d)\,\cosh(q_{//}\,d) - q_{//}\,d)}. \qquad (7.3)$$

This equation has been successfully applied to hompolymer films, from which the viscosity was extracted.[24] Under these conditions, the relaxations throughout the film are manifested in the relaxation spectrum measured using XPCS, in the off-specular mode. Hence the viscosity measured using this technique is indicative of a viscosity of the entire film of thickness *d*, as opposed to a surface viscosity. We employ this analysis for the PS/PVME blend system. However in our case, the effective film thickness, *d*, is the thickness of the surface interfacial layer.[16] In the neat blend, this layer possesses an average composition that is rich in PVME, 70%, compared to the bulk, which is 25%, as discussed previously. Due to the high PVME concentration in this layer the surface viscosity is orders of magnitude smaller than that of the remainder of the film. Hence one may consider the surface layer to relax in a manner, with non-slip boundary conditions,[26] independent of the remainder of the film. In other words, we use the approximation that the relaxation spectrum is representative of the surface layer dynamics, not that of the remainder of the film.

The composition of the free surface region of a thin film nanocomposite blend is readily examined using variable angle spectroscopic ellipsometry (VASE). Moreover the thickness of the wetting layer, *d*, may be extracted. We determined that d=7.0 ± 1.0 nm in the nanocomposite containing the 2nm Au nanoparticles, and d=8.1 ± 1.0 nm in the other nanocomposite containing the 5nm Au nanoparticles. We also learned that the effective concentration of PVME in the wetting layer was 80 ± 15 vol. % in both nanocomposites, compared to 70 ± 15 vol. % in the neat blend. These results are consistent with dynamic secondary ion mass spectroscopy (dSIMS) measurements, as discussed later.

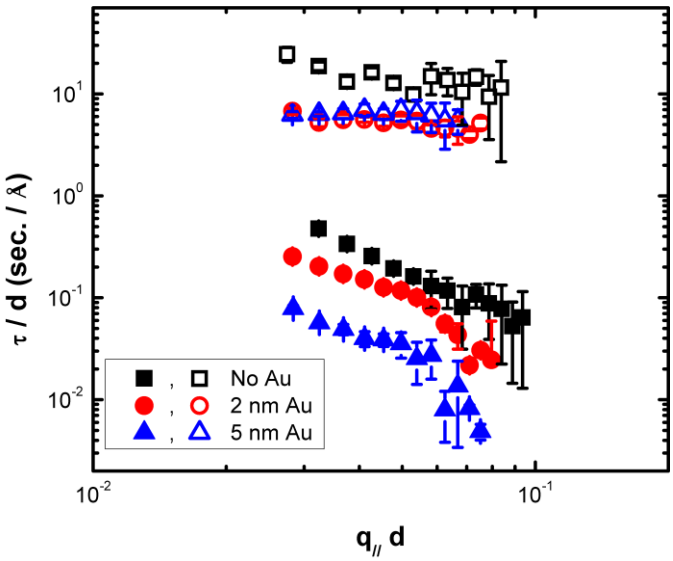

Figure 7.2 The relaxation time normalized by the surface layer thickness d, τ/d, is plotted as a function of $q_{//}d$ for measurements of the PNC blends at T=80°C. The closed symbols represent the first relaxation and the open symbols represent the second relaxation process.

The data shown in Figure 7.2, plotted as the ratio of τ/d *vs.* $q_{//}\,d$, clearly illustrates that η/γ is proportional to τ/d.[24, 27] These XPCS measurements were off-specular measurements, conducted below the critical angle ($\theta_c \approx 0.16^o$) for the neat dPS11k/PVME blends (squares), at a temperature of T=80°C. The faster relaxations represent the center of mass diffusive motions of the PVME chains in a PVME rich, 70% environment at the free surface, compared to 25% in the bulk, as has been previously discussed.[16] The second, slower relaxation is of course associated with the dynamics of PVME chains in an environment containing a higher local concentration of PS and associated with a higher local T_g.

The important observation is that the relaxation times of the polymer chains at the free surface in the nanocomposite are appreciably more rapid than those in the pure polymer/polymer blend, as shown in Figure 7.2. The second relaxations in the nanocomposites are also more rapid than those of the polymer/polymer blend. The enhanced dynamics would be consistent with the apparently enhanced fraction of PVME at the free surface in the PNC, compared with the neat blend. It is important to note moreover that there is a particle size dependence on the dynamics at the free surface, which will be discussed later.

The data in Figure 7.3 reveal that the viscosities extracted from the XPCS data are independent of film thickness. This is not unexpected because the surface layer thickness is comparable in these films. Additionally the surface region relaxes, approximately, independently of the remainder of the film because of the significant differences between the PVME composition at the free surface and in the bulk.

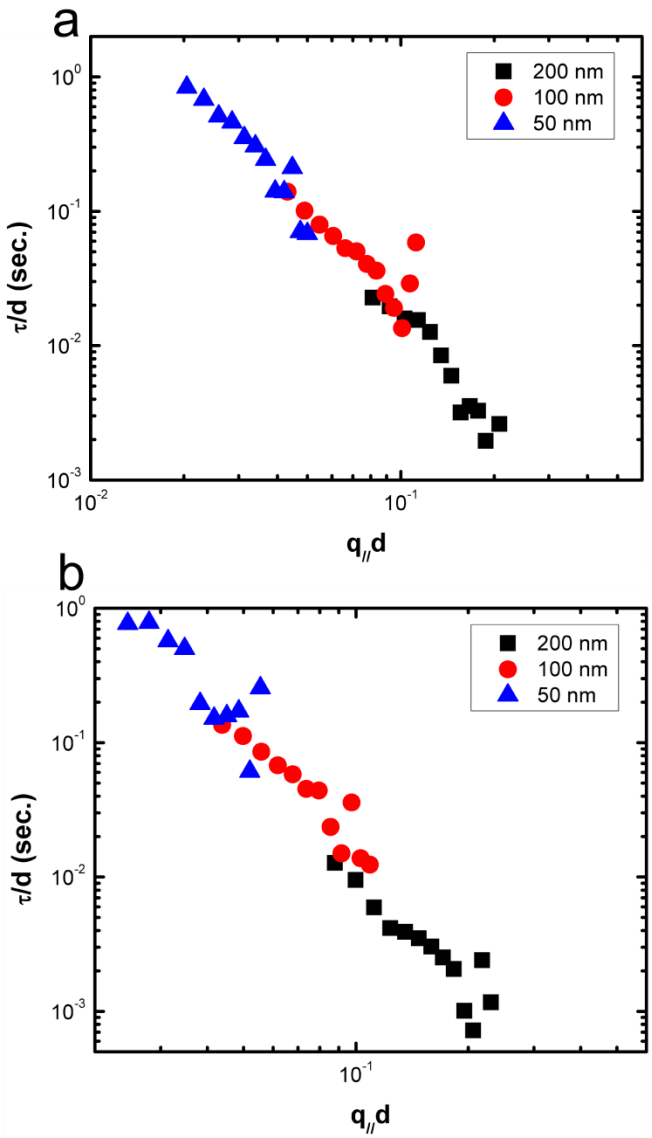

Figure 7.3 τ/d is plotted as a function of $q_{//}$ d, for 3 different film thicknesses: 200nm (black squares), 100nm (red circles) and 50nm (blue triangles), at T= 80°C for Au/dPS/PVME blends containing (a) 2nm Au NPs and (b) 5nm Au NPs.

The viscosities extracted from these data are plotted in Figure 7.4. Notably, the viscosity of the neat blend is approximately equal to the zero-shear viscosity measured by

rheology, as has previously demonstrated.[16] Similar observations have been documented for homopolymers, where the viscosity extracted from the XPCS data is equal to bulk the zero-shear viscosity measured using rheology.[24, 28] This follows from the fact that the surface relaxation spectrum manifests the influence of the relaxations throughout the entire homopolymer film, for homopolymer films that are not too thin.[24]

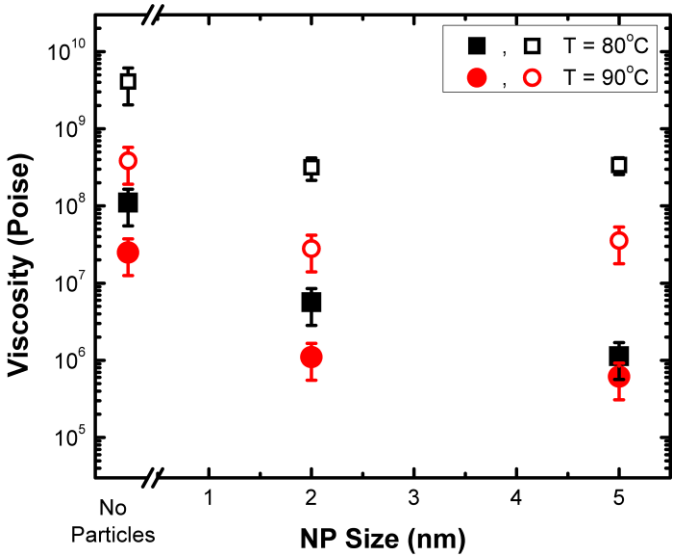

Figure 7.4 Viscosity as a function of NP diameter at 80°C (squares) and 90°C (circles). The viscosity calculated from relaxation 1 (closed symbols) and relaxation 2 (open symbols) are shown, and the viscosity of the pure polymer blend (which is indicated as no particles on the abscissa).

It is clear from the foregoing that the viscosities for the nanocomposite systems are more than an order of magnitude smaller than those of the neat blend. Moreover the viscosities of the PNC containing the 5 nm particles are a factor of 5 smaller than those containing the 2 nm particles. To understand these results, it is important to understand the following about the dynamics of miscible polymer blends. In a compatible A/B mixture the A and B chains experience different average local compositional environments, which have important consequences on their dynamics. Specifically monomer-monomer mixing of the dissimilar A/B segments is not random, due to the connectivity between monomers that constitute each chain.[29, 30] The local environment of a monomer is characterized by a self-concentration that is different from the average macroscopic concentration of the bulk; the length scale is on the order of the Kuhn step length, at least close to the glass transition.[31, 32] So spatially the local composition will vary from φ_{self} to an effective composition φ_{eff}, due to the effect of the self-concentration

and of concentration fluctuations. Natural consequences of the chain connectivity and local concentration fluctuations are that the A and B-type chains experience different, and distinct, local compositions and a distinct local glass transition temperatures T_g^{eff}. Consequently the relaxation rates of the individual components are significantly different, particularly when there is a significant difference in the T_g's of the pure components. The longest relaxation time, τ_L, of the dynamics of a polymer chain in a melt is dictated by a molecular friction factor, ζ, manifesting the "frictional drag" that the chain experiences due to local inter- and intra-molecular interactions. In other words the characteristic relaxation time of a chain is sensitive to its local composition environment.

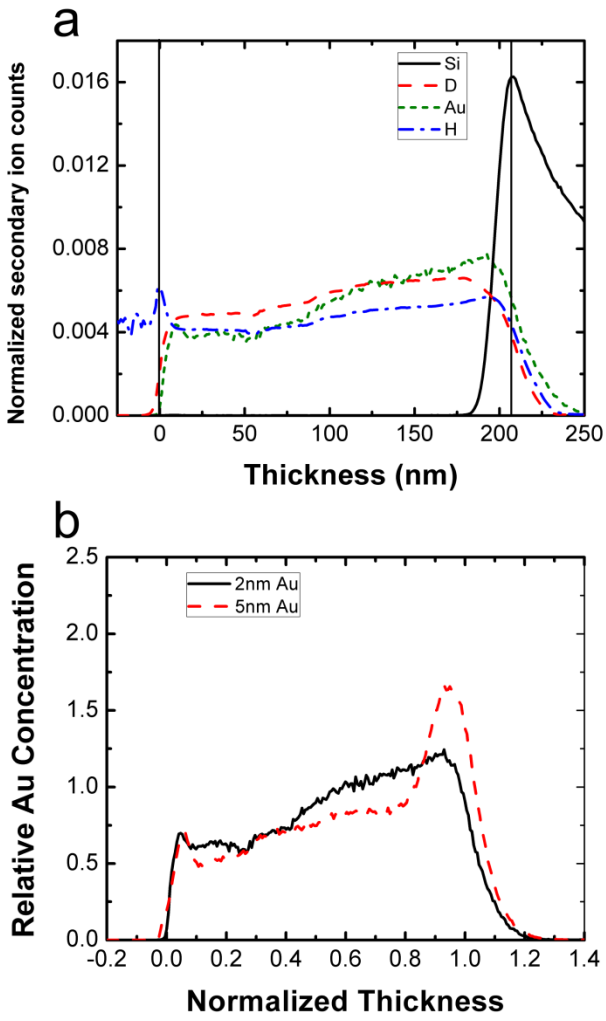

Figure 7.5 (A) The normalized depth profiles of the components, determined by dSIMS, of the nanocomposite containing 4wt% of the 2nm Au nanoparticles is shown here. (B) The depth profiles of Au in both nanocomposites are plotted.

Having discussed the dynamics in miscible blends and the effect of a free surface on the dynamics of a mixture we now turn to the question of the surface dynamics of polymer chains in polymer nanocomposites. We have shown that these nanoparticles exhibit a tendency to preferentially migrate to free surfaces of homopolymers and polymer blends,[6, 33, 34] where they modify the composition of the surface region. The depth profiles (Figures 5a and 5b), determined using secondary ion mass spectroscopy (SIMS), indicate that the brush-coated gold nanoparticles preferentially enrich the interfaces of both nanocomposites. Because the resolution of the SIMS experiment is smaller than the thickness of the wetting layer, quantitative arguments on the size and composition of the wetting layer cannot be gleaned from these results. Nevertheless it is evident from the H-profile in Figure 5A that there may be an excess of hydrogen at the free surface; this would be consistent with excess PVME in this region. This is consistent with the VASE data and anticipated, due to the lower surface tension of PVME.

The interfacial segregation of nanoparticles may be understood from the following. In athermal systems nanoparticles migrate to interfaces because the host polymer chains gain conformational entropy; this entropic gain would be mitigated by the loss of translational entropy of the nanoparticles, which increases with decreasing nanoparticle size.[35] Van der Waals interactions between the nanoparticles and an interface would contribute to a preferential attraction of the nanoparticles to a substrate.[36] The concentration profiles of the Au nanoparticles in SIMS spectra in Figure 5B show evidence of the preferential segregation of nanoparticles to both interfaces. The segregation of the 5 nm diameter Au nanoparticles is more significant than that of the 2 nm nanoparticles, due to the larger van der Waals forces associated with the larger nanoparticles. The free surface enrichment is also larger for the larger nanoparticle system, due to entropic effects. The lower interfacial segregation exhibited by the smaller particles is due to the fact that the host chains experience a much lower entropy gain when the nanoparticles segregate to the interfaces. Since the PVME chains possess a considerably lower surface energy than PS they will remain at the free surface in excess of the bulk, as shown in Figure 7.5.[22, 23]

We now comment on the reason the surface dynamics are faster in the nanocompsite than in the neat PS/PVME blend. There would be two reasons. First the

VASE measurements indicate that PVME exists at the free surface of the nanocomposites at larger concentrations than in the neat blend. Larger PVME concentrations in the surface region would be consistent with lower surface viscosities. The second reason is related to polymer brush/free chain interactions. A reduction of the viscosities of blends of PS/PS-brush-coated Au nanoparticles in relation to pure PS has been reported; this is due to a reduction of the effective friction ζ (reduction in the longest relaxation times) that the flexible PS chains experience in contact with these nanoparticles.[30, 31]

7.4 CONCLUSIONS

With the use of XPCS, we have measured the surface dynamics of miscible PS-PVME blends. We have shown that the surface dynamics of chain segments in a polymer nanocomposite are significantly faster than that of the neat polymer blend. In addition the polymer blends exhibit polymer chain dynamics of two different time-scales of dynamics, which are indicative of relaxations within two very different local compositional environments. These results provide a means to control the surface viscoelastic behavior of polymer systems, which would be useful in a range of applications involving thin films.

7.5 REFERENCES

1. Glass Transition, Dynamics and Heterogeneity of Polymer Thin Films. In *Glass Transition, Dynamics and Heterogeneity of Polymer Thin Films*, Kanaya, T., Ed. Springer-Verlag Berlin: Berlin, 2013; Vol. 252, pp 1-143.
2. Keddie, J. L.; Jones, R. A. L.; Cory, R. A. *Faraday Discussions* **1994,** 98, (Polymers at Surfaces and Interfaces), 219-230.
3. Napolitano, S.; Wubbenhorst, M. *Nature Communications* **2011,** 2.
4. Napolitano, S.; Capponi, S.; Vanroy, B. *European Physical Journal E* **2013,** 36, (6).
5. Huang, B. Y.; Glynos, E.; Frieberg, B.; Yang, H. X.; Green, P. F. *Acs Applied Materials & Interfaces* **2012,** 4, (10), 5204-5210.
6. Green, P. F. *Soft Matter* **2011,** 7, (18), 7914-7926.
7. Kumar, S. K.; Jouault, N.; Benicewicz, B.; Neely, T. *Macromolecules* **2013,** 46, (9), 3199-3214.
8. Mackay, M. E.; Dao, T. T.; Tuteja, A.; Ho, D. L.; Van Horn, B.; Kim, H. C.; Hawker, C. J. *Nature Materials* **2003,** 2, (11), 762-766.
9. Kropka, J. M.; Putz, K. W.; Pryamitsyn, V.; Ganesan, V.; Green, P. F. *Macromolecules* **2007,** 40, (15), 5424-5432.
10. Kropka, J. M.; Sakai, V. G.; Green, P. F. *Nano Letters* **2008,** 8, (4), 1061-1065.
11. Oh, H.; Green, P. F. *Nat Mater* **2009,** 8, (2), 139-143.
12. Colby, R. H.; Lipson, J. E. G. *Macromolecules* **2005,** 38, (11), 4919-4928.
13. Yang, H.; Green, P. F. *Macromolecules* **2013**, DOI: 10.1021/ma401813p.
14. Green, P. F.; Adolf, D. B.; Gilliom, L. R. *Macromolecules* **1991,** 24, (11), 3377-3382.
15. Kim, J. K.; Son, H. W. *Polymer* **1999,** 40, (24), 6789-6801.
16. Frieberg, B.; Kim, J.; Narayanan, S.; Green, P. F. *Acs Macro Letters* **2013,** 2, (5), 388-392.
17. Nakanishi, H.; Pincus, P. *Journal of Chemical Physics* **1983,** 79, (2), 997-1003.
18. Schmidt, I.; Binder, K. *Journal De Physique* **1985,** 46, (10), 1631-1644.
19. Brust, M.; Walker, M.; Bethell, D.; Schiffrin, D. J.; Whyman, R. *Journal of the Chemical Society-Chemical Communications* **1994**, (7), 801-802.
20. Ubrich, J. M.; Larbi, F. B.; Halary, J. L.; Monnerie, L.; Bauer, B. J.; Han, C. C. *Macromolecules* **1986,** 19, (3), 810-815.
21. Nishi, T.; Kwei, T. K. *Polymer* **1975,** 16, (4), 285-290.
22. Bhatia, Q. S.; Pan, D. H.; Koberstein, J. T. *Macromolecules* **1988,** 21, (7), 2166-2175.
23. Pan, D. H. K.; Prest, W. M. *Journal of Applied Physics* **1985,** 58, (8), 2861-2870.
24. Kim, H.; Ruhm, A.; Lurio, L. B.; Basu, J. K.; Lal, J.; Lumma, D.; Mochrie, S. G. J.; Sinha, S. K. *Physical Review Letters* **2003,** 90, (6).
25. Falus, P.; Borthwick, M. A.; Narayanan, S.; Sandy, A. R.; Mochrie, S. G. J. *Physical Review Letters* **2006,** 97, (6), 066102.
26. Hu, X. S.; Jiang, Z.; Narayanan, S.; Jiao, X. S.; Sandy, A. R.; Sinha, S. K.; Lurio, L. B.; Lal, J. *Physical Review E* **2006,** 74, (1).
27. Jackle, J. *Journal of Physics-Condensed Matter* **1998,** 10, (32), 7121-7131.

28. Wang, S. F.; Jiang, Z.; Narayanan, S.; Foster, M. D. *Macromolecules* **2012,** 45, (15), 6210-6219.
29. Leroy, E.; Alegria, A.; Colmenero, J. *Macromolecules* **2003,** 36, (19), 7280-7288.
30. Lorthioir, C.; Alegria, A.; Colmenero, J. *Physical Review E* **2003,** 68, (3).
31. Lodge, T. P.; McLeish, T. C. B. *Macromolecules* **2000,** 33, (14), 5278-5284.
32. Colmenero, J.; Arbe, A. *Soft Matter* **2007,** 3, (12), 1474-1485.
33. Chen, X. C.; Green, P. F. *Soft Matter* **2011,** 7, (3), 1192-1198.
34. Kim, J.; Green, P. F. *Macromolecules* **2010,** 43, (3), 1524-1529.
35. Meli, L.; Arceo, A.; Green, P. F. *Soft Matter* **2009,** 5, (3), 533-537.
36. Israelachvili, J., *Intermolecular and Surface Forces*. 2 ed.; Academic Press: New York, 1985.

CHAPTER 8
CONCLUSIONS

The work outlined in this dissertation was conducted with the goal of further understanding how complex polymer systems influence the polymer chain dynamics in both the glassy and rubbery state. Systems were investigated in both the bulk state as well as in supported films to further the understanding of how interfaces play a crucial role in governing properties when a polymer is confined in thin films. In this dissertation, we first demonstrated that with increasing functionality star-shaped molecules exhibited slower structural relaxations than their linear analogs. We then demonstrated that as the functionality was further increased, the rate of structural relaxations eventually saturated at a soft colloidal like regime; while consequently as the degree of polymerization of each arm was increased the aging behavior would return to one akin to linear polymers. In chapter 5, we demonstrated that the deviation from linear-like physical aging behavior was strongly correlated to local elastic properties in the glass state, as measured by incoherent neutron scattering. Then by confining star-shaped molecules between interfaces, the structural relaxation behavior can significantly differ from that of the bulk, which is directly connected to the changes in local glass transition temperature. The role of interfaces on the changes in dynamics was further investigated in the case of polymer blends and polymer nanocomposites taking advantage of the high surface area of nanoparticles.

In chapter 2, time-dependent structural relaxations, physical aging, of films, with thicknesses in the range 0.4 microns < h < 2 microns, of star-shaped polystyrene (SPS) macromolecules were investigated. Our studies reveal that the aging rates of star-shaped PS macromolecules are appreciably slower than their linear chain analogs. The magnitude of the difference between the aging rates of the linear and star-shaped macromolecules increases with increasing functionality, f, and decreasing degree of

polymerization per arm, N_{arm}, of the stars. Our results are consistent with the notion that constraints imposed due to the architecture of the macromolecule suppress relaxations that accommodate the reduction of free volume of the system.

In chapter 3, this phenomenon was shown to extend to higher f and larger N_{arm}. In this chapter we address the more general question regarding the structural relaxation behavior of star-shaped molecules in which there is a limit to the effect of polymer architecture as the molecules begins to exhibit more colloid like behavior with increasing f, and decreasing N_{arm}. We demonstrated that that the structural relaxation of star-shaped molecules exhibit a limit to the reduction in physical aging rate as the functionality is further increased to 32 and 64 arms. The critical functionality at which the limit occurs depends also on N_{arm}. We also demonstrate that the influence of polymer architecture diminishes at aging temperatures close to T_g. The influences of architecture were understood in terms of the competition between the departure from equilibrium and the restriction of motions at low temperature.

In chapter 4, the influence of temperature and the competition between driving force and glassy dynamics were investigated in further detail. The aging rates, were shown to exhibit a maxima at a threshold departure from T_g, $\Delta T_{th} = T_g - T_{age}$. ΔT_{th} decreased with increasing f; and the aging rate exhibited a stronger decrease with T, with increasing f. Measurements of the atomic vibrations of these polymers, using inelastic neutron scattering, rationalize this behavior in terms of the local elastic properties and their correlation with the physical aging rate.

In chapter 5, we show that the physical aging of star-shaped macromolecular glassy films in the thickness regime of a few hundred nanometers and thinner occurs significantly slower than the bulk. The slow aging of these macromolecular systems in this thickness regime is understood, universally, in terms of gradients in the local glass transition temperature, T_g, of the films in the vicinity of interfaces. In which case a gradient T_g model was employed in order to predict the thickness dependence of the aging rate based on the bulk aging rate and the local T_g.

In chapter 6, we turned our attention to miscible A/B polymer/polymer mixtures. In the case of thin films, they form a segregated layer at the free surface, associated with the preferential segregation of the lower cohesive energy density component. With the

use of X-ray photon correlation spectroscopy (XPCS) we showed that the chain dynamics at the free surface of polystyrene (PS)/polyvinyl methyl ether (PVME) thin film mixtures can be orders of magnitude faster than in the bulk. These differences in dynamics manifest from differences between the local compositions of the blend at the free surface and the bulk, as well as film thickness constraints.

In chapter 7, we reported an unusual phenomenon wherein the surface viscosity of polymer nanocomposites of PS, PVME and PS-coated gold nanoparticles (PS/PVME/PS-Au) is over an order of magnitude smaller than that of the neat miscible PS/PVME blend. Our X-ray photon correlation spectroscopy (XPCS) studies of the surface dynamics also reveal that the polymer chains manifest dynamics associated two separate average compositional environments: a PVME-rich region, significantly in excess of its bulk concentration, and a separate PS-rich environment, where the dynamics are approximately two orders of magnitude slower. The unusually rapid surface dynamics in the PS/PVME/PS-Au nanocomposite are due largely to the excess of PVME chains and the polymer/brush-coated nanoparticle interactions at the free surface.

APPENDIX A
MATERIALS LIST

A.1 MATERIALS

A list of the polymers used in this Ph.D. is displayed in Table A.1. The star-shaped molecules were synthesized by Georgios Sekallariou of the Chemistry Department at the University of Athens. Some of the low functionality stars were purchased from Polymer Source Inc, which are indicated in the table. The remaining, high functionality star-shaped PS were synthesized by means of anionic polymerization using high vacuum techniques.[1, 2] Excess of the living poly(styrenyl)lithium were reacted with the appropriate chlorosilane linking agent.[3] Sufficient time for the coupling reaction has to be allowed, and the excess arm material was removed by fractionation. The linear polystyrene molecules used in this study of various molecular weights (not shown in the table below) were purchased from Pressure Chemical.

Table A.1 A list of the star-shaped polymers used in this study.

Name	Functionality (f)[a]	M_n^{arm} (kg/mol.)[c]	PDI[d]
StarPS-3arm-19K*	3	19	1.03
StarPS-3arm-109K*	3	109	1.03
StarPS-4arm-4K*	4	4	1.03
StarPS-8arm-10K*	8	10	1.03
StarPS-8arm-13K	8	13	1.03
StarPS-8arm-25K*	8	25	1.03
StarPS-8arm-29K	8	29	1.02
StarPS-8arm-35K*	8	35	1.01
StarPS-8arm-42K*	8	42	1.03
StarPS-8arm-47K*	8	47	1.03
StarPS-8arm-57K	8	57	1.02
StarPS-16arm-13K	16	13	1.02
StarPS-16arm-29K	16	29	1.02
StarPS-16arm-57K	16	57	1.01
StarPS-32arm-9K	32	9	1.03
StarPS-32arm-36K	32	36	1.03
StarPS-32arm-52K	32	53	1.01
StarPS-32arm-80K	32	80	1.01
StarPS-32arm-140K	32	140	1.01
StarPS-64arm-9K	64	9	1.02
StarPS-64arm-36K	64	36	1.01
StarPS-64arm-52K	64	52	1.01
StarPS-64arm-80K	64	80	1.01
StarPS-64arm-140K	64	140	1.01

[a]Functionality, f ,determined by the ratio $(M_w)_{star}/(M_n)_{arm}$. [b]From Low Angle Laser Light Scattering in THF at 25 ºC. [c]From membrane osmometry in toluene at 35 ºC. [d]From SEC in THF at 40 ºC calibrated with linear PS standards. *Purchased from Polymer Source Inc.

A.2 REFERENCES

1. Hadjichristidis, N.; Iatrou, H.; Pispas, S.; Pitsikalis, M. *Journal of Polymer Science Part a-Polymer Chemistry* **2000,** 38, (18), 3211-3234.
2. Uhrig, D.; Mays, J. W. *Journal of Polymer Science Part a-Polymer Chemistry* **2005,** 43, (24), 6179-6222.
3. Roovers, J.; Zhou, L. L.; Toporowski, P. M.; Vanderzwan, M.; Iatrou, H.; Hadjichristidis, N. *Macromolecules* **1993,** 26, (16), 4324-4331.

APPENDIX B

AGING EXPERIMENT

B.1 AGING EXPERIMENTAL PROCEDURE

1. Anneal the sample in oven for 24 hours at T_g + 30°C in a vacuum oven.
2. Air cool in oven down to room temperature.
3. Anneal sample in spectroscopic ellipsometer (JA Woollam, M-2000Di) heat stage for 30 min. at 150°C.
    i. Under nitrogen gas purge.
    ii. Use liquid nitrogen to ensure cooling rates and temperature stability.
4. Measure the film thickness upon cooling to 25°C.
    i. Acquisition time 5 seconds.
    ii. Use high accuracy mode.
    iii. Only use the QTH lamp
    iv. Estimate the T_g of the polymer film by linear fit to the rubbery and glassy regions of the thickness vs. temperature curve.
5. Without removing sample from the ellipsometer heat cell, setup aging temperature profile.
6. Ramp to 40°C above T_g at 10°C/min.
7. Hold for 30 min.
8. Ramp to 25°C at 85C/min.
9. Hold for 2 min.
10. Ramp to $T_{age} = T_g - xx$, where the T_g was measured in step 4.
11. Acquire data for 360 min.
    i. Data acquisition time 15 sec.
    ii. High accuracy mode on.
    iii. Ramp step acquisition increment = 0 sec.

iv. Hold step acquisition increment = 60 sec.

B.2 FITTING TO AGING RESULTS

The film thickness from the aging experiments described in the previous sections is fit in order to determine the average aging rate of the particular film. The initial zero time value is taken to be the time in which the temperature during the quench in step 8 passes through the T_g of the material. The film thickness data is then fit to the following equation:

$$h(t) = b\log(t - t_0) + c \qquad \text{(B.1)}$$

where h is the film thickness, t is time, b is the approximate aging rate, t_0 is the time shift factor, and c is the approximate initial thickness; where b, t_0, and c are fitting parameters. Once a value for t_0 is found, the time values for the aging values are shifted according to t_0. The film thickness values are then normalized by the equilibrium value, this value is obtained by taking the thermal expansion coefficient of the rubbery regime, found in step 4 through the film thickness found during annealing at high temperature in step 7, to the aging temperature. The resultant values of aging time vs. normalized film thickness are then fit to the equation described in section 2, equation 2.2. These experiments are then repeated 3-5 times in order to obtain the average aging for the sample.

B.3 REPRODUCIBILITY MEASURMENTS

We extended experiments of our films for different durations and the aging rate was calculated from the data at numerous stages throughout the aging process. As a specific example, consider the data in Figure B.1 representing linear chain PS (LPS-152K); it was aged at ΔT_{age}= -50°C, the lowest aging temperature investigated in this study. The inset of Figure B.1 shows how the thickness of the film changed with time. The aging rate was calculated continuously along the slope of this line. It is clear from this data that the aging rate is stable for all aging times longer than 200 minutes. While the aging rate fluctuated within this time scale, it always remained within the experimental error of ~0.5 x 10^{-4}. Therefore, the experimental time of 360 minutes was more than sufficient to determine an average aging rate of the material.[1, 2] Each

experiment was repeated 3-5 times to ensure the reproducibility of the results. Our studies of supported polymer films (PS/SiO_x, SPS/SiO_x) in the thickness range 0.4 microns < h < 2 microns reveal no dependence of aging rate on film thickness. We however, note that films that are quenched in the freely standing state, exhibit thickness dependent aging behavior in this thickness range.[2-4]

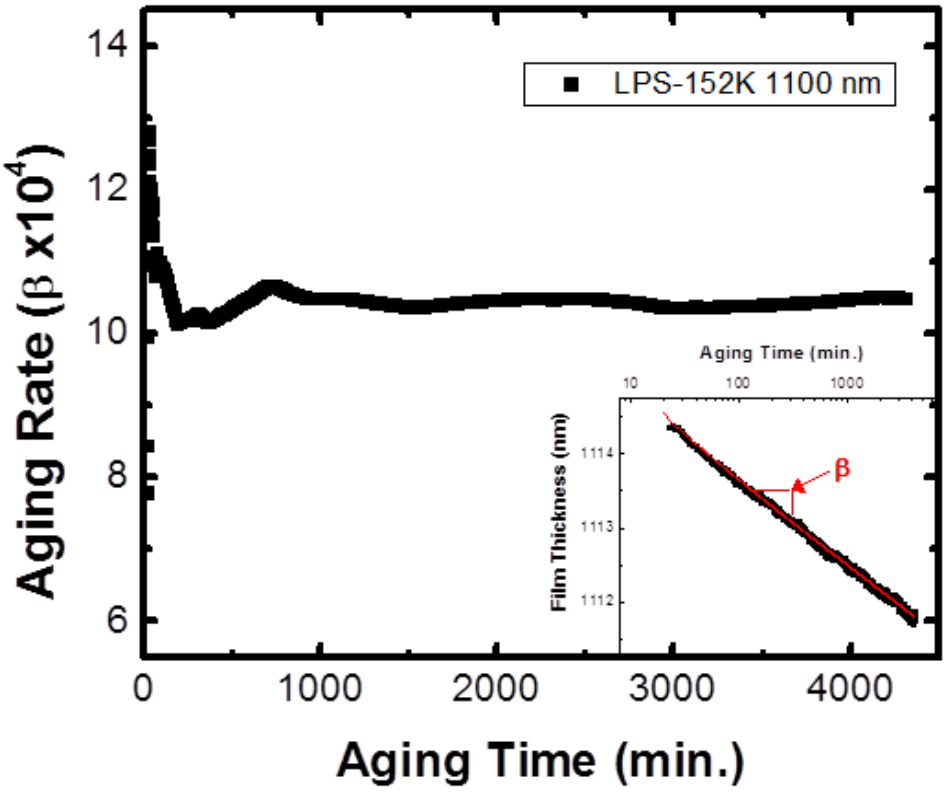

Figure B.1 The aging rate, at ΔT_{age} = -50°C, is shown here for a $H(T$=24°C) = 1.1 μm LPS-152K film. The aging rate is determined from the slope, a typical plot of which is shown in the inset.

B.4 REFERENCES

1. Baker, E. A.; Rittigstein, P.; Torkelson, J. M.; Roth, C. B. *Journal of Polymer Science Part B-Polymer Physics* **2009,** 47, (24), 2509-2519.
2. Pye, J. E.; Rohald, K. A.; Baker, E. A.; Roth, C. B. *Macromolecules* **2010,** 43, (19), 8296-8303.
3. Rowe, B. W.; Freeman, B. D.; Paul, D. R. *Polymer* **2009,** 50, (23), 5565-5575.
4. Gray, L. A. G.; Yoon, S. W.; Pahner, W. A.; Davidheiser, J. E.; Roth, C. B. *Macromolecules* **2012,** 45, (3), 1701-1709.

APPENDIX C
GLASS TRANSITION MODEL

C.1 GRADIENT TG MODEL

Kim *et. al.*, showed that a local gradient-T_g model could be used to describe the distribution of T_g throughout a supported thin film.[1] This was done by dividing the film into infinitesimally thin layers, each with its own discrete glass transition. It is important to note that the model used in the current publication is the same as the Kim model for LPS-152K and SPS-8-25K, and only a slight modification, which will be discussed in more detail later, was incorporated to account for the free surface T_g of SPS-8-10K. For a full description and derivation of these equations, please refer to the original paper by Kim and co-workers. The Kim model relies on three parameters: the glass transition temperature of the bulk polymer, T_g^{∞}, the characteristic length which the interface influences the local glass transition, ξ, and a measure of the strength of the interfacial interaction between the polymer and the interface, k. It is important to note that ξ is not the thickness of the mobile layer, 2ξ is the distance from the free surface to the point in the film, at which the bulk T_g is recovered. Kim's gradient model applies well to the LPS-152K system, but the model assumes that the free surface T_g is lower than the bulk T_g, which is not the case in SPS-8-10K. Therefore, we used a very similar model, but modified the function for the free surface T_g to allow for an increase relative to the bulk. The only modification can be observed in equation C.6, but some of the equations are repeated for clarity.

The model begins by first describing the thickness dependence of the T_g for each material, which are reported in a previous publication.[2] As the T_g versus H behavior of LPS-152K appears to follow a growth in T_g with increasing thickness while saturating at infinite values, the Michaelis-Menten (M-M) function was used. This function is predominantly been used in enzyme kinetics, but has also been used previously to

describe the T_g vs. H behavior.[1] We determined the values for T_g^{∞} and ξ by fitting the M-M function,

$$1/T_g(H) = \xi/T_g^{\infty} \cdot 1/H + 1/T_g^{\infty} \qquad \text{(C.1)}.$$

We fit equation C.1 to data previously published by our group on this system; T_g^{∞} =99 °C and ξ=2.3 nm for LPS-152K.[2] The thickness dependence of the T_g relative to the bulk is shown in Figure C.1; the results of the model calculations, obtained using equation C.2, are overlaid. The predictions of the model are drawn as solid lines on this plot. It is apparent that the trends predicted by the model are entirely consistent with experiment.

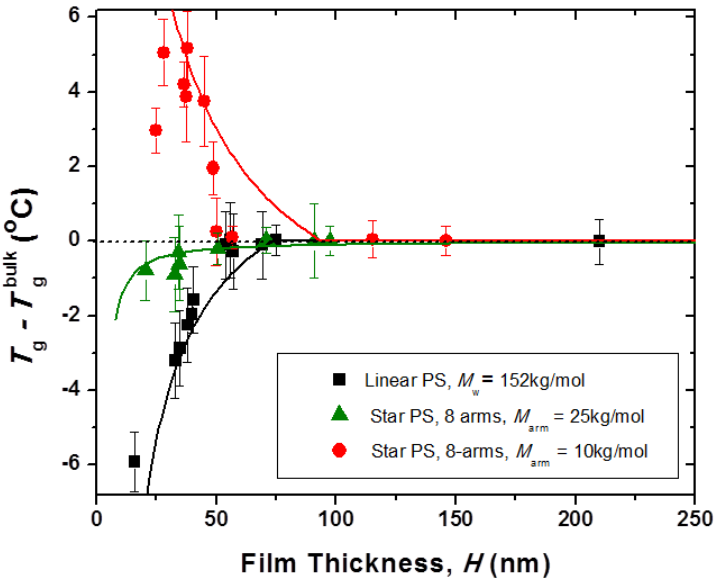

Figure C.1 The glass transition temperature is plotted as a function of film thickness, reported in Ref. [1] for LPS-152K (black squares), SPS-8-25K (green triangles) and SPS-8-10K (red circles). The solid lines represent the expected average T_g values based on the fitting described in the text.

In this model, it is assumed that the film is divided into layers that are infinitesimally thin, each with their own T_g, denoted $L_g(x)$. Because both the T_g of a film of thickness H, $T_g(H)$, and $L_g(x)$ are continuous and differentiable functions, the mean value theorem can be used to draw the local glass transition function. The average T_g of a film is related to the local *glass transition temperatures*, $L_g(x)$, throughout the film such that

$$T_g(H) = \int_0^H L_g(x)dx / \int_0^H dx. \qquad \text{(C.2)}$$

Which represents a weighted average of the local glass transition throughout the film, where the local T_g,

$$L_g(x) = S_g(x) + I_g(x) - \{S_g(0) + I_g(0)\}, \qquad \text{(C.3)}$$

where $S_g(x)$ and $I_g(x)$ are symmetric functions with respect to the film thickness representing the local glass transition of a layer at the free surface and substrate respectively. The local glass transition function was split into two symmetric functions in order to incorporate interactions from both interfaces. Thus a positive, negative or neutral interfacial interaction can be incorporated as can be seen in the following two examples (SPS-8-10K and SPS-8-25K). In this equation, the glass transition of a layer near the free surface is qualitatively represented by

$$S_g(x) = T_g^{\infty} \cdot x(2\xi + x)/(\xi + x)^2 \qquad \text{(C.4)}$$

The function for $S_g(x)$ is found by solving combining equations C.1-C.3 and solving the differential equation. The derivation is shown in detail in Ref. 2. This equation reflects the fact that the T_g at the free surface is lower than the interior. As previously stated, $I_g(x)$ is a symmetrical function to $S_g(x)$ with respect to the thickness of the film H.

$$I_g(x) = T_g^{\infty} \cdot [(H-x)(2\xi + H-x) + 2k\xi]/(\xi + H-x)^2 \qquad \text{(C.5)}$$

In addition there is an additional term that shows up in this equation, $2k\xi$. This term arises to account for and control the profile at the substrate interface, for instance to account for H-bonding or adsorption to the substrate. In the original works by Kim *et. al.* this term was not included in the function for the free surface ($S_g(x)$), because all polymer films were assumed to exhibit a decrease in T_g at the free surface. Therefore it was not necessary to allow for a positive interaction with this surface. Also, since in the linear chain (LPS-152K) PS/SiO_x system, the local T_g at the substrate is comparable to the bulk T_g, and solving for $L_g(x=H) = T_g^{\infty}$, $I_g(x=H)$ must be T_g^{∞}. In order for this to be true, $k = \xi/2$ for LPS-152K, thus accounting for a neutral interaction with the substrate. In the case of SPS-8-25K, the variable k is greater than $\xi/2$ to allow for the local glass transition at the substrate to increase in accordance with observations in previous publications.[2, 3]

In the case of SPS-8-10K, there is an increase in local T_g at both the free surface and substrate.[2] Since the T_g at the free surface of the SPS-8-10K macromolecule is higher than the interior, then for this system equation C.4, the function for the T_g of a layer near the free surface, must be modified to reflect this difference. Please note this is the only modification that is made to the Kim model, and it is only used for SPS-8-10K. Therefore in the case of the SPS-8-10K molecule equation C.4 is modified to also include a positive interaction parameter, *k*

$$S_g(x) = T_g^{\infty} \cdot [x(2\xi + x) + 2k\xi]/(\xi + x)^2 \qquad \text{(C.6)}$$

This modification was made in order to account for the increase in local glass transition at the free surface which was observed for this material measured by variable energy positron annihilation spectroscopy.[2] This modification makes $S_g(x)$ and $I_g(x)$ truly symmetrical with respect to the thickness of the film for this material. The local T_g functions, L_g-T_g^{bulk}, were calculated for 50 nm films of the polymers are plotted in Figure 5.4 of this document. The free surface T_g's of the polymers were determined using variable energy positron annihilation lifetime spectroscopy (PALS), while the T_g's of star-shaped systems, in the vicinity of the substrate, were determined from thickness dependent measurements of ultra-thin films and reported in previous publications.[2, 3] The results from PALS along with the resulting free surface T_g's are shown in the inset of Figure 5.4 of the main text.

C.2 REFERENCES

1. Kim, J. H.; Jang, J.; Zin, W. C. *Langmuir* **2001,** 17, (9), 2703-2710.
2. Glynos, E.; Frieberg, B.; Oh, H.; Liu, M.; Gidley, D. W.; Green, P. F. *Physical Review Letters* **2011,** 106, (12), 128301.
3. Glynos, E.; Frieberg, B.; Green, P. F. *Physical Review Letters* **2011,** 107, (11), 118303.